FACULTY
OF MATHEMATICS
AND PHYSICS
Charles University

DOCTORAL THESIS

Dana Křížová

The source process of Greek earthquakes

Department of Geophysics

Supervisor of the doctoral thesis: Prof. RNDr. Jiří Zahradník DrSc.

Study programme: Physics

Specialization: Geophysics

Prague 2017

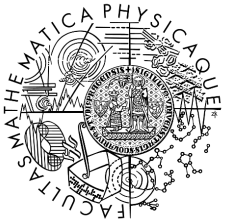

MATEMATICKO-FYZIKÁLNÍ
FAKULTA
Univerzita Karlova

DISERTAČNÍ PRÁCE

Dana Křížová

Ohniskový proces řeckých zemětřesení

Katedra geofyziky

Vedoucí disertační práce: Prof. RNDr. Jiří Zahradník DrSc.

Studijní program: Fyzika

Studijní obor: Geofyzika

Praha 2017

I declare that I carried out this doctoral thesis independently, and only with the cited sources, literature and other professional sources.

I understand that my work relates to the rights and obligations under the Act No. 121/2000 Sb., the Copyright Act, as amended, in particular the fact that the Charles University has the right to conclude a license agreement on the use of this work as a school work pursuant to Section 60 subsection 1 of the Copyright Act.

In Prague 26. 5. 2017 Dana Křížová

First, I would like to thank my supervisor Prof. Jiří Zahradník for his inspiring leadership and for his patience. My thank also belongs to Doc. František Gallovič for his usefull comments and suggestions. I am grateful to Prof. Anastasia Kiratzi for her long-term cooperation and for her advices. My thanks belongs to Martin Kříž for great help with data processing. I also thank all the teachers and students at the Department of Geophysics for creating friendly and inspiring atmosphere.

The work was supported by the grant agencies in the Czech Republic: GAUK 14509, GACR 210/11/0854, MSM 0021620860, and SVV-2012-265308. I also acknowledge partial support from the European Union (European Social Fund, ESF) and Greek national funds-Research Funding Program: Thales (MIS377335) "Investing in knowledge society through the European Social Fund" and from a Greece-Turkey bilateral project. Partial support of this work was obtained from the Czech Science Foundation Grant Number GACR-14-04372S.
I also thank Iordanis Dimitriadis for providing the average 1D model obtained from the 3D inversion for the Columbo region. The comments and suggestions of Hrvoje Tkalčić and C. P. Evangelidis are gratefully acknowledged.

Název: Ohniskový proces řeckých zemětřesení

Autor: Dana Křížová

Katedra: Katedra geofyziky

Vedoucí disertační práce: Prof. RNDr. Jiří Zahradník DrSc., Katedra geofyziky

Abstrakt:

Výzkum momentových tenzorů (MT) a jejich neurčitostí patří k úlohám moderní seismologie. Dizertace se zabývá především izotropní složkou tří mělkých zemětřesení: Jevu A v Krétském moři (M_w 5.3) a dvou nejsilnějších jevů roje u ostrova Santorini, B (M_w 4.9) a C (M_w 4.7). MT je počítán inverzí kompletních vlnových obrazů za předpokladu 1D rychlostních modelů. Obrácená úloha je nelineární v centroidální hloubce a času a lineární v šesti parametrech MT, z nichž jedním je stopa MT. Neurčitost izotropní složky je studována novým postupem (Křížová et al., 2013). Stopa MT se systematicky mění a zbývající parametry jsou optimalizovány. Metoda poskytuje obraz o vazbách mezi izotropní složkou, hloubkou a ohniskovým mechanizmem. Izotropní složka závisí na předpokládaném rychlostním modelu; ze dvou existujících modelů preferujeme model s nižším kondičním číslem. V něm je (kladná) izotropní složka nejsilněji indikována u jevu B. K rychlému odhadu existence významné izotropní složky předkládáme novou empirickou metodu (Křížová et al., 2016). Je založena na porovnání hloubkové závislosti korelace (mezi reálnými a syntetickými seismogramy) pro plný a deviatorický MT. Metoda, podložená rozsáhlými syntetickými testy, potvrdila nezanedbatelnou izotropní složku jevu B. Jev A se jeví jako deviatorický. V praxi seismických center by tato jednoduchá metoda mohla snížit riziko chybného odhadu hloubky.

Klíčová slova: zemětřesení, momentový tenzor, izotropní složka, inverze vlnových obrazů

Title: The source process of Greek earthquakes

Author: Dana Křížová

Department: Department of Geophysics

Supervisor of the doctoral thesis: Prof. RNDr. Jiří Zahradník DrSc., Department of Geophysics

Abstract:

Investigations of moment tensor (MT) and its uncertainty are topical. This thesis is focused on isotropic component of three shallow earthquakes: Event A in Cretan Sea (M_w 5.3) and two events near Santorini island, B (M_w 4.9) and C (M_w 4.7). MT is inverted from full waveforms in an assumed 1D velocity model. The inverse problem is non-linear in centroid depth and time, and linear in six MT parameters, one is the MT-trace. Uncertainty of isotropic component is studied by a new approach (Křížová et al., 2013). The trace is systematically varied, and remaining parameters are optimized. The method reveals tradeoffs between the isotropic component, depth, time, and focal mechanism. From two existing velocity models, we prefer the one with lower condition number, in which a (positive) isotropic component is indicated for event B. To rapidly assess a likely existence of isotropic component, an empirical method is proposed (Křížová et al., 2016). It is based on comparison between depth-dependences of waveform correlation in full and deviatoric modes. Based on extensive synthetic tests, the method confirms a non-negligible isotropic component of event B; event A appears to be deviatoric. Routine application in seismological centers could reduce risk of erroneous source-depth estimates.

Keywords: earthquake, moment tensor, isotropic component, full waveform inversion

Contents

Introduction

Studies of the earthquake source process belong to seismologic priorities because of their relations to seismotectonics and simulations of strong ground motions. The earthquake source investigations have been performed at the Department of Geophysics (Faculty Mathematics and Physics, Charles University) since 90's, most intensively in relation to seismic stations of the Faculty operating in Greece (since 1997) in cooperation with the University of Patras.

Although the location of earthquakes is common since the beginning of twentieth century, the moment tensor (MT) analysis starts much later, in 60's (Aki and Richards, 2002; Lay and Wallace, 1995). Study of MT on regional distances is more complicated than computation with teleseismic data because of heterogeneities in the crust and the upper mantle. However, just regional (or local) distances are important for studies of small and moderate-sized earthquakes (magnitude < 5.5); see for example Hofstetter et al. (2000). The most challenging source parameters are non-double-couple MT components, because their inversion is inherently least stable.

The present work links data processing and computational modeling to study source parameters of three carefully selected events in Greece: The Cretan Sea, M_w 5.3 event of 27 January 2012, the Santorini M_w 4.9 event of 26 June 2009, and the Santorini M_w 4.7 event of 26 June 2009. Their importance is in possible presence of the isotropic source component. The work focuses on methodical aspects of their centroid moment tensor (CMT) retrieval and its uncertainty. The main tool for this study is ISOLA software and its modifications. This package makes it possible to compute moment tensors from regional and local full-waveform data for simple or multiple earthquakes. The method is being developed since 2003 (Sokos and Zahradník, 2008).

Basic earthquake source parameters and equations, dealt with in this thesis, are listed in Chapter 1.

Special attention is paid to moment tensor and their non-double-couple components. A detailed overview of the current state-of-art of the CMT determination and uncertainty assessment is given in Chapter 2, where the three earthquakes are introduced and analyzed. Chapter 3 describes the two main methodical innovations of the thesis:

(1) We investigate on synthetic tests and real data how to resolve the isotropic component of the seismic moment tensor, and how to evaluate its uncertainty. In the non-linear inversion problems, where there are eight free parameters (e.g., six elements of the moment tensor, depth, and origin time), we propose a waveform-inversion scheme in which the moment-tensor trace is systematically varied, and the remaining seven free parameters are optimized for each specific value of the trace.

(2) We propose a simple procedure to identify earthquakes with a strong isotropic component. The method consists of a comparison of the correlation-depth dependences for two modes of the CMT inversion: full and deviatoric.

Additional calculations, not shown in main text, are presented as Supplementary material. The results have been summarized in two published papers (Křížová et al., 2013, and 2016) which are copied in the Attachments.

1. Standard earthquake parameters and basic equations

First, we must say what earthquake source process stands for in this thesis. We focus especially on moment tensor solution. We pay attention to earthquake kinematics. So, the earthquake dynamics is beyond the scope of this thesis, for more details see Madariaga and Olsen (2002), or Chapter 9 in Lee and Wallace (1995).
This Chapter is divided to the two parts:

(i) Standard earthquake parameters
(ii) Essentials for calculations

Accuracy of results will be performed separately in specialized Chapter 3.

1.1. Standard earthquake parameters

There are many publications about seismological parameters. Let us mention two well known: Aki and Richards (2002), and Dahlen and Tromp (1998). Seismic sources and source parameters are described in detail in Bormann et al. (2012). We chose six essential earthquake parameters which are commonly mentioned in earthquake reports (for example in web pages: European-Mediterranean Seismological Centre = EMSC or in Observatories & Research Facilities for European Seismology = Orfeus): origin time, depth, epicenter position, moment tensor, scalar seismic moment, magnitude.

The origin time is the time when the earthquake rupture starts. It is common to write this variable in Coordinated Universal Time (UTC). We comment here as a note that some people replace UTC by GMT (Greenwich Mean Time) which is inaccurate. GMT stands for time in time zone connected with the Royal observatory in London (Greenwich) and it is based on Earth rotation, on the other hand UTC is based on atomic clocks and it is theoretically independent on Earth rotation.

When we sort earthquakes due to depth we get three main categories. Shallow earthquakes are in the depths less than 70 kilometers, intermediate 70 – 300 km and deep earthquakes in depths greater than 300 km (Bormann et al., 2002). Earthquake occurred in the crust or in the upper mantle. The depth of earthquake could tell us some information about tectonic settings. For example, we can map subduction zones with details such as how steeply is dipping one plate beneath the other.

In this thesis, we focus on shallow earthquakes particularly on events in the crust. So, we used regional records and all calculations were made in Cartesian geometry.

The location of earthquake is one of the important things and it belongs to main information about seismic event and it is defined by origin time and hypocenter, where the hypocenter stands for initiation point of the rupture process. Then the epicenter is projection of hypocenter on the Earth surface.

Most location methods use only a part of the information from seismograms (arrival time of body waves P and S). We need a relatively high sampling frequency of seismograms (100 Hz), seismic station position and crustal model used in calculation.

We could solve inverse problem with four parameters which is linear in origin time and non-linear in other three parameters (space coordinates). Methods for solving this non-linear problem are divided to two groups:

a) Global solving: they search in whole parameter space (i.e., Monte Carlo methods, genetic algorithms, neighborhood algorithm, grid search).

b) Local solving: we search around some expected solution (zero approximation); linear approximation and the least-squares solution is common.

Let us mention the two common location programs - HYPPODD for relative location (Waldhauser and Elsworth, 2000), and NonLinLoc for absolute location (Lomax, http://alomax.net/nlloc).

1.1.1. Moment tensor

Currently in seismology, the moment tensor – symetric 3x3 tensor (MT) – is a common paremeter of earthquakes and it is routinely used in everyday practice. The MT solutions are usual product of seismic networks across the globe (i.e., Dziewonski et al., 1981; Bernardi et al. 2004; Pondrelli et al. 2006; Clinton et al., 2006).

MT and earthquake source mechanism are connected, so, we can obtain information not only about fault plane orientation and movements on it, but we can get knowledge for example about tectonic settings and understand rupture nucleation and crack opening (Šílený et al., 2004).

Standard representation of MT is beach ball. It is used to display orientation of the fault, direction of slip and stress orientation in the focus of a particular event. (Tension axis-T stands for minimum compressive stress direction, presure axis-P represents maximum compressive stress direction.) Other parameters like strike, dip, rake are, and their relation to MT is mentioned in Chapter 4 of Aki and Richards, (2002), and Brillinger et al. (1980).

Let us focus on centroid moment tensor in this work, because we calculate our solutions as a representation of major slip, not in hypocentre where the rupture propagation starts. Information about method, how to recognize which nodal plane on beachball represents faul-plane and the related relationship between hypocentre and centroid is written in Zahradník, Gallovič et al. (2008).

According to the Dahm and Krüger (2014) we can imagine MT as shown in Figure 1.1. Moment tensor could be written in many types of coordinate systems. Most common are local geographic coordinate system (NED) i.e. the Cartesian system where the first coordinate x is positive from south to north, second y is positive from west to east and the last z downward. The widely used is also local r, Θ, Φ system (USE) with coordinates positive upward, southward and eastward, respectively. The next systems are for example ENU (Jost and Herrmann, 1989) and NWU (Lay and Wallace, 1995). To avoid misinterpretation of components of MT

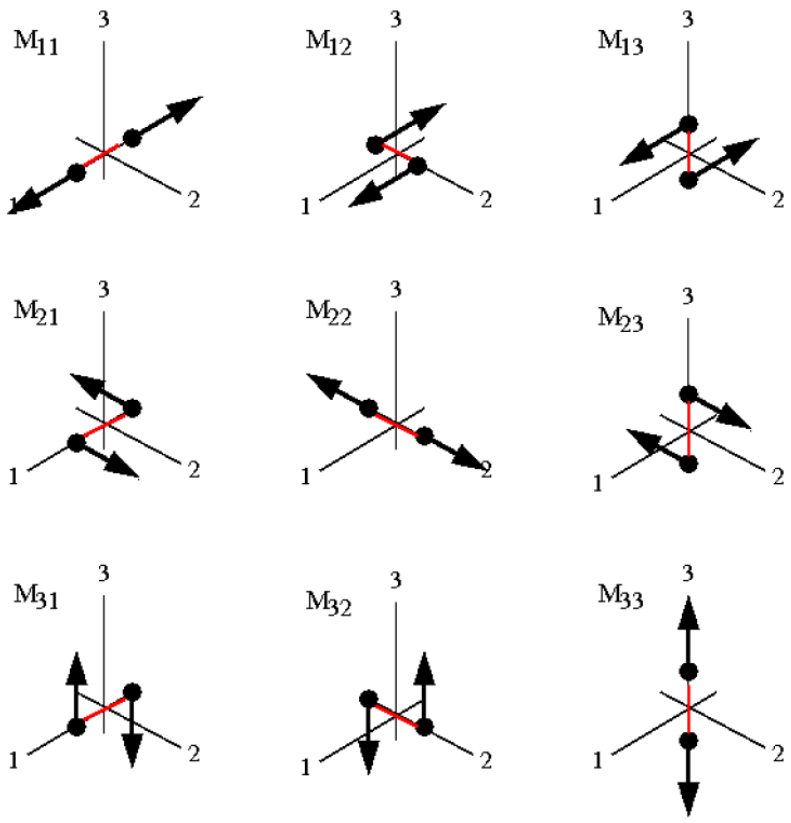

Figure 1.1. (Dahm and Krüger, 2014) The system fo force couples representing the components of a Cartesian moment tensor. Diagonal elements of the moment tensor represent linear vector dipoles, while offdiagonal elements represent force couples with moment.

and fault directions it should be mention which coordinate system is used during calculations. For example we show simple relation between NED and USE system:

$$\begin{aligned} M_{xx} &= M_{\Theta\Theta} & M_{xy} &= -M_{\Theta\Phi} \\ M_{yy} &= M_{\Phi\Phi} & M_{xz} &= M_{r\Theta} \\ M_{zz} &= M_{rr} & M_{yz} &= -M_{r\Phi} \end{aligned} \quad . \tag{1.1}$$

The full MT could be decomposet – mathematically unique – into its deviatoric (DEV) and isotropic = volumetric (ISO = VOL) part:

$$\mathbf{M} = \mathbf{M}_{\mathrm{DEV}} + \mathbf{M}_{\mathrm{ISO}}. \tag{1.2}$$

DEV part can be further decomposed. Variety of shemes exist there (Jost and Herrmann, 1989; Julian et al., 1998). Ussually $\mathbf{M}_{\mathrm{DEV}}$ is decomposed as follows:

$$\mathbf{M}_{\mathrm{DEV}} = \mathbf{M}_{\mathrm{DC}} + \mathbf{M}_{\mathrm{CLVD}}\ , \tag{1.3}$$

where DC stands for larges possible double couple and CLVD is remainder component, the so-called compensated linear vector dipole. CLVD together with ISO represents non-DC part of MT.

As Tape (2016) write, there are three different basic conventions for ISO, DC, and CLVD: Dreger et al. (2000), Vavryčuk (2001), and Chapman and Leaney (2012). We commonly use MT decomposition described in Vavryčuk (2001).

The most stable part of MT is DC, and this stability could persist even if there is noise in data or when the crustal structure is not well known (Jechumtálová and Šílený, 1998, 2001). Some earthquakes which appear to be non-DC could be in fact a superposition of two DC events which are close one to each other in time and space.

1.1.2. Scalar seismic moment

Scalar seismic moment $\mathbf{M_0}$ is defined (Silver and Jordan, 1982) as:

$$M_0 = \sqrt{\frac{\sum_{p=1}^{3}\sum_{q=1}^{3}(M_{pq})^2}{2}}\,. \tag{1.4}$$

Basically this is the Euclidian norm of the MT.

1.1.3. Magnitude

The magnitude (M) represents relative size of an earthquake. This concept was proposed by Richter (1935). According to this fact we could divide earthquakes to three categories: weak $M \leq 4.0$, moderate $4.0 < M < 6.0$, strong $M \geq 6.0$. There are defined a few scales (i.e., local magnitude, surface-wave magnitude, body-wave magnitude) but in this work, we use only moment magnitude M_w which is calculated from the scalar moment M_0 (in Nm).

$$M_w = \frac{2}{3}\log(M_0) - 6.06 \tag{1.5}$$

1.2. Essentials for calculations

In this work, we use broadband data from regional seismic network, so, all calculation was made in Cartesian geometry. Recalculation on the sphere or using earth flattening is beyond the scope of this problem. For more information see i.e., Arfken (1985), Moon and Spencer (1988).

The MT is main result for us and its calculation stands on evaluation of conditionality of normal equations system in least squares method. Calculations on real data as well as extensive synthetic tests were made.

The MT full waveform inversion was performed using ISOLA – from ISOLated Asperities – software (Sokos and Zahradník, 2008, 2013) and with its modifications. Many other codes also exist, e.g., TDMT_INVC software package – from Time-Domain Moment Tensor INVerse Code – (Dreger, 2002) and Kiwi tolls (Heimann, 2011; Cesca et al., 2010).

1.2.1. Crustal model

Nowadays many crustal models are obtained from travel-time studies, including 3D tomography, from dispersion curves or borehole experiments. We do not use elaborate gradient velocity models or 3D models, because we try to simplify our calculations.

One of the inputs to ISOLA software is crustal model. It is 1D layered structural model where we define number of layers, and in each layer: top depth of layer, constant velocity of P-waves and S-waves, density, quality factors for P-waves and S-waves. More information about suitable models is in Chapter 2.3.

1.2.2. Seismic stations and the use of seismograms

As written above broadband records were used. All our data has three components (north-south = NS, east-west = EW, vertical = Z), we obtain them in SEED (The Standard for the Exchange of Earthquake Data) format and then convert them to SAC (Seismic Analysis Code) which can be used in ISOLA software. In fact, the SEED format is well described in Incorporated Research Institutions for Seismology (IRIS, http://www.iris.edu/hq/), it is intended primarily for the archival and exchange of seismological time series data and related metadata and documented in the SEED Manual (2012) and in Tutorial (Ringler and Evans, 2015). This data format is not made for data processing and is commonly converted to other formats. This is the format defined by the Federation of Digital Seismographic Networks (FDSN) to represent seismic data. We use rdseed software (http://ds.iris.edu/ds/nodes/dmc/software/downloads/rdseed/) to make SAC files. SAC formatted data contains a single, continuous segment of time-series data with its identification (i.e., network, station, start time, channel, sample rate) and it is documented in the SAC Manual (2014).

At first, we provide information about event like origin time, location, magnitude, time length of seismograms. Then we clarify these parameters during calculations. (So, the number of tested positions of source and approximate origin time must be defined before calculations.) We set coordinates of stations and their names that we use during inversion. For more information about stations you can use registry at International Seismological Centre (ISC) web pages (http://www.isc.ac.uk/registries/search/).

From records, we use only components without disturbances and with good signal to noise ratio. That could be checked in ISOLA software or SeisGram2K from A. Lomax might be used (http://alomax.free.fr/seisgram/SeisGram2K.html).

1.2.3. Point source approximation

According to Dahlen and Tromp (1998) or Aki and Richards (2002) we consider a point source of seismic waves of a given position and origin time:

$$u_i(t) = \sum_{p=1}^{3}\sum_{q=1}^{3} M_{pq} * G_{ip,q}, \tag{1.6}$$

where displacement **u** is expressed by means of MT **M** and spatial derivatives of Green's tensor **G**; $*$ stands for temporal convolution and comma represent space derivative, p and q denote three Cartesian coordinates.

The NED coordinate system was used in this work.

1.2.4. Green's function

For solving linear partial differential equations, we use Green's functions (Green, 1828). Basically, it is impulse response of source in inhomogeneous media. As it is well described in Aki and Richards (2002), realistic source models are derived from the displacement by the unidirectional unit impulse, which is localized precisely in both space and time. Green's function is second degree tensor and depends on both receiver and source coordinates:

$$\rho \frac{\partial^2}{\partial t^2} G_{in} = \delta_{in} \delta(x-\xi)\delta(t-\tau) + \frac{\partial}{\partial x_j}\left(c_{ijkl} \frac{\partial}{\partial x_l} G_{kn} \right), \tag{1.7}$$

where unit impulse is applied at $\mathbf{x} = \xi$ and $t = \tau$ in the n-direction, than we denote the *i*th component of displacement at general ($\mathbf{x}$, t) by $G_{in}(\mathbf{x}, t; \xi, \tau)$.

For the strong events which were recorded on teleseismic distances, the MT calculation is relatively straightforward, because waves in P and S groups could be described by Green's function in ray approximation (Kikuchi and Kanamori, 1991). For moderate earthquakes which are registered at regional (or local) stations, computing of MT is more complicated due to stronger interferential effects in crust (i.e., L_g waves; Kulhánek, 1990), that's why Green's functions for full waveform field are calculated (Bouchon, 1981).

1.2.5. Elementary mechanisms

The MT is symmetric and it can be expressed in the form of a linear combination of six elementary (dimensionless) tensors $\mathbf{M}^i$:

$$M_{pq} = \sum_{i=1}^{6} a_i M^i_{pq} \,. \tag{1.8}$$

It represents a convenient parametrization because in this way the source is characterized by six scalar coefficients a_i.

These elementary tensors are implemented in the discrete-wavenumber code AXITRA (Bouchon, 1981; Countant, 1989). The other methodic aspects are similar like in Kikuchi and Kanamori (1991), but elementary MTs in that article differ from ours.

$$M^1 = \begin{pmatrix} 0 & 1 & 0 \\ 1 & 0 & 0 \\ 0 & 0 & 0 \end{pmatrix} \quad M^2 = \begin{pmatrix} 0 & 0 & 1 \\ 0 & 0 & 0 \\ 1 & 0 & 0 \end{pmatrix} \quad M^3 = \begin{pmatrix} 0 & 0 & 0 \\ 0 & 0 & -1 \\ 0 & -1 & 0 \end{pmatrix}$$

$$M^4 = \begin{pmatrix} -1 & 0 & 0 \\ 0 & 0 & 0 \\ 0 & 0 & 1 \end{pmatrix} \quad M^5 = \begin{pmatrix} 0 & 0 & 0 \\ 0 & -1 & 0 \\ 0 & 0 & 1 \end{pmatrix} \quad M^6 = \begin{pmatrix} 1 & 0 & 0 \\ 0 & 1 & 0 \\ 0 & 0 & 1 \end{pmatrix}. \tag{1.9}$$

The $\mathbf{M}^1$ – $\mathbf{M}^5$ tensors represent five DC focal mechanisms, whereas $\mathbf{M}^6$ is purely ISO source.

This elementary MT are shown in the Figure 1.2. The six elementary tensors used here to aid the MT inverson should not be confused with various tensors used to decompose the MT for purposes of its physical interpretation, for example, to

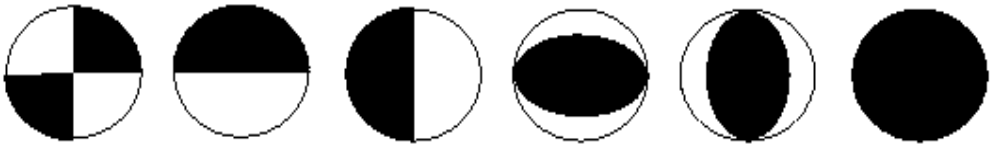

Figure 1.2. Elementary mechanisms which are related to equation (1.9).

decompose into the isotropic part and three DC tensors (e.g., Julian, 1998, Jost and Herrmann, 1989).

The *a*-coefficients in equarion (1.8) are related to **M** as:

$$M = \begin{pmatrix} -a_4 + a_6 & a_1 & a_2 \\ a_1 & -a_5 + a_6 & -a_3 \\ a_2 & -a_3 & a_4 + a_5 + a_6 \end{pmatrix}. \tag{1.10}$$

The moment trace is related with just a single *a*-coefficient:

$$a_6 = \frac{tr(M)}{3}. \tag{1.11}$$

1.2.6. Moment tensor inversion

Moment tensor inversion belongs to the standard inverse problems. Theory of inverse issues is well written in Tarantola (2005).

Combining (1.6) and (1.8) we get

$$u_i(t) = \sum_p \sum_q (\sum_{j=1}^{6} a_j M_{pq}^j) * G_{ip,q}\,, \tag{1.12}$$

and then

$$u_i(t) = \sum_j^6 a_j (\sum_p \sum_q M_{pq}^j * G_{ip,q}) = \sum_{j=1}^6 a_j E_i^j(t)\,, \tag{1.13}$$

where $\mathbf{E}^j$ denotes the *j*th elementary seismogram corresponding to the *j*th elementary moment tensor and **G** is Green's tensor.

If displacement **u** and elementary seismograms are known than inverse problem for *a*-coefficients can be solved. That is formally overdetermined problem becauce number of data (u_i) is much bigger than number of parameters (a_j).

Here we assume that the moment temporal function is known, and it has the form of a step function, which is a good approximation at frequencies below the corner frequency of the event. In matrix notation

$$\mathbf{u} = \mathbf{E}\mathbf{a}\,. \tag{1.14}$$

This linear inverse problem for **a** can be solved by the least-squares method. That could be written like system of equation

$$\mathbf{E^T}\,\mathbf{u} = \mathbf{E^T}\,\mathbf{E}\,\mathbf{a}\,, \tag{1.15}$$

with solution

$$\mathbf{a_{opt}} = (\mathbf{E^T E})^{-1}\mathbf{E^T u}\,, \tag{1.16}$$

where superscripts T and -1 stands for matrix transposition and inversion respectively.

If the centroid position and time belong to the unknown parameters, they are sought through a spatiotemporal grid search in vicinity of a previously estimated position, and (together with **M**) they collectively represent the CMT (centroid moment tensor) solution. In other words, we still solve linear problem (1.14) for **a** but do so repeatedly with different **E**.

The grid search maximizes the correlation between the observed (**u**) and synthetic (**s**) seismograms

$$Corr = \frac{\int us}{\sqrt{\int u^2 s^2}}, \tag{1.17}$$

where

$$\int us = \sum_i \int u_i(t) s_i(t) dt \tag{1.18}$$

and summation is over components and stations.

The match between real and best-fitting seismograms is measured by the L2-norm misfit

$$misfit = \int (u - s)^2 \tag{1.19}$$

and/or by means of the global variance reduction (VR):

$$VR = 1 - \frac{misfit}{\int u^2} = 1 - \frac{\int (u - s)^2}{\int u^2} = Corr^2 . \tag{1.20}$$

Let us mention the fact that if synthetics *s* are found by the least-squares misfit minimization of $\int(u\text{-}s)^2$, then $\int us = \int ss$ (see, e.g., equations 1-6 of Kikuchi and Kanamori, 1991).

2. Basic information for chosen earthquakes

2.1. Main information about selected areas in Greece

Greece is in general one from most seismically active areas in Europe. Its official name is the Hellenic Republic. It covers an area of almost 132,000 km^2 and about 11 million inhabitants live there. The capital city is Athens. The mountains cover about 80% percent of land; so, the Greece is one from the most mountainous state in Europe. (See Hellenic Statistical Authority – ELSTAT, http://www.statistics.gr/en/home.) Greek has more than 1,000 islands (about 6,000 if we defined the smallest parts of land like isles; around 225 of these islands are inhabited). The time zone is UTC + 2 hours. Greece is divided into 13 regions plus there is one autonomous area. We would like to focus on two of them: Crete and South Aegean. From the past, we could mention our interest in Movri Mountain earthquake in Western Greece region (Gallovič et al., 2009).

Our areas of interest are earthquakes with possible nonzero isotropic component. Shallow events located not only on tectonic faults were chosen. There are 8 volcanoes on the Aegean Sea islands (Kos, Methana, Milos, Nisyros, Poros, Santorini (Columbo), Santorini (Nea Kameni), and Yali). We focused on south-central Aegean region not far from Columbo volcano. The tectonic settings and stress field characteristics of this area are well described and depicted in Karagianni et al. (2005).

A moderate earthquake swarm started on 26 June 2009 northeast of the Santorini (Thira) Island, close to Mt. Columbo, an active submarine volcano in the Cyclades, Aegean Sea. The swarm occurred at the western boundary of the Santorini–Amorgos zone, a major structural unit in the Hellenic volcanic arc, where the strongest instrumentally recorded event occurred on 9 July 1956 (reported M_w ranging from 7.5 to 7.8), producing a great tsunami (e.g., Ambraseys, 1960; Galanopoulos, 1960; Papazachos and Papazachou, 2003; Okal et al., 2009; Konstantinou, 2010). The region around the Columbo volcano features strong temporal variations of shallow (< 10 km) seismic activity on a high background level, interpreted as due to magma and fluid migrations (Bohnhoff et al., 2006). Dimitriadis et al. (2009) complemented the analysis of the Columbo volcano activity by joint relocation and inversion of the upper crustal structure; focal mechanisms of 20 small events were reported, proving a prevailing normal-faulting pattern with a northwest-southeast extension at shallow depths (6-9 km).

We investigate also shallow event of the south-central Aegean region: the 27 January 2012 M_w 5.3 Cretan Sea earthquake, the strongest event of the January 2012 earthquake sequence in Cretan Sea.

MT solutions for the events are also available online; for their preliminary agency reports, we refer to the European-Mediterranean Seismological Centre (EMSC) web pages (www.emsc-csem.org/).

Broadband waveforms were retrieved from the permanent stations of the Hellenic Unified Seismic Network (HUSN), operated jointly by the National Observatory of Athens (NOA, doi:10.7914/SN/HL), the Aristotle University of Thessaloniki (AUTH, doi:10.7914/SN/HT), the University of Patras (UPSL, doi:10.7914/SN/HP), and the University of Athens (UOA). The records from one station of the National Seismic Network of Turkey (DDA) were also used. A few UPSL stations are co-operated by the Charles University.

The selection of the events is motivated by the following:

1. events were well recorded by broadband instruments of a reasonable azimuthal coverage;
2. they occurred at a region where tectonic and volcanic events occur, making them candidates for possibly large ISO components;
3. the previous analyses have revealed that the events may have a quite different ISO content, in particular a large ISO during the strongest event of Santorini earthquake swarm.

Although we basically focus on synthetics tests, we start with real data because in the synthetics tests we will use the same source-station configuration.

2.2. Brief review of related calculations

One of possible physical models of the full-MT source, including the ISO, DC, and CLVD components, is the tensile earthquake model, in which the slip vector is generally nonparallel with the fault plane (Vavryčuk, 2011). Full moment tensor can be combined with an additional nontectonic isotropic component (Dufumier and Rivera, 1997).

Significant isotropic components may occur, for example, during man-made explosions, volcanic events, seismic events related to migration of fluids, and gas or rupture on non-planar faults. As certain types of these events may have a very long duration, the inversion of the MT temporal variation is also important (Auger et al., 2006; Yang and Bonner, 2009). The temporal variations of the isotropic and shear components of the source may be different (e.g., Davi et al., 2010). Vavryčuk and Kuhn (2012) developed a new method to retrieve the time function and analyze the stability of the isotropic component as a function of a random noise in waveform amplitudes and temporal shifts.

From the published research so far, it is indicated that moment tensors calculated for volcanic events do not necessarily involve an isotropic component. Tkalčić et al. (2009), who also provide a thorough literature review on non-DC earthquakes, used a sensitivity test in which they systematically decreased the number of stations down to a single one. Their test revealed no isotropic change for a M_w 5 volcanic earthquake. Dreger et al. (2000) found significant isotropic

components for two M_w 4.6 and 4.9 earthquakes in the Long Valley caldera, possibly related to hydrothermal or magmatic processes; however, a comprehensive stability testing of the MT inversion for 33 events with $M_w > 3.5$ in the same volcanic region, made by Templeton and Dreger (2006), showed that 28 of them are best characterized by a pure double-couple model.

Here, we focus on shallow earthquakes, but studies of isotropic component (Kawakatsu, 1996) or non-DC components (Vavryčuk, 2004) for deep earthquakes are available. Earthquake swarms often include non-DC events. For example, in West Bohemia (Czech Republic), the non-DC components could be caused by fluid injection (Horálek et al., 2002), and several earthquakes in that region can be classified as tensile earthquakes (Vavryčuk, 2011). Earthquakes with noticeable compensated linear vector dipole (CLVD) or ISO components could be observed during borehole experiments. Vavryčuk et al. (2008) discovered two main types of these events. One type looked like a response to injection, while the other could relate to anisotropy of rocks.

Full-MT calculation provides a pathway to understand the fracturing process (Song and Toksöz, 2011), and how to differentiate natural from induced seismicity (Ford et al., 2009; Cesca et al., 2013). The full-MT inversion is useful in the studies of nuclear explosions (Minson and Dreger, 2008). Non-DC components can be substantial during volcanic earthquakes, for example, Long Valley caldera in California (Foulger et al., 2004; Templeton and Dreger, 2006). Among several types of non-DC volcanic events, it is worth mentioning the case of vertical-CLVD earthquakes (Shuler et al., 2013), or earthquakes with large CLVD component but missing the ISO component (Tkalčić et al., 2009). Recently, Mustać and Tkalčić (2016) used a nonlinear Bayesian inversion in which noise represents a free parameter and is implemented via empirical covariance matrix.

2.3. Crustal models for Greece, seismic stations and insight to moment tensor inversion

2.3.1. Crustal velocity models for Greece

Since the beginning of the twentieth century the earth velocity models were used. Summary of global Earth models (1-D and also 3-D) is accurately performed in Bormann (2012).

The most common models for Greece are i.e., Haslinger et al. (1999), Latorre et al. (2004), Rigo et al. (1996), and Karagianni et al. (2005). Model "M1" (Tselentis et al, 1996) is occasionally used for locations. 1-D regional crustal models Novotný et al. (2001), and Dimitriadis et al. (2010) were used for moment tensor inversion in this thesis. Summary of these two models is in Table 2.1. and in the Figure 2.1. The model by Novotný et al. (2001) was obtained from the regional surface-wave dispersion, in which *Lg* waves dominate, and it is routinely used for MT inversions at AUTH; and the model by Dimitriadis et al. (2010) based on local first-arrival times. The attenuation quality factors (Q_p, Q_s) reported in the Table 2.1. represent rough

Table 2.1.: Crustal models used in inversion

Model	Layer top (km)	v_p (km/s)	v_s (km/s)	ρ (g/cm^3)	Q_p	Q_s
Novotný	0.	2.3	1.292	2.16	300	300
et al. (2001)	1.	4.3	2.416	2.56	300	300
	2.	5.5	3.090	2.80	300	300
	5.	6.2	3.483	2.94	300	300
	16.	6.4	3.596	2.98	300	300
	33.	8.3	4.663	3.36	1000	1000
Dimitriadis	0.	4.85	2.74	2.67	300	150
et al. (2010)	1.	5.03	2.84	2.71	300	150
	3.	5.52	3.12	2.80	300	150
	5.	5.69	3.21	2.84	300	150
	7.	6.31	3.56	2.96	300	150
	9.	6.16	3.48	2.93	300	150
	11.	6.23	3.52	2.95	300	150
	13.	6.27	3.54	2.96	300	150
	17.	6.17	3.48	2.93	300	150
	19.	6.32	3.57	2.96	300	150
	21.	7.02	3.96	3.10	300	150
	23.	7.46	4.21	3.19	300	150
	25.	7.52	4.25	3.20	300	150
	30.	7.56	4.27	3.21	1000	500

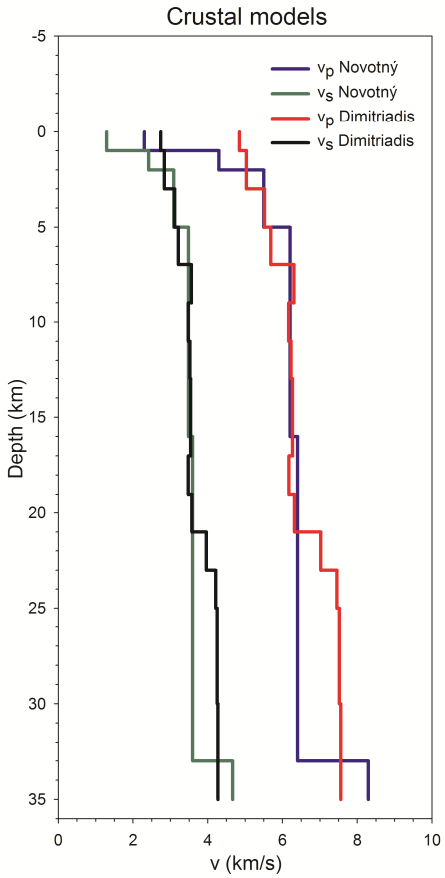

Figure 2.1. 1-D Crustal models Novotný et al. (2001) and Dimitriadis et al. (2010) used in inversion.

estimates; density ρ (g/cm^3) is calculated using simple formula:

$$\rho(g/cm^3) = 1.7 + 0.2\ v_p(km/s); \qquad (2.1)$$

the waveform inversion is almost insensitive to their particular values in the studied range of epicentral distances and frequencies.

Here the Green's functions are calculated in 1D velocity models by the discrete wavenumber method (Bouchon, 1981), including near-field terms.

2.3.2. Seismic stations used

Twenty stations were used during calculations. Their position is shown in the Figure 2.2. and brief information are summarized in the Table 2.2. Data for the table are taken from http://www.isc.ac.uk/registries/search/. The records from the broadband seismographs are used, so, instrumental corrections of data were made. Stations Nisiros Isl. and Nisiros are on the same island, so, they are shown very close one to the other in the map.

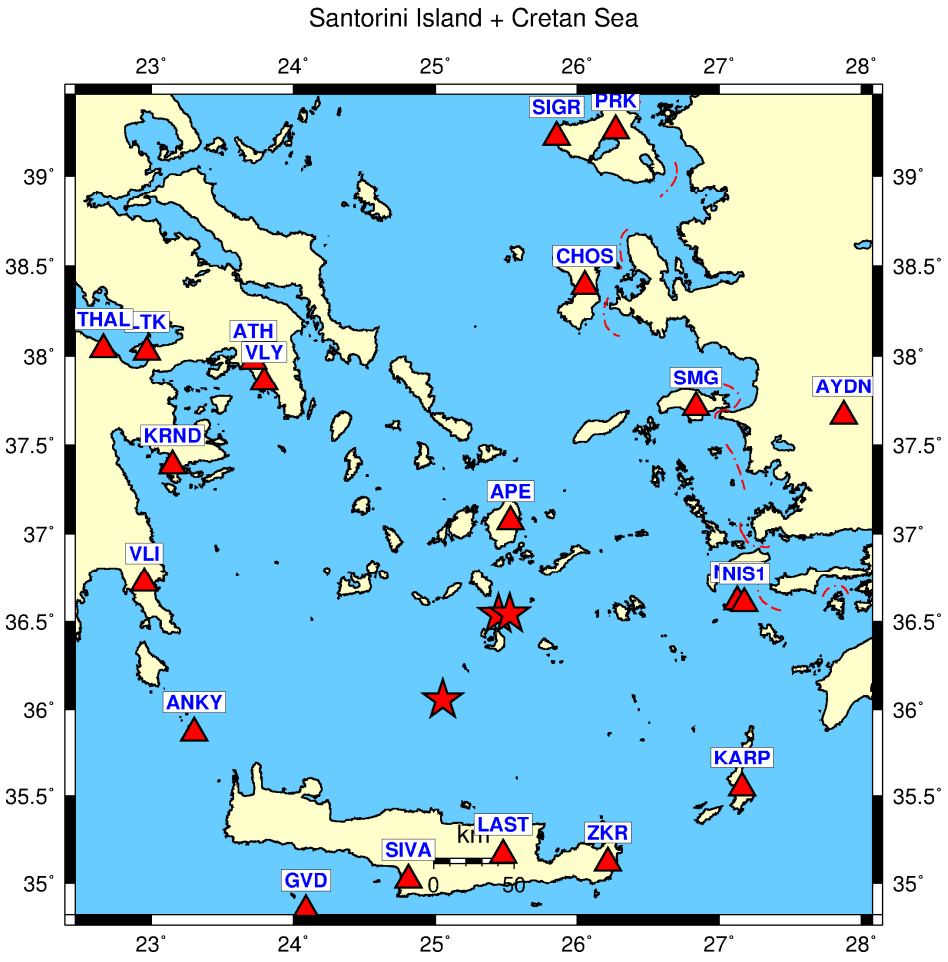

Figure 2.2. Broadband seismic stations (triangles) used in calculations for papers Křížová et al. (2013) and Křížová et al. (2016). Epicenters for selected events are marked with asterisks.

Table 2.2.: Stations used in MT inversions

Station Code	Name	Latitude (°)	Longitude (°)	Elevation (m)	Utilization *
ANKY	Antikythira Island	35.86703	23.30117	143.0	S1, Cre
APE	Apeiranthos	37.06890	25.53060	620.0	S1, S2, Cre
ATH	Athens Observatory	37.97220	23.71670	95.0	S1, S2
AYDN	Tasoluk	37.66080	27.87920	716.0	S1
CHOS	Chios island	38.38680	26.05500	842.0	S1, S2, Cre
GVD	Gavdhos	34.83911	24.08736	180.0	Cre
KARP	Karpathos	35.54717	27.16117	528.0	S1, S2, Cre
KRND	KRANIDI	37.38300	23.15020	140.0	Cre
LAST	Lasithi	35.16111	25.47861	870.0	S1, S2
LTK	Loutraki	38.02300	22.96700	410.0	S1, S2
NIS1	Nisiros Isl.	36.60230	27.17820	378.0	S1
NISR	Nisiros	36.61167	27.12833	48.0	Cre
PRK	Paraskevi	39.24610	26.27170	100.0	S1, S2
SIGR	SIGRI	39.21140	25.85530	83.0	S1, S2
SIVA	Sivas	35.01750	24.81000	95.0	S1, Cre
SMG	Samos	37.70867	26.83700	340.0	Cre
THAL	Thalero	38.03720	22.66310	129.0	S1
VLI	Veliai	36.71820	22.93700	220.0	S1, S2, Cre
VLY	Voula, Athens	37.85240	23.79420	256.0	Cre
ZKR	Zakros	35.11469	26.21700	270.0	S1, S2, Cre

*... S1 Santorini Island earthquake – strongest event; 15 station used, and synthetic tests B, C
S2 Santorini Island earthquake – strongest event; 10 station used, and Santorini Island earthquake – weaker event
Cre Cretan sea earthquake and synthetic test A

2.3.3. Insight to moment tensor inversion

The MT inversion was performed using ISOLA software (Sokos and Zahradník, 2008). ISOLA (from ISOLated Asperities) is a program package based on the multiple point-source iterative deconvolution of complete regional waveforms. This is based on method from Kikuchi and Kanamori (1991). Green's functions are calculated by the discrete-wavenumber method (Bouchon, 1981; AXITRA code of Coutant, 1989). The moment tensor is solved by the least-squares method, and the origin time and 3D position of the point source (centroid) are both grid searched, the latter in the vicinity of the (independently) located hypocenter. (The correlation between real = observed and synthetic seismograms – eq. 1.17 – is maximized. In the preliminary stage, we considered variations of the centroid position both in the horizontal direction and depth. In the following discussions, for simplicity, we concentrate only on grid searching the centroid depth (Křížová et al., 2013; 2016). The method is routinely used in the Seismological Laboratory of the University of Patras to calculate moment tensors in western Greece. From the other users Cambaz and Mutlu (2016) should be mentioned. ISOLA also proved useful in a number of earthquake studies (e.g., Zahradník, Jánský, et al., 2008; Gallovič et al., 2009; Zahradník and Gallovič, 2010). Currently ISOLA became one of standard software for MT calculation and it is widely used (i.e., Hicks and Rietbrock, 2015). Here we use a single point-source approximation. The additional condition on DC mechanism could be used (Henry et al., 2002). The noisy components at a few stations were

excluded from the inversion. Each event is characterized by its strike, dip, rake, centroid depth, scalar moment M_0, moment magnitude M_w, the percentages of ISO, DC, and abs(CLVD), the global VR.

2.4. Santorini Island earthquakes

We investigate two strongest events ($M_w > 4$) of moderate earthquake swarm which started on 26 June 2009 close to an active submarine volcano in Aegean Sea. The sequence was rich in earthquakes, with about 25 events with M_w larger than 2.5 within the first five days. The earthquakes were recorded with a good azimuthal coverage at epicentral distances approximately from 60 to 310 km. We use the records from 15 and 10 stations of events 1 and 2, respectively. The seismograms which provided a good signal-to-noise ratio even at relatively low frequencies (0.02-0.1 Hz) were chosen.

The stability of the MT solution was further examined by jackknifing the data (i.e., systematically removing one station from the inverted data set). The results are summarized in Supplementary material.

As has been said, all calculations were provided in two crustal models: model N - Novotný et al. (2001) and model D - Dimitriadis et al. (2010). Full MT, deviatoric MT, and DC-constrained MT were calculated. Basic informations and results are summarized in the Table 3 in Křížová et al. (2013).

2.4.1. Strongest event – Santorini earthquake

We made calculations with records from all 15 available stations and also using only 10 stations which are accessible for weaker event (the second strongest Santorini Island earthquake); see Table 2.2. This earthquake M_w 4.9 occurred 26 June 2009 at 20:37:38.10 UTC and it was located in the depth 9.7 km at position: 36.531°N; 25.434°E.

Some station components were excluded due to low signal to noise ratio. In the Table 2.3. there is the list of used components.

In the first step, we search MT solution under epicenter (located by the Aristotle University of Thessaloniki, Department of Geophysics) with the depth step 0.5 km. Then we try to find better solution in the area close to previous result, so, 3D grid search was made. Then we use coordinates from new centroid position for further calculations. The results for specified position are in Table 3 in Křížová et al. (2013) where new position for model N is: 36.5400 °N; 25.4452°E, and for model D is: 36.5490 °N; 25.4563 °E. For simplicity and to avoid misinterpretation in synthetic tests (especially in the test C) in Křížová et al. (2016) only one geographical position – same as for model N in previous article – during calculations was used. The results for deviatoric MT and full MT calculations below epicenter are summarized in the Table 2.4. and in the Figure 2.3. Note that results mentioned in the Table 3 in Křížová et al. (2013) and in the Table 3 in Křížová et al. (2016) slightly differ one from the each other because in the first case we use depth step 0.5 km during

Table 2.3.: List of used components for strongest event of Santorini Island earthquake swarm

	Component				Component				Component		
Station Code	NS	EW	Ver.	Station Code	NS	EW	Ver.	Station Code	NS	EW	Ver.
APE	+	+	+	KARP	---	---	+	AYDN	+	---	+
LAST	+	+	+	ANKY	+	---	---	LTK	---	---	+
NIS1	+	+	+	CHOS	+	+	+	THAL	---	---	+
ZKR	+	+	+	ATH	+	+	+	SIGR	+	+	+
SIVA	---	---	+	VLI	+	+	+	PRK	+	+	+

Ver. ... vertical component

In each column are stations sorted by distance (APE ... closest to epicenter, PRK ... furthermost)

Table 2.4.: Solution for MT inversion for strongest event of Santorini Island earthquake swarm

	Model N						Model D					
	Full MT			Dev. MT			Full MT			Dev. MT		
strike; dip; rake (°)	252	68	-59	240	62	-78	248	66	-63	244	65	-76
	13	36	-142	36	29	-111	16	35	-136	34	28	-117
M_w	4.7			4.6			4.7			4.7		
M_0 (Nm)	1.146×10^{16}			9.931×10^{15}			1.328×10^{16}			1.192×10^{16}		
depth (km)	6.5			3.5			6.0			2.5		
Centroid time (s)	20: 37: 37.65			20: 37: 37.65			20: 37: 39.15			20: 37: 39.15		
DC	28.3			70.5			36.1			69.0		
CLVD	16.6			29.5			10.5			31.0		
ISO	55.1			0.0			53.4			0.0		
VR	0.65			0.64			0.68			0.68		

Dev. ... Deviatoric

M_0 ... scalar seismic moment (eq. 1.4)

M_w ... magnitude (eq. 1.5)

VR ... variance reduction (eq. 1.20)

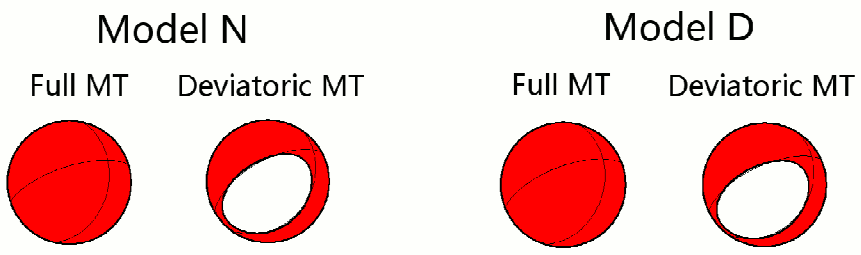

Figure 2.3. MT solutions for strongest event of Santorini Island earthquake swarm.

calculations and 1.0 km in the second case.

2.4.2. Weaker event – Santorini earthquake

The second strongest earthquake M_w 4.7 from the swarm occurred 26 June 2009 at 22:14:53.50 UTC and it was located in the depth 4.1 km at position: 36.544 °N;

25.523°E. Results of MT inversions are summarized in the Table 3 in Křížová et al. (2013).

We made calculations with records from 10 stations. Some station components were excluded due to low signal to noise ratio. In the Table 2.5. there is the list of used components.

As same as for the strongest event of the swarm, in the first step, we search MT solution under epicenter (located by the Aristotle University of Thessaloniki, Department of Geophysics) with the depth step 0.5 km. Then we try to find better solution in the area close to previous result, so, 3D grid search was made. Then we use coordinates from new centroid position for further calculations.

The results for specified position are in Table 3 in Křížová et al. (2013) where new position for both model N and D is: 36.5440 °N; 25.4668°E. The results for deviatoric MT and full MT calculations below epicenter are summarized in the Table 2.6 and in the Figure 2.4.

Table 2.5.: List of used components for the second strongest event of Santorini Island earthquake swarm

	Component				Component		
Station Code	NS	EW	Ver.	Station Code	NS	EW	Ver.
APE	+	+	+	ATH	---	---	+
LAST	+	+	+	VLI	+	+	+
ZKR	+	+	+	LTK	---	---	+
KARP	---	---	+	SIGR	+	+	+
CHOS	+	+	+	PRK	+	+	+

Ver. ... vertical component

In each column are stations sorted by distance (APE ... closest to epicenter, PRK ... furthermost)

Table 2.6.: Solution for MT inversion for the second strongest event of Santorini Island earthquake swarm

	Model N				Model D			
	Full MT			Dev. MT			Full MT			Dev. MT		
strike; dip; rake (°)	265	55	-40	257	50	-57	244	45	-71	244	45	-70
	21	57	-137	31	49	-123	28	47	-108	37	47	-108
M_w	4.4			4.4			4.5			4.5		
M_0 (Nm)	4.467×10^{15}			4.051×10^{15}			5.600×10^{15}			5.327×10^{15}		
depth (km)	6.5			4.5			4.0			4.5		
Centroid time (s)	22: 14: 52.80			22: 14: 52.80			22: 14: 53.80			22: 14: 53.75		
DC	40.5			75.7			78.7			80.4		
CLVD	26.6			24.3			9.6			19.6		
ISO	32.9			0.0			-11.8			0.0		
VR	0.62			0.61			0.65			0.66		

Dev. ... Deviatoric

M_0 ... scalar seismic moment (eq. 1.4)

M_w ... magnitude (eq. 1.5)

VR ... variance reduction (eq. 1.20)

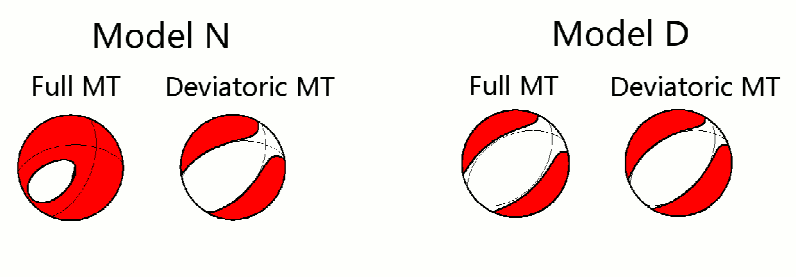

Figure 2.4. MT solutions for the second strongest event of Santorini Island earthquake swarm.

2.5. Cretan Sea earthquake

The earthquake sequence occurred in southwest direction from Santorini Island. The Cretan Sea earthquake is the strongest event of the January 2012 earthquake sequence in Cretan Sea. For this earthquake only crustal model Novotný was used, because hypocenter of this event is in the slightly different place than in case of Santorini Island events and model Dimitriadis seems to be inappropriate.

This earthquake M_w 5.3 occurred 27 January 2012 at 01:33:24.0 UTC and it was located in the depth 10 km at position: 36.044°N; 25.064°E.

We made calculations with records from 12 stations. All station components have quite good signal to noise ratio. In order from closest to furthermore they are: SIVA - APE - ZKR - ANKY - GVD - NISR - KARP - VLI - KRND - VLY - SMG - CHOS.

As same as for the Santorini earthquakes, in the first step, we search MT solution under epicenter (located by the Aristotle University of Thessaloniki, Department of Geophysics), but in this case the depth step 1 km was used. Then we try to find better solution in the area close to previous result, so, 3D grid search was made. Then we use coordinates from new centroid position for further calculations.

The results for specified position are in Table 2 in Křížová et al. (2016) where new position is: 36.056 °N; 25.053°E. The results for deviatoric MT and full MT calculations below epicenter are summarized in the Table 2.7 and in the Figure 2.5.

The stability of the MT solution was further examined by jackknifing the data (i.e., systematically removing one station from the inverted data set). The results are summarized in Supplementary material.

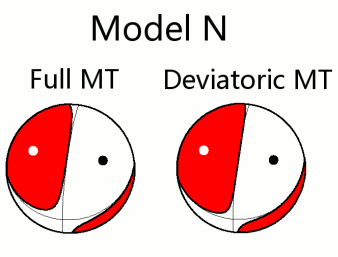

Figure 2.5. MT solutions for the strongest event of Cretan Sea earthquake swarm.

Table 2.7.: Solution for MT inversion for the strongest event of Cretan Sea earthquake swarm

	Full MT	Dev. MT
strike; dip; rake (°)	182 84 -110 82 21 -16	187 84 -110 81 21 -16
M_w	5.4	5.4
M_0 (Nm)	1.247×10^{17}	1.245×10^{17}
depth (km)	7.	7.
Centroid time (s)	01: 33:24.5	01: 33: 24.5
DC	84.3	89.4
CLVD	10.1	10.6
ISO	-5.6	0.0
VR	0.63	0.63

Dev. ... Deviatoric
M_0 ... scalar seismic moment (eq. 1.4)
M_w ... magnitude (eq. 1.5)
VR ... variance reduction (eq. 1.20)

2.6. Synthetic tests

For synthetic tests, we will use the same source-station configuration as for two shallow events of the south-central Aegean region: the 27 January 2012 M_w 5.3 Cretan Sea earthquake and the 26 June 2009 M_w 4.9 Santorini earthquake.

Motivation of the synthetic tests comes from observatory practice. Besides the centroid position and the strike/dip/rake angles, we are often interested in the DC% because this is the simplest parameter characterizing a possible deviation of the earthquake from pure shear faulting. We seek to understand how the obtained DC% depends on the adopted MT-inversion mode.

All tests have a common feature. We calculate synthetic waveforms for an assumed centroid position and for a given full MT. We then invert the synthetic waveforms in either a full-MT or deviatoric-MT mode and we leave the centroid depth and time free. We investigate the effects of the deviatoric constraint on the obtained source parameters (strike/dip/rake, depth, DC%, etc.). Three tests are made (A–C), each one with six subtests (1-6). For simplicity, all models have CLVD% = 0.

Technically, the subtests are created as follows: we choose the strike/dip/rake angles and calculate the *a*-coefficients (eq. 1.10) a_1, ..., a_5, of the deviatoric MT. Then, we create full MTs of several ISO components by choosing appropriate values of the sixth coefficient a_6 (Tables A1 and A2 in Křížová et al., 2016).

The MT-inversion results for synthetic tests A-C including the subtests 1-6 are mentioned in corresponding Tables A3–A5 of Křížová et al. (2016). Several interesting features are discussed in this article mentioned above.

2.6.1. Test A

Test A corresponds to Cretan Sea earthquake. It means the centroid depth and strike/dip/rake angles are same as in real case for full MT (see Table 2 in Křížová et al., 2016). The true depth for this test is 8 km. The subtests differ in their ISO%

(rounded to integer values): ±90, ±46, and ±30. The plus and minus signs correspond to explosion and implosion, respectively. Synthetic data are forward simulated and inverted using the same velocity model (N-model).

2.6.2. Test B

Test B corresponds to Santorini earthquake (the strongest event from swarm). It means the centroid depth and strike/dip/rake angles are same as in real case for full MT in model N (see Table 3 in Křížová et al., 2016). The true depth for this test is 6 km. The subtests differ in their ISO% (rounded to integer values): ±90, ±48, and ±32. Synthetic data are forward simulated and inverted using the same velocity model (N-model).

2.6.3. Test C

Test C corresponds to Santorini earthquake (the strongest event from swarm). It means the centroid depth and strike/dip/rake angles are same as in real case for full MT in model N (see Table 3 in Křížová et al., 2016). The true depth for this test is 6 km. The subtests differ in their ISO% (rounded to integer values): ±90, ±48, and ±32. Test C is more complicated than previous two tests. To illustrate possible effects of inaccurate velocity models, we forward simulate synthetic waveforms in one model (N-model), but invert them in the other (D-model). That is why in Test C, variance reduction (eq. 1.20) is always less than 85%. We could also see difference between "real" ISO values and values obtained from MT calculations (-90 vs -70; +90 vs +75; ±48 vs ±50; ±32 vs ±34).

3. Accuracy of results

The analysis of resolvability and uncertainty of the MT belongs to main part of modern seismology. The focal mechanism (i.e. the strike, dip, rake and scalar moment) is relatively stable with respect to inaccuracies of the routinely available velocity models and also with respect to possible errors in the assumed source positions. Nevertheless, to make the focal mechanism even more reliable, the source (centroid) position and time are in our case jointly inverted with the mechanism. Contrarily to the focal mechanism, the non-DC components of MT (CLVD and ISO) are difficult to determine because they are unstable. It means that they vary a lot with small changes of the velocity model, source-station configuration, and frequency range, among others.

We would like to answer the question if it is necessary always calculate full MT instead of deviatoric MT, while we know that only its strike/dip/rake (and moment) are reliable. Is the percentage of the DC part (hereafter, DC%) well determined if derived from the deviatoric MT? We would like to analyze how the deviatoric constraint affects the MT inversion results such as the DC%, the centroid depth, and the strike/dip/rake angles.

The treatment of the isotropic component in moment tensor inversions and its uncertainty is a significant issue in theoretical seismology, with a variety of approaches proposed to remedy the problem. Vasco (1990) used the method of extremal models to rigorously estimate the bounds of the MT trace. The graphic approach of Riedesel and Jordan (1989) provides the tools to visualize the MT uncertainties and deviations of the MT from a pure DC model. For the inversion schemes that provide families of acceptable solutions (in addition to the best-fitting solution), the family itself is used to experimentally construct the confidence intervals of the source parameters. A representative example is the work of Šílený (1998), who used genetic algorithms to construct probabilistic estimates of the model parameters, including the posterior probability density function of the model parameters. Ford et al. (2010) proposed the network-sensitivity solution. They grid searched the parameter space in terms of the MT invariants, and, using the source-type plots of Hudson et al. (1989), were able to effectively identify the non-DC sources in practice. Panza and Saraò (2000) emphasized the role of synthetic tests in evaluating the reliability of the non-DC components. Nakano et al. (2008) discussed the trade-off between the source position and the non-DC components and recommended to use the DC assumption when determining the source position. Zahradník, Sokos, et al. (2008) emphasized the trade-off between the non-DC components and centroid time.

Full-MT calculation provides a pathway to understand the fracturing process (Song and Toksöz, 2011), and how to differentiate natural from induced seismicity (Ford et al., 2009; Cesca et al., 2013). The full-MT inversion is useful in the studies of nuclear explosions (Minson end Dreger, 2008). Non-DC components can be substantial during volcanic earthquakes, for example, Long Valley caldera in

California (Foulger et al., 2004; Templeton and Dreger, 2006). Among several types of non-DC volcanic events, it is worth mentioning the case of vertical-CLVD earthquakes (Shuler et al., 2013), or earthquakes with large non-DC component but missing the ISO component (Tkalčić et al., 2009). Recently, Mustać and Tkalčić (2016) used a nonlinear Bayesian inversion in which noise represents a free parameter and is implemented via empirical covariance matrix.

In the following text in this chapter we would like to focus on evaluation of results of MT inversion.

3.1. Moment tensor inversion - rating

There exist many methods how to analyze results of MT inversion. Before to concentrate on comparing outcomes we should mention how we try to avoid wrong evaluation of calculations.

In the first step, we select satisfactory data with good signal to noise ratio and without disturbances. Then we try to find a suitable frequency range for full waveform inversion. Chosen seismograms with good, fairly good, and bad signal to noise ratio are shown in the Figure 3.1. as an example. In this thesis, we used band pass filtering defined by four frequencies, it means that the filter has two cosine tapered windows, one on each side, and in the inner interval the filter is constant. For both Santorini events, it is 0.02 – 0.05 – 0.08 – 0.1 Hz and for Cretan Sea earthquake it is 0.03 – 0.05 – 0.08 – 0.1 Hz. It is worth mentioning that this filter is non-causal. Currently, a causal Butterworth filter has been implemented into ISOLA software, which is defined only with two corner frequencies. In both cases (causal or non-causal) the same filter is applied to real and synthetic data. In Figure 3.2 is comparison for the strongest Santorini event, where causal filter is 0.04 – 0.09 Hz. The comparison of results from these calculations is listed below in this chapter. The main uncertainties became from insufficient knowledge of the Greens function, which means crustal model and seismic source position. To reduce crustal model uncertainty, we are trying to use as longest periods as possible.

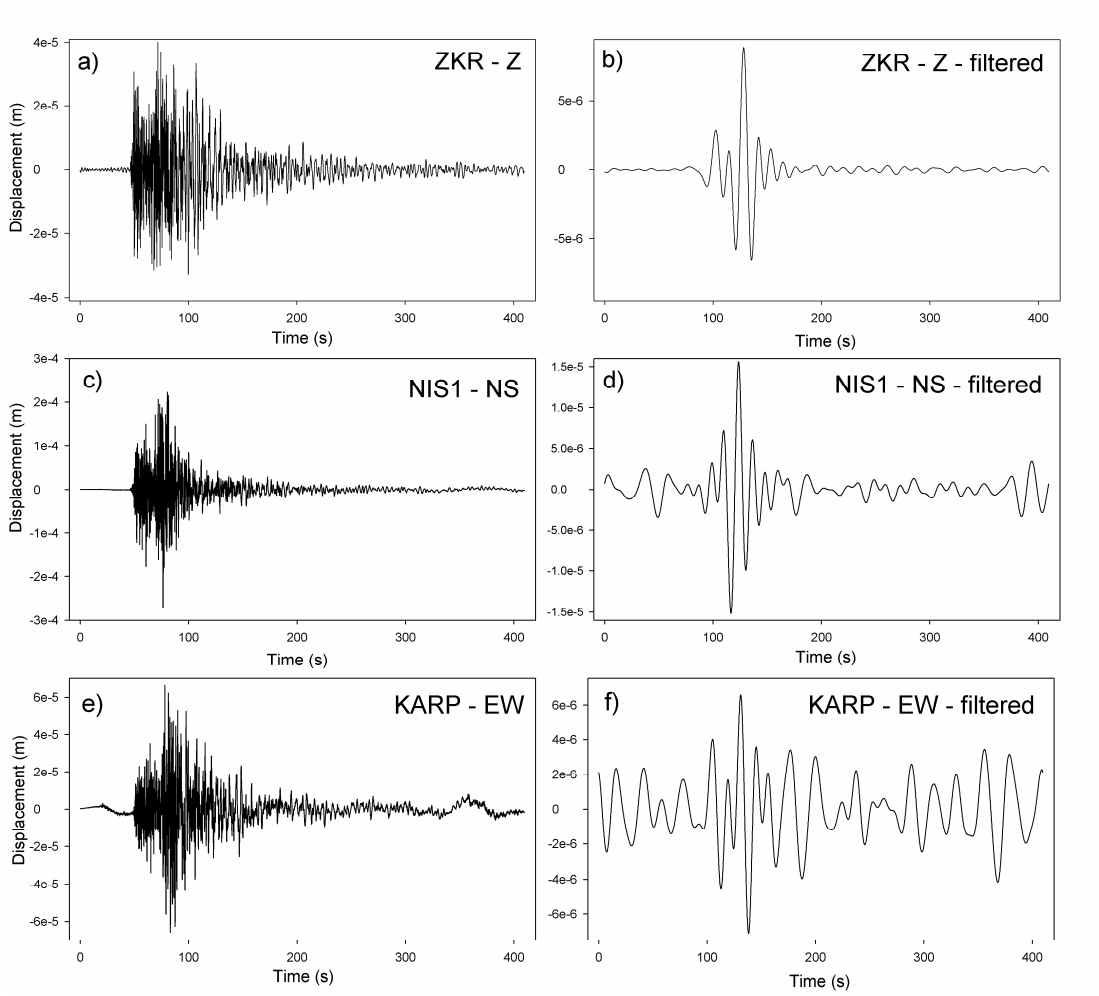

Figure 3.1. Example of seismograms for strongest event of Santorini earthquake swarm. In the first column are data without filtration and in the second column are filtered data. a), b) displacement at station ZKR – Z component with good signal to noise ratio; c), d) displacement at station NIS1 – NS component with fairly good signal to noise ratio; e), f) displacement at station KARP – EW component which was not used during MT calculations.

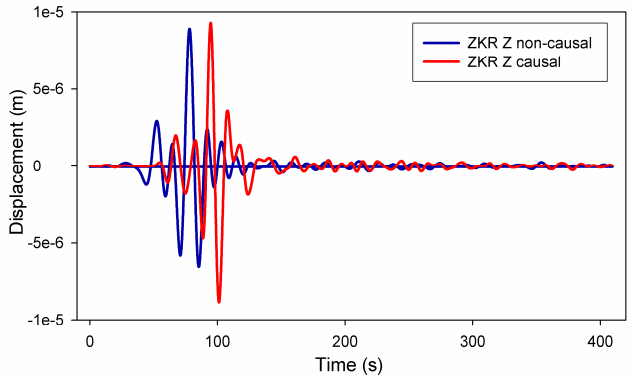

Figure 3.2. Comparison for causal filter (0.04 – 0.09 Hz) and non-causal filter (0.02 – 0.05 – 0.08 – 0.1 Hz) for strongest Santorini event at station ZKR – Z component in full MT inversion.

3.1.1. Conventional methods – results comparison

Correlation and variance reduction

As stated in Chapter 2, we try to maximize correlation between the observed (u) and synthetic (s) seismograms (eq. 1.17). We suppose that the moment rate function is a delta function, which is a good approximation at frequencies below the corner frequency of the event. Then eq. (1.13) can be understood as a linear inverse problem for unknown *a*'s, hence, the unknown moment tensor **M**. The full MT inversion seeks all six *a*'s, while the deviatoric inversion (DEV) assumes a_6=0, therefore only the first five *a*'s are calculated. The synthetics seismograms (s) are in inverse problem searched by the least-squares misfit minimization. Like an optimal source depth (position) and origin time are considered results for which the shape match between observed and synthetic seismograms is the best. The main tool to evaluate results is then correlation and variance reduction (eq. 1.20).

Correlation diagrams

The correlation between observed and synthetic data is depicted as a function of position, which at the same time show appropriate source mechanism for all tested positions. At each position, we plot the best result from the temporal grid search.

Here we analyze whether there is any simple feature in these complex results, at least for some specific values of ISO%. Therefore, we further concentrate on the variation of the waveform correlation with trial source depth, and we will show that indeed the events with a large ISO% may have a specific correlation-depth behavior. As an example, see Figures 7 and 8 of Křížová et al. (2016).

Kagan angle

To measure the angular departure of any two DC solutions, under comparison, we use Kagan angle (Kagan, 1991). The solutions are comparable (quite similar) if the angle is < 10°-20°, and highly dissimilar if the angle is > 40°. For examples, see Zahradník and Custódio (2012).

The Kagan angle is simply the smallest angle you need to rotate the system of PTN (pressure, tension, normal) axes of MT to merge two solutions. In our case, we calculate Kagan angle from strike, dip, rake of two solutions. It is independent of choice which nodal plane from first solution and from second solution is taken. But, because we obtained strike, dip, rake rounded up to integer numbers as our results then the Kagan angle is dependent on choice of nodal plane, fortunately the difference between solutions is relatively small (less than 2°). As an example, we took results of Kagan angle for tables A3 - A5 in Křížová et al (2016) and specify them in the Table 3.1. Let us mention that full MT and deviatoric MT for first subtest B are enormously different (Kagan angle = 88°), also full MT in model D in the second subtest C differ a lot from right solution (Kagan angle = 91°).

Table 3.1.: Kagan angle for synthetic tests

tests	A	B	C-full	C-dev
1aa	57.534	88.108	32.119	46.841
1ab	56.876	87.957	32.292	46.535
1ba	56.722	87.387	32.761	47.437
1bb	56.056	87.242	32.910	47.106
2aa	34.892	29.759	91.652	36.944
2ab	34.500	30.132	91.544	37.653
2ba	36.359	29.723	91.008	37.102
2bb	35.968	30.025	90.923	37.765
3aa	15.118	12.719	2.767	13.401
3ab	15.961	12.468	1.938	13.471
3ba	16.520	13.396	3.631	14.101
3bb	15.823	13.066	2.756	14.057
4aa	11.569	13.464	5.257	13.057
4ab	10.948	13.549	4.739	13.754
4ba	12.735	13.642	5.848	13.152
4bb	12.139	13.597	5.233	13.774
5aa	7.719	6.324	3.270	7.931
5ab	6.902	5.976	3.679	8.377
5ba	8.970	7.189	4.132	8.759
5bb	8.152	6.838	4.335	9.152
6aa	6.841	5.746	5.426	9.374
6ab	6.639	6.529	5.515	9.748
6ba	8.012	5.382	6.188	9.557
6bb	7.692	6.005	6.064	9.810

The letters a,b in subtests 1 - 6 means that we take first (a) or second (b) strike, dip, rake set from Tables A3 - A5 in Křížová et al. (2016) for chosen subtest and then we compare them. The first letter stands for full MT solution and the second for deviatoric one.
For test C (Table A5) stands first letter for corresponding full MT solution for model N (Table A4).
i.e., 5ba for test A means that we compare for the fifth subtest in Table A3 - the second set of strikes, dip, rake for full MT with the first set of strike dip, rake for deviatoric MT.

Condition number

To examine how well or ill posed the inverse problem is we additionally use the condition number CN. The condition number (CN), is defined by

$$CN = \frac{\max\limits_{i=1,\ldots 6}(w_i)}{\min\limits_{i=1,\ldots 6}(w_i)}. \tag{3.1}$$

Here w denotes the singular numbers of the matrix of elementary seismograms. CN is useful in judging, at least in a relative sense, how well or ill posed is the inverse problem; small singular values (large CN) indicate an unstable solution. The w_i are expressed in eq. (3.6) below in this section.

The CN is a relative measure; a larger CN signalizes a worse (less stable) resolvability of MT. Actually, we do not mention value of CN for all results stated in this thesis (some of them are listed in Křížová et al., 2013, 2016), it is not if they are relatively small - less than 5. E.g. some cases of large CN for model D: CN = 16 for full MT inversion - strongest Santorini event for ten stations used during calculations, CN = 6 for full MT inversion - second strongest Santorini event.

Other standard methods for results evaluation

Like a standard stability tests the jackknife tests were performed. This means that we made calculations repeatedly and in each calculation one station was excluded from data set. The results are listed in Supplementary material.

For comparison of moment tensors, we can use also another parameter, μ. According to Pasyanos et al. (1996):

$$\mu = \sqrt{\frac{\sum_{i=1}^{3}\sum_{j=1}^{3}\left(\frac{M_{1ij}}{M_{01}} - \frac{M_{2ij}}{M_{02}}\right)^2}{8}}\ , \tag{3.2}$$

where indices 1, 2 mark the first and the second result respectively. M_{ij} stands for components of MT and M_0 is scalar seismic moment (eq. 1.4). Values of μ range from 0. to 1., where 0. stands for identical solutions and for μ les than 0.25 the results are considered to be highly similar, and good agreement is for μ les than 0.35. In this thesis the Kagan angle is preffered instead of μ for solution comparison.

3.1.2. New approach for results assessment

Now, we would like to focus on isotropic component of MT. Prior to the application using observed data, we performed a number of tests to validate the approach.

Probability density function (pdf)

First, we deal with the linear MT inversion with six parameters (a fixed centroid position and time) and present a theoretical 1D pdf allowing for the simplest estimate of the ISO uncertainty in the 6D parameter space (Zahradník and Custódio, 2012). Then we propose an extension into the nonlinear MT inversion in the 8D parameter space (i.e., the six-component MT, centroid depth, and time).

First, we assume that the centroid depth H and time O are known (fixed), the MT inverse problem has 6 parameters and is linear, and thus the uncertainty analysis is straightforward. Since tr(**M**)/3 = a_6 is one of the model parameters, we can analytically calculate its standard deviation σ_{a6}. For theoretical reasons, we have to introduce a standard deviation σ_u of the data. Its squared value is the data variance. We assume the simplest possible case that σ_u has the same value for all the data components and is independent of time. As extensively discussed in Zahradník and Custódio (2012), it is not easy to estimate the true value of σ_u, however, in problems such as the one solved in this paper, where we investigate the uncertainty in a relative sense only, we just prescribe a reasonable value of σ_u , and keep it constant in all the compared models. Here by 'reasonable value' we mean σ_u of the same order of magnitude as the peak-to-peak amplitude of the displacement data in the studied frequency range at the most distant station, i.e. $\sigma_u = 1 \times 10^{-5}$ m.

In this section, we proceed according to Press et al. (1997). Normalizing **u** and **E** of Equation (1.14) by the standard deviation, we obtain

$$\tilde{u} = \frac{u}{\sigma_u};\ \tilde{E} = \frac{E}{\sigma_u};\ \tilde{u} = \tilde{E}\,\mathrm{a}\ , \tag{3.3}$$

where $\tilde{\mathbf{E}}$ is the design matrix. The design matrix depends on the position of the source and stations, on the crustal model and the considered frequency range, but does not depend on the waveforms. We can assess the *theoretical* parameter uncertainty even without recorded seismograms. Any single parameter a_i then has a 1D Gaussian probability density function (pdf). For a_6 we have

$$pdf(a_6) = \frac{e^{-\frac{1}{2}\frac{(a_6 - a_{6opt})^2}{\sigma_{a_6}^{\ 2}}}}{\sigma_{a_6} \cdot \sqrt{2\pi}} \quad , \tag{3.4}$$

where the true value of a_6 is denoted a_{6opt}, and the standard deviation σ_{a6} is given by the explicit formula (Press et al., 1997, section 15.4)

$$\sigma_{a_6}^{\ 2} = \sum_{i=1}^{6} \left(\frac{V_{6i}}{w_i} \right)^2 \quad . \tag{3.5}$$

Here V_{6i} is the 6th component of the i-th singular vector of the design matrix $\tilde{\mathbf{E}}$, and w_i is its i-th singular value. In practice, we do not need the singular decomposition of matrix $\tilde{\mathbf{E}}$, since the singular vectors $\mathbf{V}$ of $\tilde{\mathbf{E}}$ are simply eigenvectors of matrix $\mathbf{E^T E}$, and the singular values of $\tilde{\mathbf{E}}$ can be calculated from the eigenvalues λ_i of $\mathbf{E^T E}$:

$$w_i = \sqrt{\frac{\lambda_i}{\sigma_u^{\ 2}}} , \qquad \text{i=1,2,...6} \tag{3.6}$$

Now consider $\Delta\chi^2$, i.e. the theoretical misfit between data and synthetics, normalized by the data variance. The surfaces of constant theoretical misfit $\Delta\chi^2$ (a 6D ellipsoid) are given by (Press et al., 1997 section 15.6.)

$$\Delta\chi^2 = w_1^2(V_{(1)} \cdot \boldsymbol{\delta a})^2 + ... + w_6^2(V_{(6)} \cdot \boldsymbol{\delta a})^2 \tag{3.7}$$

where $\boldsymbol{\delta a}$ is the radius vector connecting the center of the ellipsoid and a point in the parameter space. It enables us also to *numerically* study misfit as a function of a_1 – a_6, or its particular projection onto a single parameter axis (the a_6-axis). Theoretical justification of the projected misfit and its relation to confidence intervals of the single parameter comes from section 15.6., Theorem D of Press et al. (1997). We discretize a_6, and for each value of a_6 we extract the points inside the ellipsoid (a_1, a_2, ... a_5)$|a_6$; here $|a_6$ denotes a fixed value of a_6. Each point is characterized by the theoretical misfit $\Delta\chi^2(a_6) \leq 1$, and we determine its minimum value $\Delta\chi^2_{min}$ over all points (a_1, a_2, ... a_5)$|\ a_6$.

$$Theor\_pdf(a_6; H = fixed; O = fixed) = e^{-\frac{1}{2}\min theor\_misfit(a_1,...a_5)|a_6} \quad . \tag{3.8}$$

Here the minimum theoretical misfit $\Delta\chi^2_{min}$ was denoted min *theor_misfit;* note that a_6 is a free parameter that is varied, not computed by the inversion. Similar function was further used in a non-linear case. For consistency with the published paper, we use the term "1D probability density function" also here, making warning, that it is a formal quantity which should not be confused with the statistically justified marginal probability density function of a_6.

In non-linear case, the inverse problem has 8 parameters: a_1, …a_6, H, and O. The non-linearity is due to the effect of the centroid depth H and centroid time O. The theoretical misfit function is no longer available. Thus, we use waveforms and evaluate the real misfit between the data and synthetic seismograms, i.e. misfit eq. (1.19) normalized by the data variance. In analogy to eq. (3.8), the so-called *experimental* probability density function can be evaluated:

$$Exper\_pdf(a_6; H = free; O = free) = const \cdot e^{-\frac{1}{2}\min real\_misfit(a_1,...a_5,H,O)|a_6} . \qquad (3.9)$$

Here the minimal real misfit is denoted min *real_misfit*. The meaning of eq. (3.9) is as follows: A value of a_6 is chosen, and the real misfit is minimized by the least-squares method in a_1, … a_5, and by a grid search in H and O. Repeating this for a set of discrete a_6 values, we obtain a 1D pdf(a_6) reflecting the linear effect of a_1, … a_5 and non-linear effects of H and O. The value of *const* normalizes the integral of pdf(a_6) to unity. The 1D experimental pdf in eq. (3.8) is the main new tool proposed in this study.

Remark: Again, we emphasize that we study projection of 8D misfit onto one of the parameter axes (the a_6-axis), not a marginal probability density of a_6.

The only technical issue related to eq. (3.9) that requires caution is the minimization of the misfit for each fixed value of a_6. For each a_6 we must find the optimal centroid depth H and time O common to all a_1, … a_6. The algorithm is the following: We choose a discrete value of a_6, (close to the previously computed optimal value, but not equal to this value) and a given trial value of H and O. We minimize the misfit between real data **u** and synthetics **s**, thus obtaining a_1, …a_5. Combining these inverted coefficients with the chosen coefficient a_6 we obtain $\mathbf{a_{opt.}}$ The correlation between **u** and $\mathbf{s=E\,a_{opt}}$ is calculated using eq. (1.17). The procedure is repeated for each trial O and H (still fixing the same a_6), and the H and O with maximum correlation are found for the chosen value of a_6. The whole procedure is repeated for each value of a_6. As a result we obtain the best-fitting parameters (a_1, …a_5, H,O), as well as the minimum misfit value (i.e. the min *real_misfit* value), all as a function of a_6. Thus, we construct the desired experimental pdf(a_6) according to eq. (3.9).

Another way of obtaining probability density functions of various source parameters (including ISO) has been recently proposed by Vackář et al. (2017). At each trial depth and time the best-fitting MT tensor is calculated by the least-squares method, and the minimum misfit is converted into an exponential PDF (probability density function). The individual PDF's are used to provide Gaussian random MT samples whose number at each depth is determined by integrating PDF over the MT parameters. This procedure normalizes the complete (generally non-Gaussian) PDF to unity. Complete set of the MT samples (for all trial depths and times) enables construction of histograms (marginal PDF's) of the source parameters, including ISO.

Determination of depth during full MT and deviatoric MT inversions

The centroid position is commonly searched together with MT. We would like to answer the question if it is necessary to calculate full MT instead of deviatoric MT even if we are not interested in value of ISO. The synthetic tests were performed in Křížová et al. (2016) for this reason.

The inversion of the synthetic data in deviatoric mode in our case clearly shows that neglecting the isotropic component has a strong effect upon the correlation-depth variations. In particular, sub-tests with high ISO component (in absolute value) show very deep local minima, but weaker local minima can be observed also in the other sub-tests. The minima are close (but not identical) to the true source depth. This remarkable feature is common to all our tests. The tests indicate that if a real event has a very large ISO% (low DC%), the correlation-depth graph may get an apparent minimum near the correct source depth, i.e. the depth will be incorrectly determined.

The significantly different correlation-depth profiles can be simply explained. Imagine a source at depth D with a large ISO component and negligible CLVD. This ISO component constitutes a significant part of the waveforms. In the full-MT inversion the waveforms can be best fitted at the depth D. However, in the deviatoric-MT inversion the true waveforms are approximated with synthetics lacking the ISO part. It means that real data are interpreted in terms of an inappropriate model (DC and CLVD only), hence deteriorating the match at depth D. As the inappropriate model does not contain ISO, real data could be partially fit only by a source model at depth D having a different focal mechanism, biased with respect to the true one in a way compensating the missing ISO. However, if no biased deviatoric MT can compensate the lack of ISO, a correlation minimum is created. At another trial depth, D'≠D, some deviatoric-MT source model can exist (for example, a model with a spurious CLVD, and/or with biased strike, dip, and rake angles) that produces synthetics fitting real data almost as well as the full-MT synthetics at depth D. Hence the source depth estimate in the deviatoric-MT inversion may be biased from D to D'.

3.2. Appraisal of results

Standard results obtained during calculations are mentioned in Křížová et al. (2013, 2016), so we do not repeat all results from articles and we focus only on some of them.

3.2.1. Santorini island - strongest event - results

In this section, we would like to compare results for eq. (3.9) with calculations according equations (5-7) of Vackář et al. (2017), recently implemented in ISOLA. Let us mention that in the first case (eq. 3.9) we use "old" ISOLA software with non-causal filter 0.02 – 0.05 – 0.08 – 0.1 Hz and in the second case (eqs. 5-7 in Vackář et al, 2017) the causal filter 0.04 – 0.1 Hz was used.

For this reason, let us start with summary of the results for standard full MT inversions, which are summarized in the Table 3.2 and shown in the Figure 3.3. We can see that results almost non-differ one from the each other for full MT inversion in model N and D respectively. The solutions for causal filter have larger variance reduction and smaller condition number. The main difference is in value of ISO component for model D. According to lower CN, we prefer the value 47.3 % obtained for inversion with causal filter. (Note that we obtain and introduce the DC, CLVD, and ISO values to one decimal place instead of rounded them to integers, but this is due to the fact that then is easier to put their sum equal to 100% correctly.)

The results for pdf function calculations according to eq. (3.9) and histograms corresponding to equations (5-7) of Vackář et al. (2017) are shown in the Figures 3.4 – 3.6. In the Figure 3.4 we can see that resolvability of ISO component is better if real velocity structure is closer to model N than D, and the same applies for histograms in the Figure 3.5. In this sense, the two methods are in rough agreement. Comparison of thesis methods is shown in the Figure 3.6 where a_6 from eq. (3.9) are

Table 3.2.: Solution for full MT inversion for strongest event of Santorini Island earthquake swarm for using non-causal and causal filtration during calculations

	Model N				Model D			
	non-causal		causal		non-causal		causal	
strike; dip; rake (°)	255 69 -57 15 38 -144		255 69 -57 16 37 -143		253 65 -67 27 32 -130		250 65 -63 20 35 -133	
M_w	4.7		4.7		4.7		4.7	
M_0 (Nm)	1.124×10^{16}		1.126×10^{16}		1.167×10^{16}		1.224×10^{16}	
depth (km)	6.5		6.5		4.0		5.5	
Centroid time (s)	20: 37: 37.75		20: 37: 37.85		20: 37: 39.25		20: 37: 39.30	
DC	41.9		44.0		48.5		49.9	
CLVD	5.0		2.5		28.0		2.8	
ISO	53.1		53.5		23.5		47.3	
VR	0.66		0.70		0.70		0.73	
CN	3.34		3.06		5.09		3.10	

Dev. ... Deviatoric
M_0 ... scalar seismic moment (eq. 1.4)
M_w ... magnitude (eq. 1.5)
VR ... variance reduction (eq. 1.20)
CN ... condition number (eq. 3.1)

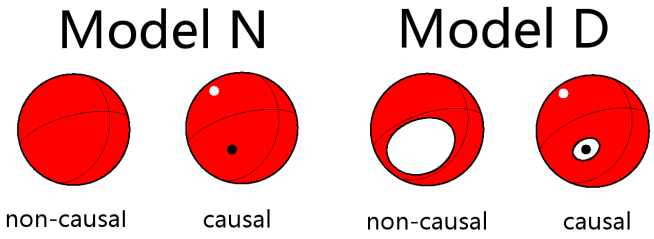

Figure 3.3. Full MT solutions for strongest event of Santorini Island earthquake swarm.

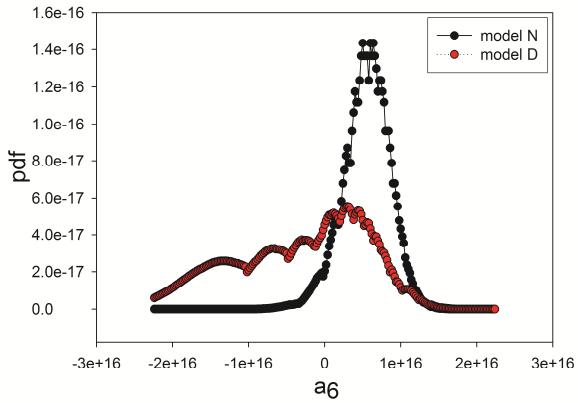

Figure 3.4. The uncertainty assessment of the isotropic component, pdf(a_6), calculated using equation (3.9) in two crustal models, N and D.

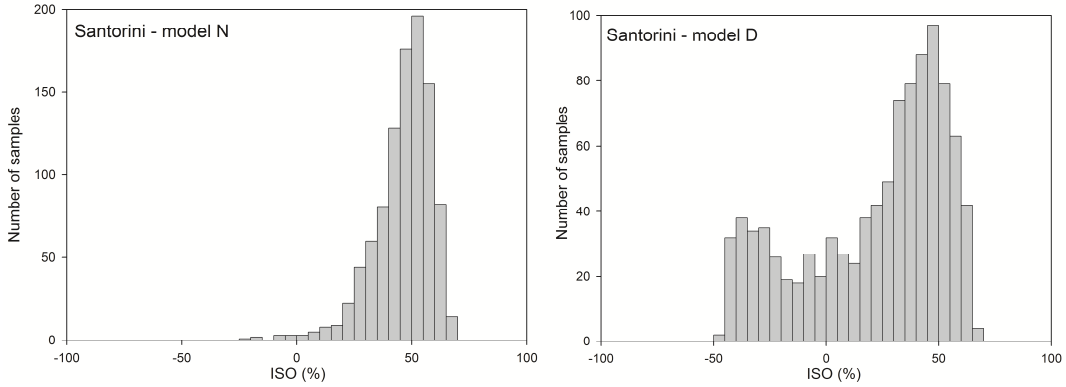

Figure 3.5. The uncertainty assessment of the isotropic component, calculated using equations (5-7) from Vackář et al. (2017) in two crustal models, N and D.

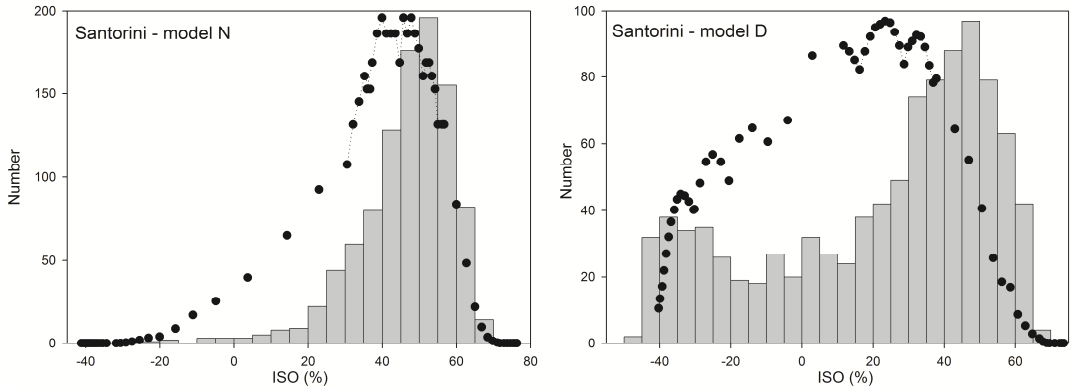

Figure 3.6. The uncertainty assessment of the isotropic component, calculated using equations (5-7) from Vackář et al. (2017) in two crustal models, N and D compared with results of pdf(a_6), calculated using equation (3.9).

recalculated to ISO and maximum value of pdf function is formally adjusted on the same level as maximum in histogram.

3.2.2. Santorini island - weaker event - results

The results for pdf function calculations according to eq. (3.9) are shown in the Figure 3.7. We can see that in this case the ISO component is smaller than for the strongest event of Santorini earthquake swarm. For the model D we can not distinguish which value of ISO is correct.

Although we believe that both chosen earthquakes from Santorini earthquake swarm have positive isotropic component of MT, we get negative values of ISO for calculations in model D (ISO = -24%), accompanied with large values of CN (CN = 6). The similar conclusions about poor resolvability of ISO component in model D we can get from jackknife tests (see Supplementary material S1.2) In all results for model N the value of CN is less than 5.0. In the sense of CN, the results for full MT in model D are less stable than for full MT in model N. Therefore, the values of ISO are more trustable for model N than for model D. It seems that if CN is larger than 6.00 the value of ISO could be completely wrong (although strike, dip, rake values have reasonable values).

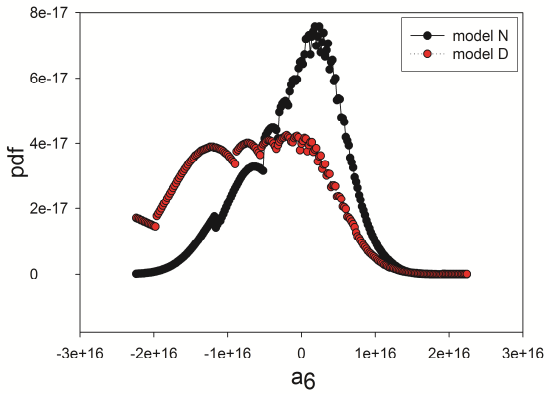

Figure 3.7. The uncertainty assessment of the isotropic component, pdf(a_6), calculated using equation (3.9) in two crustal models, N and D for Santorini earthquake – second strongest event.

3.2.3. Cretan Sea earthquake - results

The results for pdf function calculations according to eq. (3.9) are shown in the Figure 3.8. We can see that this outcome is in good agreement with result obtained during full MT calculation where in this case the ISO component is negative and has relatively small value (ISO = -9.6 %). The resolvability of ISO component according to Figure 3.8 is great. The similar conclusions about ISO we can get from jackknife tests (see Supplementary material S1.3). Probability of a6 = 0 (ISO = 0) is high thus indicating that vanishing volume change for this event can be a reasonable interpretation.

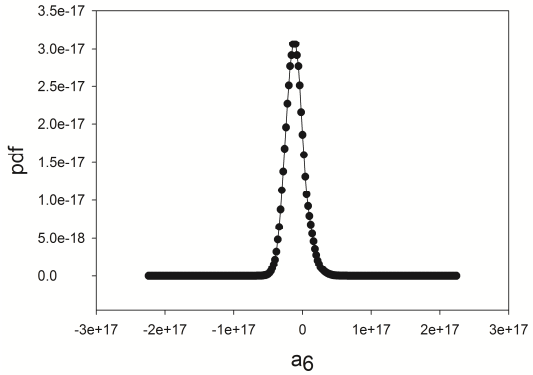

Figure 3.8. The uncertainty assessment of the isotropic component, pdf(a_6), calculated using equation (3.9) for Cretan Sea earthquake.

3.2.4. Synthetic tests - results

All correlation diagrams are shown in the figures S6 – S11 in Supplementary material (S2).

In most sub-tests of Test A, the strike/dip/rake of the deviatoric inversion differ only marginally from the correct solution. However, there are two exceptions, corresponding to the MT with the largest ISO +/-89.5%. For these cases, the deviatoric inversion produces a MT whose CLVD is greater than 90%, and the fault-plane solution of the deviatoric inversion differs quite significantly from the correct one. However, nodal lines on beach balls make very limited sense if the ISO component of MT is (in absolute value) close to 90% or higher than that.

The sub-tests of Test B, representing similar experiment but with different strike/dip/rake angles and a slightly shallower depth, give almost the same results. For details see Tables A3-A5 in Křížová et al. (2016).

In Test C, where the inversion is performed for the incorrect velocity model, we obtain deviations from the correct solution even in the full-MT inversion. The prescribed (correct) values are those of test B, due to the incorrect velocity model, in this case C. The latter is the case of sub-tests C1D and C2D, with "real" ISO= -90.3% and +90.4% where we obtain only ISO=-70.1 and +75.1, respectively. For sub-test C2D-full we get Kagan angle as large as 91°. For two smaller (absolute) values of ISO, the full MT inversion gives a higher VR and small K-angle. The deviatoric inversion in the incorrect model provides relatively small deviation of the nodal lines from the correct solution. It means that, in this example, the inversion of the fault plane solution is robust. For the deviatoric inversion, the DC% is almost always biased, for the low input DC% (sub-test 1, also accompanied by a very wrong retrieved depth). However, for the full inversion the retrieved DC% is relatively close to the true one (or somewhat lower). The DC% for the full MT inversion is retrieved well in case 1 and 2, but in tests 3-6 it is lower than the true value. Our results show that an incorrect velocity model introduces bias in estimating the DC% in both the full and deviatoric inversions.

We should mention that we generate synthetic data without noise and then invert them, that is why the results for full MT inversion in model N are considered to be correct.

We inverted the synthetic data in full-MT mode and as seen from the correlation diagrams (Figures S6 – S11 – left column) no pronounced local maxima can be detected. In other words, for this particular event-station geometry and velocity model, the centroid depth resolvability is almost none. The (weak) depth variation is almost independent on ISO%. There is a weak dependence on depth for sub-tests 3-6, but the shape of curves is almost the same. The correlation seems to be least dependent on depth in subtests 1 and 2, the curves are almost flat. Despite the use of the inappropriate velocity model, the depth dependence in Figures S10 – S11 has similar shape as in Figures S8 – S9, just the correlation values are lower.

The inversion of the same synthetic data in deviatoric mode (Figures S6 – S11 – right column), clearly shows that neglecting the isotropic component has a strong effect upon the correlation-depth variations. In particular, sub-tests 1 and 2 show very deep local minima, but weaker local minima can be observed also in the other sub-tests. The minima are close (but not identical) to the true source depth. This remarkable feature is common to all tests A-C. The tests indicate that if a real event has a very large ISO% (low DC%), the correlation-depth graph may get an apparent minimum near the correct source depth, i.e. the depth will be incorrectly determined.

3.3. Summary of Chapter 3

The three earthquakes were investigated: two strongest event of Santorini Island earthquake swarm and strongest event of Cretan Sea earthquake swarm. Group of synthetic tests with same station source distribution like in real case for two of chosen earthquakes was performed.

To more deeply investigate possible non-DC components, we study the depth-dependent correlation in two modes – full and deviatoric. For Cretan sea earthquake, our CLVD value (~6%) is smaller than the CLVD value (43%) obtained in previous modeling, using a different code and station geometry (Kiratzi, 2013). For Santorini earthquake – strongest event, we expect big ISO component because standard deviatoric centroid MT inversion indicated the double-couple percentage as low as 59%. Two velocity models for Santorini earthquake were used (D-model and N-model).

The two events studied in Křížová et al. (2016) are very different. The Cretan Sea has a large DC% for both inversion modes in a broad range of the trial source depths, and the correlation-depth variations are almost identical. These are indications of a low ISO component. Contrarily, the Santorini Island earthquake (strongest event of swarm) has a lower DC% at the depths where the correlation takes its maximum values. Most importantly, the full-MT and deviatoric-MT inversions provide considerably different correlation-depth dependences. Compared

to the synthetic tests we interpret these features as an indicator for a large isotropic component of the Santorini Island event. On the other hand, the missing local minimum in correlation function for Cretan Sea earthquake indicates relatively low ISO component.

The detailed synthetic tests have some practical implications. We think that the message of the synthetic tests is quite strong. They suggest that if the data processing indicates a small DC%, the correlation-depth analysis should be made twice, both in the full-MT and deviatoric-MT mode. If these two results strongly differ from each other, they may indicate the presence of a large isotropic component.

As an earthquake with possible large isotropic component of MT the strongest event from the Santorini Island earthquake swarm was studied. This event has relatively large ISO in model N in jackknife tests (see Supplementary material S1.1). Although results for model D have higher values of variance reduction (eq. 1.20) we accepted more the outcomes for model N because of smaller value of CN (eq. 3.1), this is especially true for ISO component of MT.

Conclusions

While the centroid moment tensor (CMT) calculations belong to routine seismological tasks, the uncertainty estimate of CMT is still rather a research problem, particularly regarding the isotropic component.

Therefore, new and robust techniques applicable in seismological practice are necessary, particularly in volcano seismology, in studies of geothermal regions, or in nuclear-test monitoring, where the isotropic component may be significant.

Two new approaches to assess resolvability of isotropic component of CMT were proposed in this thesis. The main results were published in two papers, Křížová et al. (2013; 2016), and are briefly summarized below. The approaches were validated on synthetic tests and real data. For testing the methods, three shallow earthquakes from Greece were chosen: The Cretan Sea, M_w 5.3 event of 27 January 2012, the Santorini M_w 4.9 event of 26 June 2009, and the Santorini M_w 4.7 event of 26 June 2009. We focused on the use of near-regional, low-frequency broad band waveforms.

First approach

In linearized inversion problems, where the earthquake or explosive-source location and origin time are fixed (e.g. assumed to be known), the uncertainty of the moment tensor can be studied through the eigenvalues and eigenvectors of the design matrix, which allows the representation of the theoretical misfit by means of a 6D error ellipsoid. Because the design matrix depends only on the structural model and receiver source geometry, the analysis can be performed using recorded seismic waveforms, or even without. In the non-linear inversion problems, where the free parameters are eight (e.g., the six elements of the moment tensor, depth, and origin time), we propose a waveform-inversion scheme in which the moment-tensor trace is systematically varied, and the remaining seven free parameters are optimized for each specific value of the trace. In this way, the waveform misfit can be studied as a function of the moment tensor, centroid depth, and centroid time. In particular, misfit as a function of the moment-tensor trace enables a relative comparison of events as regards their isotropic component. To account for uncertain crustal structure the method is applied in this thesis repeatedly in two velocity models available in the studied region.

Applying this method to the two shallow earthquakes (M_w 4.9 and 4.7) with epicenters close to the Columbo volcano, located 20 km northeast of the island of Santorini, Aegean Sea, Greece we found that a notable feature is the strong trade-off between the isotropic component and source depth. It is stronger than the trade-off of the isotropic component with the seismic moment, source angles (strike, dip, and rake) and origin time. Very prominent is the effect of the crustal models used: model N (Novotný et al., 2001) and model D (Dimitriadis et al., 2010). Both structural models provide satisfactory waveform match of observed and synthetic seismograms, however, if the true structure of the Earth is closer to model D, then

the isotropic component is almost irresolvable. From these two existing velocity models, we prefer the model N with lower condition number, in which a large positive isotropic component is indicated for strongest event of Santorini Island earthquake swarm.

Second approach

We formulated and partly verified a hypothesis that events with a significant isotropic component can be detected by a simple comparison of the full-MT and deviatoric-MT inversions, and that the centroid depth determination of such events under deviatoric constraint may be highly inaccurate.

Current MT determinations are often made in deviatoric approximation, and they include a grid search of the centroid position and time. The centroid is identified with a trial source position that maximizes correlation between real and synthetic waveforms. We proposed that the waveform inversion should be made in two modes: the full MT and the deviatoric MT. If the two inversion modes provide remarkably different correlation-depth functions and, in particular, if the correlation of the deviatoric inversion possess a deep local minimum, although in the full-MT inversion such a minimum is absent, we obtain an indication of a strong isotropic component. The likely source depth is close to that local minimum. Because in routine practice just the maximum of the correlation-depth function provides an estimate of the centroid depth, we infer that in case of the deviatoric inversion of an event with large ISO this traditional approach may fail, returning an incorrect depth (and possibly also an incorrect fault-plane solution).

Interestingly, synthetic tests indicating the mentioned features of the correlation-depth functions are quite robust. Indeed, the characteristic features were found even in the case when synthetic waveforms simulated in one velocity model were inverted in another model available for the same region.

Applying this method to the two studied earthquakes we found that for the Santorini island earthquake (strongest event of swarm) the full-MT and deviatoric-MT inversions provide considerably different correlation-depth dependences. Based on the synthetic tests we interpret these features as an indicator for a large isotropic component of the Santorini Island event. On the other hand, the missing local minimum in correlation function for Cretan Sea earthquake indicates relatively low ISO component.

In this sense, the second approach provided an independent confirmation of a significant isotropic component of strongest event of Santorini Island earthquake swarm, previously indicated from the first approach.

Final remark

Both the proposed approaches are comprehensible and they are usable in practice. Use of the first approach would be facilitated by its inclusion in ISOLA released software package. Use of the second approach is quite straightforward. Real usefulness of the developed methods should be tested in future on more earthquakes, in particular on such events for which uncertainty estimates of the isotropic component by independent techniques would be available.

Bibliography

Aki, K., and P. G. Richards (2002), *Quantitative seismology,* University Science Books, Sausalito, California, 704 pp.

Ambraseys, N. N. (1960). The seismic sea wave of July 9th 1956, in the Greek Archipelago, *J. Geophys. Res.* **84,** 1561–1568.

Arfken, G. (1985), Spherical Polar Coordinates. §2.5 in *Mathematical Methods for Physicists, 3rd ed.* Orlando, FL: Academic Press, pp. 102-111.

Auger, E., L. D'Auria, M. Martini, B. Chouet, and P. Dawson (2006). Real-time monitoring and massive inversion of source parameters of very long period seismic signals: An application to Stromboli Volcano, Italy, *Geophys. Res. Let.* **33,** L04301, doi:10.1029/2005GL024703.

Bernardi, F., J. Braunmiller, U. Kradolfer, D. Giardini (2004). Automatic regional moment tensor inversion in the European-Mediterranean region. *Geophys. J. Int.*, **157**, 703– 716.

Bohnhoff, M., M. Rische, T. Meier, D. Becker, G. Stavrakakis, and H.-P. Harjes (2006). Microseismic activity in the Hellenic Volcanic Arc, Greece, with emphasis on the seismotectonic setting of the Santorini-Amorgos zone, *Tectonophysics* **423,** 17-33.

Bormann, P. (Ed.) (2012). New Manual of Seismological Observatory Practice (NMSOP-2), IASPEI, GFZ German Research Centre for Geosciences, Potsdam; http://nmsop.gfz-potsdam.de; DOI: 10.2312/GFZ.NMSOP-2 (CHAPTER 2: Seismic Wave Propagation and Earth Models (P. Bormann, E. R. Engdahl and R. Kind) - DOI: 10.2312/GFZ.NMSOP-2_CH2; CHAPTER 3: Seismic Sources and Source Parameters (P. Bormann, S. Wendt and D. DiGiacomo) - DOI: 10.2312/GFZ.NMSOP-2_CH3)

Bouchon, M. (1981). A simple method to calculate Green's functions for elastic layered media, *Bull. Seismol. Soc. Am.* **71,** 959-971.

Brillinger, D. R., A. Udías, and A. B. Bolt (1980). A probabilitymodel for regional focal mechanism solutions, *Bull. Seismol. Soc Am.* **70**, 1, 149-170.

Cambaz, M. D., and A. K. Mutlu (2016). Regional Moment Tensor Inversion for Earthquakes in Turkey and Its Surroundings: 2008–2015. *Seismol. Res. Lett*. **87**(5), 1082-1090.

Cesca S, S. Heimann, K. Stammler, T. Dahm (2010). Automated procedure for point and kinematic source inversion at regional distances. *J. Geophys. Res.* 115:B06304. doi:10.1029/2009JB006450

Cesca, S., A. Rohr, and T. Dahm (2013). Discrimination of induced seismicity by full moment tensor inversion and decomposition. *J. Seismol.* **17,** no. 1, 147-163.

Chapman, C. H., and W. S. Leaney (2012). A new moment-tensor decomposition for seismic events in anisotropic media, Geophys. J. Int., 188, 343–370.

Clinton, J.F., E. Hauksson, K. Solanki (2006). An evaluation of the SCSN moment tensor solutions: Robustness of the Mw magnitude scale, style and automation of the method. *Bull. Seis. Soc. Am.* **96,** 1689-1705.

Coutant, O. (1989). Program of numerical simulation AXITRA, *Tech. rep.*, LGIT, Grenoble, France (in French).

Dahlen, F. A., and J. Tromp (September 1998). Theoretical Global Seismology.

Dahm T., F. Krüger (2014). Moment tensor inversion and moment tensor interpretation DOI:10.2312/GFZ.NMSOP 2_IS_3.9

Davi, R., G. S. O'Brien, I. Lokmer, C. J. Bean, P. Lesage, and M. M. Mora (2010). Moment tensor inversion of explosive long period events recorded on Arenal volcano, Costa Rica, constrained by synthetics tests, *Journal of Volcanology and Geothermal Research*, **194,** 189-200.

Dimitriadis, I., E. Karagianni, D. Panagiotopoulos, C. Papazachos, P. Hatzidimitriou, M. Bohnhoff, M. Rische, and T. Meier (2009). Seismicity and active tectonics at Coloumbo Reef (Aegean Sea, Greece): Monitoring an active volcano at Santorini Volcanic Center using a temporary seismic network, *Tectonophysics* **465,** 136-149.

Dimitriadis, I., C. Papazachos, D. Panagiotopoulos, P. Hatzidimitriou, M. Bohnhoff, M. Rische, and T. Meier (2010). P and S velocity structures of the Santorini-Coloumbo volcanics system (Aegean Sea, Greece) obtained by non-linear inversion of travel times and its tectonic implications, *J. Volcanol. Geoth. Res.* **195,** 13-30.

Dreger, D. S. (2002). Time-Domain Moment Tensor INVerse Code (TDMT-INVC); Chapter 85.11 of the IASPEI International Handbook of Earthquake and Engieneering Seismology (ftp://www.orfeus-eu.org/pub/software/iaspei2003/8511_tutorial.pdf - last accesed May 2017)

Dreger, D. S., H. Tkalčic, and M. Johnston (2000). Dilational processes accompanying earthquakes in the Long Valley caldera. *Science* **288,** 122 (2000), DOI: 10.1126/science.288.5463.122.

Dufumier, H., and L. Rivera (1997). On the resolution of the isotropic component in moment tensor inversion, *Geophys. J. Int.* **131,** 595-606.

Dziewonski, A.M., T.-A. Chou, J. H. Woodhouse (1981). Determination of earthquake source parameters from waveform data for studies of global and regional seismicity. *J. Geophys. Res.* **86**, 2825–2852.

Ford, S. R., D. S. Dreger, and W. R. Walter (2009). Identifying isotropic events using a regional moment tensor inversion. *J. Geophys. Res.* **114,** no. B1, doi: 10.1029/2008JB005743.

Ford, S. R., D. S. Dreger, and W. R. Walter (2010). Network sensitivity solutions for regional moment-tensor inversions, *Bull. Seismol. Soc. Am.* **100,** 1962-1970.

Foulger, G. R., B. R. Julian, D. P. Hill, A. M. Pitt, P. E. Malin, and E. Shalev (2004). Non-double-couple microearthquakes at Long Valley caldera, California, provide evidence for hydraulic fracturing. *J. Volcanol. Geoth. Res.* **132,** no. 1, 45-71.

Galanopoulos, A.G. (1960). Tsunamis observed on the coasts of Greece from Antiquity to present time, *Ann. di Geofis.* **13,** 369-386.

Gallovič, F., J. Zahradník, D. Křížová, V. Plicka, E. Sokos, A. Serpetsidaki, and G-A. Tselentis (2009). From earthquake centroid to spatial-temporal rupture

evolution: Mw 6.3 Movri Mountain earthquake, June 8, 2008, Greece, *Geophys. Res. Let.* **36,** L21310, doi: 10.1029/2009GL040283.

Green, G. (1828). An essay on the application of mathematical analysis to the theories of electricity and magnetism. Nottingham [Eng.: Printed for the author, by T. Wheelhouse].

Haslinger, F., E. Kissling, J. Ansorge, D. Hatzfeld, E. Papadimitriou, V. Karakostas, K. Makropoulos, H.-G. Kahle, and Y. Peter (1999). 3D crustal structure from local earthquake tomography around the Gulf of Arta (Ionian region, NW Greece). *Tectonophysics*, **304**(3), 201-218.

Heimann S (2010). A robust method to estimate kinematic earthquake source parameters. PhD Thesis, University of Hamburg, Germany, pp 145

Henry, C., J. H. Woodhouse, S. Das (2002). Stability of earthquake moment tensor inversions: effect of the double-couple constraint. *Tectonophysics* **356**, 115-124.

Hicks, S. P., and A. Rietbrock (2015). Seismic slip on an upper-plate normal fault during a large subduction megathrust rupture. *Nature Geoscience*, *8*(12), 955-960, doi:10.1038/ngeo2585.

Hofstetter R, G. Örgülü, M. Aktar (2000). Application of Regional Moment tensor Inversion. ORFEUS Newsletter – March 2000- vol. 2 – no. 1 page 6

Horálek, J., J. Šílený, and T. Fischer (2002). Moment tensors of the January 1997 earthquake swarm in NW Bohemia (Czech Republic): double-couple vs. non-double-couple events. *Tectonophysics*, **356,** no. 1, 65-85.

Hudson, J. A., R. G. Pearce, and R. M. Rogers (1989). Source type plot for inversion of the moment tensor, *J. Geophys. Res.* **94,** 765-774.

Janský, J., O. Novotný, V. Plicka, and J. Zahradník (2012). Earthqake location from P-arrival times only: problems and some solutions, *Stud. Geophys. Geod.* **56,** 553-566, DOI: 10.1007/s11200-011-9036-2.

Jánský, J., J. Zahradník, and V. Plicka (2009). Shallow earthquakes: shallower than expected?, *Stud. Geophys. Geod.* **53,** 261-268.

Jechumtálová, Z., J. Šílený (1998). Smoothing the source time function – a tool to soften inadequate modelling of the medium during inversion of local waveforms? *Journal of Seismology*, **2,** 145-158.

Jechumtálová, Z., J. Šílený (2001). Point-source Parameters from Noisy Waveforms: Error Estimate by Monte-Carlo Simulation. *Pure Appl. Geophys*. **158**, 1639-1654.

Jost, M. L., and R. B. Herrmann (1989). A students guide to and review of moment tensors, *Seismol. Res. Lett.* ***60,*** 37–57.

Julian, B. R., A. D. Miller, and G. R. Foulger (1998). Non-double-couple Earthquakes, 1, *Rev. Geophys.* **36,** 525-549.

Kagan, Y. Y. (1991). 3-D rotation of double-couple earthquake sources, *Geophys. J. Int.* **106**, 709-716, doi 10.1111/j.1365-246X.1991.tb06343.x.

Karagianni, E. E., C. B. Papazachos, D. G. Panagiotopoulos, P. Suhadolc, A. Vuan, and G. F. Panza (2005). Shear velocity structure in the Aegean area obtained by inversion of Rayleigh waves. *Geophys. J. Int.,* **160**(1), 127-143.

Kawakatsu, H. (1996). Observability of the isotropic component of a moment tensor. *Geophys. J. Int.* **126,** no. 2, 525-544.

Kikuchi, M., and H. Kanamori (1991). Inversion of complex body waves. III, *Bull. Seismol. Soc. Am.* **81,** 2335–2350.

Kiratzi, A. (2013). The January 2012 earthquake sequence in the Cretan Basin, south of the Hellenic Volcanic Arc: Focal mechanisms, rupture directivity and slip models, *Tectonophysics,* **586,** 160-172, doi: 10.1016/j.tecto.2012.11.019.

Konstantinou, K. (2010). Crustal rheology of the Santorini–Amorgos zone: Implications for the nucleation depth and rupture extent of the 9 July 1956 Amorgos earthquake, southern Aegean, *J. Geodyn.* **50,** 400–409.

Křížová, D., J. Zahradník, and A. Kiratzi (2013). Resolvability of Isotropic Component in Regional Seismic Moment Tensor, Inversion, *Bull. Seismol. Soc. Am.* **103,** no. 4, 2460 - 2473, doi: 10.1785/0120120097.

Křížová, D., J. Zahradník, and A. Kiratzi (2016). Possible Indicator of a Strong Isotropic Earthquake Component: Example of Two Shallow Earthquakes in Greece, *Bull. Seismol. Soc. Am.* **106,** no. 6, 2784 - 2795, doi: 10.1785/0120160086.

Kulhánek, O. (1990). Anatomy of Seismograms: Development in Solid Earth Geophysics, 178 pp.

Latorre, D., J. Virieux, T. Monfret, V. Monteiller, T. Vanorio, J. L. Got, and H. Lyon-Caen (2004). A new seismic tomography of Aigion area (Gulf of Corinth, Greece) from the 1991 data set. *Geophys. J. Int.* **159**(3), 1013-1031.

Lay, T. , T. C. Wallace (1995), Modern global seismology. Academic Press 1995.

Madariaga, R., and K. B. Olsen (2002). 12 Earthquake dynamics. *International Geophysics*, *81*, 175-III.

Minson, S. E., and D. S. Dreger (2008). Stable inversions for complete moment tensors. *Geophys. J. Int.* **174,** no. 2, 585-592.

Molnar, P., and H. Lyon-Caen (1989). Fault plane solutions of earthquakes and active tectonics of the Tibetan Plateau and its margins., *Geophys. J. Int.* **99,** 123–154.

Moon, P. and D. E. Spencer (1988). Spherical Coordinates (r, θ, ψ). *Field Theory Handbook, Including Coordinate Systems, Differential Equations, and Their Solutions, 2nd ed.* New York: Springer-Verlag, pp. 24-27, 1988.

Mustać, M., and H. Tkalčić (2016). Point source moment tensor inversion through a Bayesian hierarchical model. *Geophys. J. Int.* **204,** no. 1, 311-323, doi: 10.1093/gji/ggv458.

Nakano, M., H. Kumagai, and H. Inoue (2008). Waveform inversion in the frequency domain for the simultaneous determination of earthquake source mechanism and moment function, *Geophys. J. Int.* **173,** 1000-1011.

Novotný, O., J. Zahradník, and G-A. Tselentis (2001). Northwestern Turkey earthquakes and the crustal structure inferred from surface waves observed in Western Greece, *Bull. Seismol. Soc. Am.* **91,** 875-879.

Okal, E.A., C. E. Synolakis, B. Uslu, N. Kalligeris, and E. Voukouvalas (2009). The 1956 earthquake and tsunami in Amorgos, Greece. *Geophys. J. Int.* **178,** 1533–1554, doi:10.1111/j.1365–246X.2009.04237.x.

Panza, G. F., and A. Saraò (2000). Monitoring volcanic and geothermal areas by full seismic moment tensor inversion: are non-double-couple components always artifacts of modelling?, *Geophys. J. Int.* **143,** 353–364.

Papazachos, B.C., and K. Papazachou (2003). The earthquakes of Greece, Ziti Publ., pp.286.

Pasyanos, M., D. S. Dreger, and B. Romanowicz (1996). Towards real-time determination of regional moment tensors. *Bull. Seismol. Soc. Am.* **86**, 1255–1269.

Pondrelli, S., S. Salimbeni, G. Ekström, A. Morelli, P. Gasperini and G. Vannucci (2006). The Italian CMT dataset from 1977 to the present, *Phys. Earth Planet. Int.*, **159,** 286-303.

Press, W. H., S. A. Teukolsky, W. T. Vetterling, and B. P. Flannery (1997). *Numerical recipes in Fortran 77:. The art of Scientific Computing*, Cambridge University Press, 2nd ed., 992 pp.

Richter, C. F. (1935). An instrumental earthquake magnitude scale. *Bull. Seismol. Soc. Am.* **25** (1–2): 1–32.

Riedesel, M. A., and T. H. Jordan (1989). Display and assessment of seismic moment tensors, *Bull. Seismol. Soc. Am.* **79,** 85-100.

Rigo, A., H. Lyon-Caen, R. Armijo, A. Deschamps, D. Hatzfeld, K. Makropoulos, P. Papadimitriou, and I. Kassaras (1996). A microseismic study in the western part of the Gulf of Corinth (Greece): Implications for large-scale normal faulting mechanisms. *Geophys. J. Int.* **126**(3), 663-688.

Ringler, A. T., and J. R. Evans (2015). A Quick SEED Tutorial. *Seismol. Res. Lett.* **86** (6), 1-9. doi: 10.1785/0220150043

Shuler, A., G. Ekström, and M. Nettles (2013). Physical mechanisms for vertical-CLVD earthquakes at active volcanoes, *J. Geophys. Res.* **118**, 1569–1586, doi:10.1002/jgrb.50131.

Šílený, J. (1998). Earthquake source parameters and their confidence regions by a genetic algorithm with a 'memory', *Geophys. J. Int.* **134,** 228-242.

Šílený, F., and R. Hofstetter (2002). Moment tensor of the 1999 Dead Sea calibration shot: limitations in the isotropic source retrieval without a detailed earth model, *Tectonophysics* **356,** 157– 169.

Šílený, J., V. Vavryčuk, J. Zahradník (2004). Střižná a nestřižná zemětřesení, *Čs. čas. fyz.* **54**, 173-178.

Silver, P. G., and T. H. Jordan (1982). Optimal estimation of scalar seismic moment, *Geophys. J. Roy. Astron. Soc.* **70,** 755-787, doi: 10.1111/j.1365-246X.1982.tb05982.x.

Sokos, E. N., and J. Zahradník (2008). ISOLA a Fortran code and a Matlab GUI to perform multiple-point source inversion of seismic data. *Comput. Geosci.* **34,** 967-977.

Sokos, E. N., J. Zahradník, A. Kiratzi, J. Janský, F. Gallovič, O. Novotný, J. Kostelecký, A. Serpetsidaki, and G.-A. Tselentis (2012). The January 2010 Efpalio earthquake sequence in the western Corinth Gulf (Greece), *Tectonophysics* **530-531,** 299-309.

Sokos, E. and J. Zahradník (2013). Evaluating centroid moment tensor uncertainty in new version of ISOLA software, *Seismol. Res. Lett.* **84**, 656-665.

Song, F., and M. N. Toksöz (2011). Full-waveform based complete moment tensor inversion and source parameter estimation from downhole microseismic data for hydrofracture monitoring, *Geophysics* **76,** no. 6, WC103-WC116.

Tarantola, A. (2005). Inverse Problem Theory and Methods for Model Parameter Estimation. Institut de Physique du Globe de Paris, Université de Paris 6, Paris, France. DOI: http://dx.doi.org/10.1137/1.9780898717921

Templeton, D. C., and D. S. Dreger (2006). Non-double-couple earthquakes in the Long Valley volcanic region, *Bull. Seismol. Soc. Am.* **96,** 69-79.

Tkalčić, H., D. S. Dreger, G. R. Foulger, and B. R. Julian (2009). The puzzle of the 1996 Bárdarbunga, Iceland, earthquake: No volumetric component in the source mechanism, *Bull. Seismol. Soc. Am.* **99,** 3077-3085.

Tselentis, G.-A., N.S. Melis, E. Sokos, and K. Papatsimpa (1996). The Egion June 15, 1995 (6.2 ML) earthquake, Western Greece. *Pure Appl. Geophys.* **147**, 83–98.

Vackář J., J. Burjánek, and J. Zahradník (2015). Automated detection of disturbances in seismic records; MouseTrap code. *Seismol. Res. Lett.* **86**, 442-450.

Vackář, J., J. Burjánek, F. Gallovič, J. Zahradník, and J. Clinton (2017). Bayesian ISOLA: new tool for automated centroid moment tensor inversion. *Geophys. J. Int.* doi: https://doi.org/10.1093/gji/ggx158

Vasco, D. W. (1990). Moment-tensor invariants: Searching for non-double-couple earthquakes, *Bull. Seismol. Soc. Am.* **80,** no. 2, 354–371.

Vavryčuk, V. (2001). Inversion for parameters of tensile earthquakes, *J. Geophys. Res.* **106,** 16,339-16,355.

Vavryčuk, V. (2004). Inversion for anizotropy from non-double-couple components of moment tensors. *J. Geophys. Res.* **109**, no. B07306, doi: 10.1029/2003JB002926.

Vavryčuk, V. (2007). On the retrieval of moment tensors from borehole data, *Geophys. Prospect.* **55,** 381-391.

Vavryčuk, V. (2011). Tensile earthquakes: Theory, modeling, and inversion, *J. Geophys. Res.* **116,** B12320, doi:10.1029/2011JB008770.

Vavryčuk, V., and D. Kuhn (2012). Moment tensor inversion of waveforms: a two-step time-frequency approach, *Geophys. J. Int.* **190,** no. 3, 1761-1776, doi: 10.1111/j.1365-245X.2012.05592.x.

Vavryčuk, V., M. Bohnhoff, Z. Jechumtálová, P. Kolář, and J. Šílený (2008). Non-double-couple mechanisms of microearthquakes induced during the 2000 injection experiment at the KTB site, Germany: A result of tensile faulting or anisotropy of a rock? *Tectonophysics*, **456,** no. 1, 74-93.

Waldhauser, F., and W. L. Ellsworth (2000). A double-difference earthquake location algorithm: Method and application to the northern Hayward fault, California. *Bulletin of the Seismological Society of America*, **90(6)**, 1353-1368.

Wéber, Z. (2006). Probabilistic local waveform inversion for moment tensor and hypocentral location, *Geophys. J. Int.* 165, 607-621.

Yang, X., and J. L. Bonner (2009). Characteristics of chemical explosive sources from time-dependent moment tensors, *Bull. Seismol. Soc. Am.* **99,** 36-51.

Zahradník, J., and S. Custódio (2012). Moment tensor resolvability: Application to southwest Iberia. *Bull. Seismol. Soc. Am.* 102, 1235-1254, doi: 10.1785/0120110216.

Zahradník, J., and F. Gallovič (2010). Toward understanding slip inversion uncertainty and artifacts, *J. Geophys. Res.* **115,** no. B9, B09310, doi: 10.1029/2010JB007414.

Zahradník, J., and A. Plešinger (2005). Long-period pulses in broadband records of near earthquakes *Bul. Seismol. Soc. Am.* **95**, no. 5, 1928-1939.

Zahradník, J., and A. Plešinger (2010). Toward understanding subtle instrumentation effects associated with weak seismic events in the near field. *Bull. Seismol. Soc. Am.* **100**, 59-73.

Zahradník, J., and E. Sokos (2011). Multiple-point source solution of the Mw7.2 Van earthquake, October 23, 2011, Eastern Turkey. *Research Report,* EMSC, 1 November 2011, http://www.emsc-csem.org/Files/event/239856/Van_ISOLA.pdf (last accessed April 2013).

Zahradník, J., J. Janský, and V. Plicka (2008). Detailed waveform inversion for moment tensors of M ~ 4 events: Examples from the Corinth Gulf, Greece, *Bull. Seismol. Soc. Am.* **98,** 2756-2771.

Zahradník, J., E. Sokos, G-A. Tselentis, and N. Martakis (2008). Non-double-couple mechanism of moderate earthquakes near Zakynthos, Greece, April 2006; explanation in terms of complexity, *Geophys. Prospect.* **56,** 341-356.

Zahradník, J., F. Gallovič, E. Sokos, A. Serpetsidaki, and G-A. Tselentis (2008). Quick fault-plane identification by a geometrical method: application to the Mw 6.2 Leonidio earthquake, January 6, 2008, Greece. *Seismol. Res. Lett.* **79**, 653-662, doi: 10.1785/gssrl.79.5.653.

Web pages:

http://gmt.soest.hawaii.edu/ - last accesed May 2017 (GMT – PaulWessel and Walter H. F. Smith)

www.emsc-csem.org/ - last accesed May 2017 (European-Mediterranean Seismological Centre (EMSC))

http://www.orfeus-eu.org/ - last accesed May 2017 (Observatories & Research Facilities for European Seismology = Orfeus)

http://alomax.net/nlloc - last accesed May 2017 (NonLinLoc for absolute location, A. Lomax)

http://www.giseis.alaska.edu/input/carl/research/beach/beachnotes_percent.pdf - last accesed May 2017 (Tape, C. (2016). "Percentages" of DC, CLVD, ISO for moment tensors should be dropped)

http://www.iris.edu/hq/ - last accesed May 2017 (IRIS, Incorporated Research Institutions for Seismology)

https://www.fdsn.org/seed_manual/SEEDManual_V2.4.pdf - last accesed May 2017 (SEED Reference Manual - Standard for the Exchange of Earthquake Data, Version 2.4 (2012))

http://ds.iris.edu/ds/nodes/dmc/software/downloads/rdseed/ - last accesed May 2017 (rdseed software)

https://ds.iris.edu/files/sac-manual/sac_manual.pdf - last accesed May 2017 (Seismic Analysis Code Users Manual, Version 101.6a (2014))

http://www.isc.ac.uk/registries/search/ - last accesed May 2017 (ISC, International Seismological Centre, Station search)

http://alomax.free.fr/seisgram/SeisGram2K.html - last accesed May 2017 (SeisGram2K from A. Lomax)

http://www.statistics.gr/en/home - last accesed May 2017 (Hellenic Statistical Authority – ELSTAT)

Attachments

Articles published in Bulletin of the Seismological Society of America (Křížová et al., 2013 and Křížová et al., 2016) which are crucial for this thesis are copied here.

A1. Resolvability of isotropic component in regional seismic moment tensor inversion

by **Dana Křížová**[1], **Jiří Zahradník**[1], and **Anastasia Kiratzi**[2]

[1] Charles University, Faculty of Mathematics and Physics, Czech Republic

[2] Aristotle University of Thessaloniki, Department of Geophysics, Greece

ABSTRACT

We propose a new approach to resolve the isotropic component of the seismic moment tensor and its uncertainty. In linearized inversion problems, where the earthquake or explosive-source location and origin time are fixed (e.g. assumed to be known), the uncertainty of the moment tensor can be studied through the eigenvalues and the eigenvectors of the design matrix, which allows the representation of the theoretical misfit by means of a 6D error ellipsoid. Because the design matrix depends only on the structural model and receiver source geometry, the analysis can be performed using recorded seismic waveforms, or without. In the non-linear inversion problems, where the free parameters are eight (e.g., the six elements of the moment tensor, depth, and origin time), we propose a waveform-inversion scheme in which the trace of the moment tensor varies systematically and the remaining seven free parameters are optimized for each specific value of the trace. In this way, a 1D experimental probability density function of the moment tensor trace is constructed. To demonstrate the applicability of the method, we apply it to two shallow earthquakes (M_w 4.9 and 4.7) with epicenters close to the Columbo volcano, located 20 km northeast of the island of Santorini, Aegean Sea, Greece. We use 15 near-regional (60–310 km) records at frequencies below 0.1 Hz and two alternative crustal models. We conclude that the main uncertainties are attributed to the crustal model and to the trade-off between the isotropic component and the source depth.

INTRODUCTION

The resolvability of the seismic moment tensor (MT) and its uncertainty are among the topical issues of modern seismology. The full MT can be decomposed into its deviatoric (DEV) and isotropic (ISO) part. An equivalent name for the isotropic part is volumetric. This decomposition is mathematically unique. It is the deviatoric part that can be further decomposed following a variety of schemes (e.g., Jost and Herrmann, 1989; Julian et al., 1998); for example, the most common approach is the decomposition of the deviatoric part into the largest possible double couple (DC) that has a remainder component, the so-called compensated linear vector dipole (CLVD).

The definition of the relative size of the components (i.e., the so-called ISO, DC and CLVD percentages) may have several forms (Vavryčuk, 2001).

The moment tensor can be used in a purely formal way to relate the seismic wave field and the elastic response of the Earth (Green's function). Some authors attempt to give a physical interpretation of the moment tensor. One of possible physical models of the full-MT source, including the ISO, DC, and CLVD components, is the tensile earthquake model, in which the slip vector is generally nonparallel with the fault plane (Vavryčuk, 2011). Dufumier and Rivera (1997) combined the full moment tensor with an additional, so-called nontectonic isotropic component.

Compared to the DC component, CLVD and ISO are the most unstable parameters in the moment tensor inversions. They often trade off with other source parameters, such as depth, source time function, source multiplicity, as well as with the structural parameters (heterogeneity, anisotropy). A number of attempts to resolve these issues have been proposed. Vasco (1990) used the method of extremal models to rigorously estimate the bounds of the MT trace. A number of approaches are more experimental, as for example, to rerun the inversions using data contaminated by artificial noise or to artificially perturb the crustal models used (e.g., Šílený and Hofstetter, 2002; Wéber, 2006; Vavryčuk, 2007). The graphic approach of Riedesel and Jordan (1989) provides the tools to visualize the moment tensor uncertainties and the deviations of the MT from a pure DC model. For the inversion schemes that provide families of acceptable solutions (in addition to the best-fitting solution), the family itself is used to experimentally construct the confidence intervals of the source parameters. A representative example is the work of Šílený (1998), who used genetic algorithms to construct probabilistic estimates of the model parameters, including the posterior probability density function of the model parameters. Ford et al. (2010) proposed the network-sensitivity solution. They grid searched the parameter space in terms of the MT invariants, and, using the source-type plots of Hudson et al. (1989), were able to effectively identify the non-DC sources in practice. Panza and Saraò (2000) emphasized the role of synthetic tests in evaluating the reliability of the non-DC components.

Nakano et al. (2008) discussed the trade-off between the source position and the non-DC components and recommended to use the DC assumption when determining the source position. In this line of work, Zahradník and Sokos (2011) had to use a DC-constrained solution to determine the centroid position of the 2011 M_w 7.2 Van earthquake, Turkey, from near-regional accelerograms. Dufumier and Rivera (1997), within the frame of the linear theory, broadly analyzed the condition numbers of the MT inverse problem and applied regularizations. Thus, they were able to theoretically interpret the previously observed trade-offs between the isotropic-source component, hypocentral depth, and source time function. Zahradník, Sokos, et al. (2008) emphasized the trade-off between the non-DC components and centroid time.

Significant isotropic components may occur, for example, during man-made explosions, volcanic events, seismic events related to migration of fluids, and gas or

rupture on non-planar faults. As certain types of these events may have a very long duration, the inversion of the MT temporal variation is also important (Auger et al., 2006; Yang and Bonner, 2009). The temporal variations of the isotropic and shear components of the source may be different (e.g., Davi et al., 2010). Vavryčuk and Kuhn (2012) developed a new method to retrieve the time function and analyze the stability of the isotropic component as a function of a random noise in waveform amplitudes and temporal shifts.

From the published research so far, it is indicated that moment tensors calculated for volcanic events do not necessarily involve an isotropic component. Tkalčić et al. (2009), who also provide a thorough literature review on non-DC earthquakes, used a sensitivity test in which they systematically decreased the number of stations down to a single one. Their test revealed no isotropic change for a M_w 5 volcanic earthquake. Dreger et al. (2000) found significant isotropic components for two M_w 4.6 and 4.9 earthquakes in the Long Valley caldera, possibly related to hydrothermal or magmatic processes; however, a comprehensive stability testing of the MT inversion for 33 events with $M_w > 3.5$ in the same volcanic region, made by Templeton and Dreger (2006), showed that 28 of them are best characterized by a pure double-couple model.

From the above brief review of the state-of-the-art methods it follows that the treatment of the isotropic component in moment tensor inversions and its uncertainty is a significant issue in theoretical seismology, with a variety of approaches proposed to remedy the problem. However, new and robust techniques applicable in the routine seismological analysis are necessary, as for example in the cases of volcano monitoring or in nuclear-test monitoring, where to resolve the uncertainty of the isotropic component is significant. In an effort to contribute to this broad goal, the specific objective of this paper is to propose a new simple numerical method for constructing a 1D experimental probability density function (PDF) related to the isotropic component. The paper is structured as follows. It starts with the description of the MT inversion and continues with the methodical details of the uncertainty estimate. First, we deal with the linear MT inversion with six parameters (a fixed centroid position and time) and present a theoretical 1D PDF allowing for the simplest estimate of the ISO uncertainty in the 6D parameter space (Zahradník and Custódio, 2012). Then we propose an extension into the nonlinear MT inversion in the 8D parameter space (i.e., the six-component MT, centroid depth, and time). The innovation is a simple way of constructing an experimental 1D PDF of the isotropic component. In the remaining sections, we apply both the traditional and the new methods to two moderate-size earthquakes with epicenters close to an active submarine volcano in the Aegean Sea and discuss the uncertainty of the obtained isotropic component in the seismic moment tensor.

Prior to the application using observed data, we performed a number of tests to validate the new codes. Extensive synthetic tests were not conducted for several reasons: (1) Synthetic tests are mainly important in multiparameter and/or strongly nonlinear inverse problems, where the inversion may provide solutions qualitatively different from the true model and/or when the solution is highly nonunique. This is

not the case of the MT inversion. (2) A number of synthetic tests have been already published (see the above cited papers) that effectively indicate how spurious non-DC components may arise in a MT inversion due to imperfections in modeling; for example, seismic noise, mislocation, mismodeling of the wave propagation (inaccurate Green's functions), to mention a few. (3) The synthetic tests have a very limited practical significance. For example, they may predict the MT uncertainties for a given variation of the crustal model, say within the 5% or 10% of the assumed model, but this is of no practical value if we do not know how far from reality our model is.

METHOD

Forward and Inverse Problem

We consider a point source of seismic waves of a given position and origin time, and express displacement **u** by means of moment tensor **M** and spatial derivatives of Green's tensor **G** (Aki and Richards, 2002):

$$u_i(t) = \sum_{p=1}^{3} \sum_{q=1}^{3} M_{pq} * G_{ip,q}, \tag{1}$$

where * stands for temporal convolution, and *p, q* denotes three Cartesian coordinates. The moment tensor can be expressed in the form of a linear combination of six elementary (dimensionless) tensors $\mathbf{M^i}$**:**

$$M_{pq} = \sum_{i=1}^{6} a_i M^i_{pq} . \tag{2}$$

It represents a convenient parametrization because in this way the source is characterized by six scalar coefficients a_i.

We use the elementary tensors implemented in the discrete-wavenumber code AXITRA (Bouchon, 1981, Coutant, 1989):

$$M^1 = \begin{pmatrix} 0 & 1 & 0 \\ 1 & 0 & 0 \\ 0 & 0 & 0 \end{pmatrix} \quad M^2 = \begin{pmatrix} 0 & 0 & 1 \\ 0 & 0 & 0 \\ 1 & 0 & 0 \end{pmatrix} \quad M^3 = \begin{pmatrix} 0 & 0 & 0 \\ 0 & 0 & -1 \\ 0 & -1 & 0 \end{pmatrix}$$

$$M^4 = \begin{pmatrix} -1 & 0 & 0 \\ 0 & 0 & 0 \\ 0 & 0 & 1 \end{pmatrix} \quad M^5 = \begin{pmatrix} 0 & 0 & 0 \\ 0 & -1 & 0 \\ 0 & 0 & 1 \end{pmatrix} \quad M^6 = \begin{pmatrix} 1 & 0 & 0 \\ 0 & 1 & 0 \\ 0 & 0 & 1 \end{pmatrix}. \tag{3}$$

The $\mathbf{M}^1$ to $\mathbf{M}^5$ tensors represent five DC focal mechanisms, while $\mathbf{M}^6$ is a purely isotropic source.

We must note that the six elementary tensors used here to aid the MT inversion should not be confused with various tensors used in the literature to decompose the MT for purposes of its physical interpretation, for example, to decompose the MT into the isotropic part and three DC tensors (e.g., Figure 3 of Julian 1998, or p. 42 of Jost and Herrmann, 1989). The interpretation of the MT used in this paper is defined in *Decomposition of MT*.

Combining (2), (3) we arrive at

$$\mathbf{M} = \begin{pmatrix} -a_4 + a_6 & a_1 & a_2 \\ a_1 & -a_5 + a_6 & -a_3 \\ a_2 & -a_3 & a_4 + a_5 + a_6 \end{pmatrix} \tag{4}$$

where a_i (with the dimension of moment) are coefficients of the linear combination in equation (2). Note that the trace of the moment tensor is tr(**M**) = $3a_6$. The scalar seismic moment is defined as the Euclidian norm of the MT (Silver and Jordan, 1982),

$$M_0 = \sqrt{\frac{\sum_{p=1}^{3}\sum_{q=1}^{3}(M_{pq})^2}{2}} \quad . \tag{5}$$

Combining (1) and (2) yields:

$$u_i(t) = \sum_p \sum_q \left(\sum_{j=1}^{6} a_j M_{pq}^j\right) * G_{ip,q} \, , \tag{6}$$

and then

$$u_i(t) = \sum_{j}^{6} a_j \left(\sum_p \sum_q M_{pq}^j * G_{ip,q}\right) = \sum_{j=1}^{6} a_j E_i^j(t) \, , \tag{7}$$

where $\mathbf{E}^j$ denotes the *j*th elementary seismogram corresponding to the *j*th elementary moment tensor. Here we assume that the moment temporal function is known, and it is assumed to have the form of a step function, which is a good approximation at frequencies below the corner frequency of the event. In matrix notation,

$$\mathbf{u = E\,a} \, . \tag{8a}$$

The overdetermined linear inverse problem (8a) for **a** can be solved by the least-squares method

$$\mathbf{a_{opt} = (E^T E)^{-1} E^T u} \, , \tag{8b}$$

where superscripts T and -1 stand for matrix transposition and inversion. This least-squares formulation is standard (e.g., Kikuchi and Kanamori, 1991), but in our case the elementary moment tensors (3) differ from those of the referenced paper. The difference is formal and has no effect on the solution. Technically, the processing of the complete observed seismograms **u** and the calculation of the elementary seismograms **E** for a given time function, as well as the inversion of $\mathbf{a_{opt}}$, are all performed using ISOLA software (Sokos and Zahradník, 2008). No station-dependent temporal adjustment to improve the fit between the observed and synthetic seismograms is introduced (Zahradník, Jánský, et al., 2008).

In case of an unknown source position and time, which are related to the displacement in a nonlinear way, we seek these additional parameters (centroid position and time, hidden in **E**) by grid search. In other words, we still solve linear problem (8a) for **a** but do so repeatedly with different **E**.

The grid search maximizes the correlation between the observed (**u**) and synthetic (**s**) seismograms

$$Corr = \frac{\int us}{\sqrt{\int u^2 s^2}}, \tag{9}$$

where $\int us = \sum_i \int u_i(t) s_i(t) dt$ and summation is over components and stations.

The match between real and best-fitting seismograms is measured by the L2-norm misfit

$$misfit = \int (u - s)^2 \tag{10}$$

and/or by means of the global variance reduction (VR):

$$VR = 1 - \frac{misfit}{\int u^2}. \tag{11}$$

If synthetics **s** are found by least-squares misfit minimization, that is,

$$\mathbf{s}=\mathbf{E}\mathbf{a}_{\mathbf{opt}}, \tag{12a}$$

where $\mathbf{a}_{\mathbf{opt}}$ is given by (8b), then

$$\int u \cdot s = \int s \cdot s, \tag{12b}$$

and the correlation is related with the variance reduction through the simple formula

$$Corr^2 = VR. \tag{13}$$

Decomposition of MT

As previously mentioned there are a number of schemes to interpret the resulting MT (i.e., to decompose it into components with a simple meaning). We follow the most common decomposition $\mathbf{M} = \mathbf{M}_{ISO} + \mathbf{M}_{DEV}$, where $\mathbf{M}_{ISO}$ and $\mathbf{M}_{DEV}$ are the isotropic and deviatoric parts, respectively. Furthermore, $\mathbf{M}_{DEV} = \mathbf{M}_{DC} + \mathbf{M}_{CLVD}$ (e.g., Julian, 1998, p. 530). The eigenvalues of $\mathbf{M}_{DEV}$ define commonly used parameter ε, ranging from 0 (pure DC) to ±0.5 (pure CLVD): $\varepsilon = -e_1/\mathrm{abs}(e_2)$, where e_1 and e_2 are the eigenvalues of $\mathbf{M}_{DEV}$ with the minimum and maximum absolute values, respectively. The relative size of the individual components is expressed in percentages. Their definition has not been standardized in the literature; in this paper we use the percentages defined in equation (8) of Vavryčuk (2001): ISO = 100[tr(**M**)/3]/abs(e^*), where e^* is the eigenvalue of the full moment tensor **M**, which has the maximum absolute value. CLVD = 2ε[100 – abs(ISO)], DC = 100 - abs(ISO) - abs(CLVD). Alternatively, in this paper we measure the isotropic part of MT also directly by means of the a_6 coefficient because, according to equation (4), a_6 = tr(**M**)/3.

Isotropic Component - Uncertainty in the Linear Case

First, we assume that the centroid depth H and time O are known (fixed), the MT inverse problem has six parameters and is linear, and thus the uncertainty analysis is straightforward. Because tr(**M**)/3 = a_6 is one of the model parameters, we can easily calculate its standard deviation σ_{a6}.

For theoretical reasons, we have to introduce a standard deviation σ_u of the data. Its squared value is the data variance. We assume the simplest possible case

that σ_u has the same value for all the data components and is independent of time. As extensively discussed in Zahradník and Custódio (2012), it is not easy to estimate the true value of σ_u; however, in problems such as the one solved in this paper, where we investigate the uncertainty in a relative sense only, we just prescribe a reasonable value of σ_u and keep it constant in all the compared models. Here we use σ_u of the same order of magnitude as the peak-to-peak amplitude of the displacement data in the studied frequency range at the most distant station (i.e., $\sigma_u = 1 \times 10^{-5}$ m).

Normalizing **u** and **E** of Equation (8a) by the standard deviation, we obtain

$$\tilde{u} = \frac{u}{\sigma_u}, \qquad \tilde{E} = \frac{E}{\sigma_u}, \qquad \tilde{u} = \tilde{E}\,\mathrm{a}\,, \tag{14}$$

where $\tilde{\mathbf{E}}$ is the design matrix (Press et al., 1997). The design matrix depends on the position of the source and stations, on the crustal model, and the considered frequency range, but does not depend on the waveforms. We can assess the theoretical parameter uncertainty even without recorded seismograms, and in the following, we demonstrate how. Any single parameter a_i then has a 1D Gaussian PDF. For example, if a_1 to a_5 take their optimal values, for a_6 we have

$$PDF(a_6) = \frac{e^{\frac{1}{2}\frac{(a_6 - a_{6opt})^2}{\sigma_{a_6}^{\ 2}}}}{\sigma_{a_6} \cdot \sqrt{2\pi}}\,, \tag{15}$$

which is independent of a particular value of $a_{6\mathrm{opt}}$, and the standard deviation σ_{a6} is given by the explicit formula (Press et al., 1997, section 15.4)

$$\sigma_{a_6}^{\ 2} = \sum_{i=1}^{6} \left(\frac{V_{6i}}{w_i} \right)^2 . \tag{16}$$

Here V_{6i} is the 6th component of the ith singular vector of the design matrix $\tilde{\mathbf{E}}$, and w_i is its ith singular value. In practice, we do not need the singular decomposition of matrix $\tilde{\mathbf{E}}$, as the singular vectors **V** of $\tilde{\mathbf{E}}$ are simply eigenvectors of matrix $\mathbf{E^T E}$, and the singular values of $\tilde{\mathbf{E}}$ can be calculated from the eigenvalues λ_i of $\mathbf{E^T E}$:

$$w_i = \sqrt{\frac{\lambda_i}{\sigma_u^{\ 2}}}\,, \qquad \mathrm{i}=1,2,...6 \tag{17}$$

The condition number (CN), is defined by

$$CN = \frac{\max\limits_{i=1,...6} (w_i)}{\min\limits_{i=1,...6} (w_i)}. \tag{18}$$

CN is useful in judging, at least in a relative sense, how well or ill posed is the inverse problem; small singular values (large CN) indicate an unstable solution.

Now consider $\Delta\chi^2$ (i.e., the theoretical misfit between data and synthetics, normalized by the data variance). The surfaces of constant theoretical misfit $\Delta\chi^2$ (a 6D ellipsoid) are given by (Press et al., 1997 section 15.6.)

$$\Delta\chi^2 = w_1^2(\mathbf{V}_1 \cdot \delta\mathbf{a})^2 + ... + w_6^2(\mathbf{V}_6 \cdot \delta\mathbf{a})^2\,, \tag{19}$$

where $\delta\boldsymbol{a}$ is the radius vector connecting the center of the ellipsoid and a point in the parameter space. It enables us to numerically construct a 1D probability density function of the a_6 parameter. The points can be found by numerically grid searching the 6D parameter space, and the grid limits are given by the standard deviations of the individual parameters. For algorithmic details, see the appendix of Zahradník and Custódio (2012). We discretize a_6, and for each value of a_6 we extract the points inside the ellipsoid $(a_1, a_2, ... a_5)|a_6$; here $|a_6$ denotes a fixed value of a_6. Each point is characterized by the theoretical misfit $\Delta\chi^2(a_6) \leq 1$, and we determine its minimum value $\Delta\chi^2_{\min}$ over all points $(a_1, a_2, ...a_5)|a_6$. Thus, we obtain a numerical approximation of the theoretical Gaussian 1D probability density function (15).

$$Theor_{PDF}(a_6; H = fixed; O = fixed) = e^{-\frac{1}{2}\min theor_{misfit}(a_1,...a_5)|a_6} . \quad (20)$$

Here the minimum theoretical misfit $\Delta\chi^2_{\min}$ was denoted min $\text{theor}_{\text{misfit}}$; note that a_6 is a free parameter that is varied, not computed by the inversion.

The theoretical justification of this approach comes from Section 15.6., Theorem D of Press et al. (1997). A simpler approach has been applied by Molnar and Lyon-Caen (1989) in the teleseismic waveform inversion; they determine the uncertainty of a parameter by fixing that parameter at a series of values and inverting for the other parameters. Although the numerical approximation equation (20) of the theoretical Gaussian distribution equation (15) is quite obvious and has no practical value, it serves as a good hint as to how proceed in the nonlinear case.

Isotropic Component – Uncertainty in the Nonlinear Case

In this case, the inverse problem has eight parameters: a_1, …a_6, H, and O. The nonlinearity is due to the effect of the centroid depth H and centroid time O. Contrary to the preceding section, the theoretical misfit function is no longer available. Thus, we use waveforms and evaluate the real misfit between the data and synthetic seismograms (i.e., misfit equation (10) normalized by the data variance). In analogy to equation (20), the so-called experimental probability density function can be evaluated:

$$Exper_{PDF}(a_6; H = free; O = free) = const \times e^{-\frac{1}{2}\min real_{misfit}(a_1,...a_5,H,O)|a_6} . \quad (21)$$

Here, the minimal real misfit is denoted min $\text{real}_{\text{misfit}}$. The meaning of equation (21) is as follows: A value of a_6 is chosen, and the real misfit is minimized by the least-squares method in a_1, …a_5 and by a grid search in H and O. Repeating this for a set of discrete a_6 values, we obtain a 1D PDF(a_6) reflecting the linear effect of a_1, …a_5 and nonlinear effects of H and O. The value of const normalizes the integral of PDF(a_6) to unity. The 1D experimental PDF in equation (21) is the main new tool proposed in this study.

New Algorithm

The only technical issue related to equation (21) that requires caution is the minimization of the misfit for each fixed value of a_6. For each a_6 we must find the

optimal centroid depth H and time O common to all a_1, …a_6. The algorithm is the following:

1. We choose a discrete value of a_6, (close to the previously computed optimal value, but not equal to this value) and a given trial value of H and O. We minimize the misfit between real data **u** and synthetics **s**, thus obtaining a_1, …a_5. Combining these inverted coefficients with the chosen coefficient a_6 we obtain $\mathbf{a}_{\mathbf{opt}}$.
2. The correlation between **u** and $\mathbf{s}=\mathbf{E}\,\mathbf{a}_{\mathbf{opt}}$ is calculated using equation (9).
3. The procedure is repeated for each trial O and H (still fixing the same a_6), and the H and O with maximum correlation are found for the chosen value of a_6. The corresponding misfit equation (10) is recorded for the given a_6, too.
4. The whole procedure is repeated for each value of a_6. As a result, we obtain the best-fitting parameters (a_1, …a_5, H,O), as well as the minimum misfit value (i.e., the min $\text{real}_{\text{misfit}}$ value), all as a function of a_6. Thus, we construct the desired experimental PDF(a_6) according to equation (21).

Although the proposed method yields a 1D PDF(a_6), it correctly takes into account the 8D nature of the problem, as well as its nonlinearity. On the other hand, the uncertainty of the crustal structure model is not included. It must be solved by repeating the analysis using several models that are available.

DATA AND CONVENTIONAL ANALYSIS

A moderate earthquake swarm started on 26 June 2009 northeast of the Santorini (Thira) Island, close to Mt. Columbo, an active submarine volcano in the Cyclades, Aegean Sea. The swarm occurred at the western boundary of the Santorini–Amorgos zone, a major structural unit in the Hellenic volcanic arc, where the strongest instrumentally recorded event occurred on 9 July 1956 (reported M_w ranging from 7.5 to 7.8), producing a great tsunami (e.g., Ambraseys, 1960; Galanopoulos, 1960; Papazachos and Papazachou, 2003; Okal et al., 2009; Konstantinou, 2010). The region around the Columbo volcano features strong temporal variations of shallow (< 10 km) seismic activity on a high background level, interpreted as due to magma and fluid migrations (Bohnhoff et al., 2006). Dimitriadis et al. (2009) complemented the analysis of the Columbo volcano activity by joint relocation and inversion of the upper crustal structure; focal mechanisms of 20 small events were reported, proving a prevailing normal-faulting pattern with a northwest-southeast extension at shallow depths (6-9 km).

Here we focus on the two largest events (26 June, $M_w > 4$) of the 2009 Mt. Columbo swarm. Table 1 gives the routine location parameters, determined by the Aristotle University of Thessaloniki (AUTH). The earthquakes were recorded with a good azimuthal coverage by the broadband stations of the Hellenic Unified Seismic Network (HUSN), spanning the epicentral distances approximately from 60 to 310 km (Fig. 1a). We use the records from 15 and 10 stations of events 1 and 2, respectively, which provided a good signal-to-noise ratio even at relatively low frequencies (0.02-0.1 Hz), which are feasible for modeling. By “feasible” we mean

Table 1

Hypocentral Parameters of the Investigated Events

	Date (yyyy/mm/dd)	Time (hh:mm:ss.ss in UTC)	Latitude (°N)	Longitude (°E)	Depth (km)	M_w
Event 1	2009/06/26	20:37:38.10	36.531	25.434	9.70	4.9
Event 2	2009/06/26	22:14:53.50	36.544	25.523	4.10	4.7

Reported by the Aristotle University of Thessaloniki, Department of Geophysics.

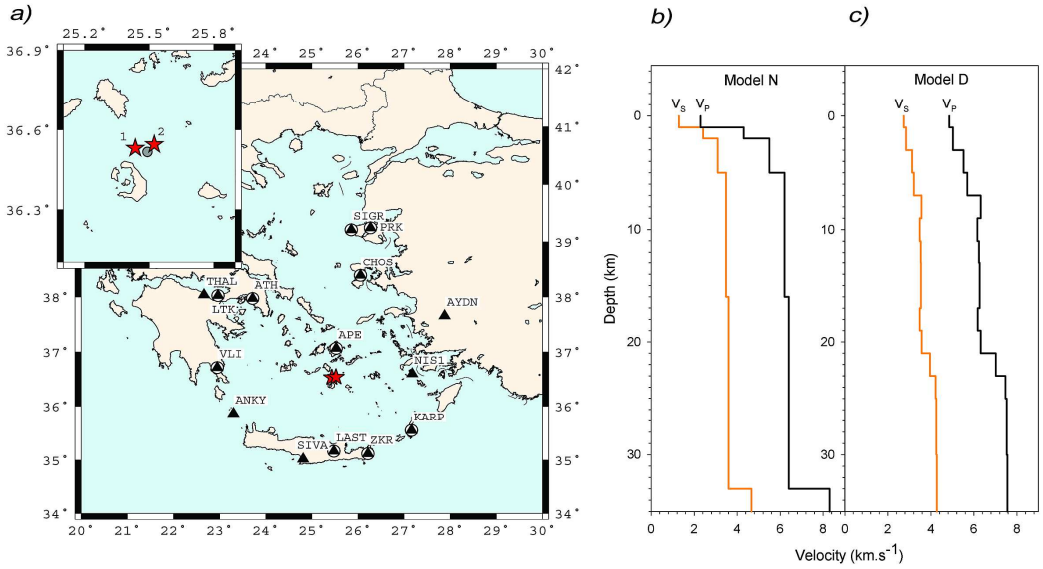

Figure 1. (a) Broadband stations (triangles) whose records were used to study the two earthquakes, marked as event 1 and 2 (stars) in the inset, with epicenters close to Mt Columbo volcano (circle in the inset). Marked with encircled triangles are the stations available for both event 1 and 2. (b) Crustal model N (Novotný et al., 2001). (c) Crustal model D (Dimitriadis et al., 2010); see also Table 2. The color version of this figure is available only in the electronic edition.

that the available crustal models are adequate to model the wave propagation effects and provide satisfactory waveform match up to frequency of 0.1 Hz in the studied epicentral distances. Two 1D models are employed: (1) the model by Novotný et al. (2001), hereafter "model N", obtained from the regional surface-wave dispersion, in which *Lg* waves dominate, and it is routinely used for MT inversions at AUTH; and (2) the model by Dimitriadis et al. (2010), hereafter "model D", sufficiently predicting local first-arrival times (Table 2 and Fig. 1b,c). The attenuation quality factors reported in the footer of Table 2 represent rough estimates; the waveform inversion is almost insensitive to their particular values in the studied range of epicentral distances and frequencies.

The MT inversion was performed using ISOLA software (Sokos and Zahradník, 2008). ISOLA (from ISOLated Asperities) is a program package based on the multiple point-source iterative deconvolution of complete regional waveforms. Green's functions are calculated by the discrete-wavenumber method (Bouchon,

Table 2
The Two 1D Crustal Models Used

Model N*		Model D†	
Layer Top (km)	V_P(km/s)	Layer Top (km)	V_P(km/s)
0.0	2.30	0.0	4.85
1.0	4.30	1.0	5.03
2.0	5.50	3.0	5.52
5.0	6.20	5.0	5.69
16.0	6.40	7.0	6.31
33.0	8.30	9.0	6.16
		11.0	6.23
		13.0	6.27
		17.0	6.17
		19.0	6.32
		21.0	7.02
		23.0	7.46
		25.0	7.52
		30.0	7.56

Density(g/cm^3) $= 1.7 + 0.2V_P$(km/s)
*$V_P/V_S = 1.78$, $Q_P = 300$, $Q_S = 300$.
†$V_P/V_S = 1.77$, $Q_P = 300$, $Q_S = 150$.

1981; AXITRA code of Coutant, 1989). The moment tensor is solved by the least-squares method, and the origin time and 3D position of the point source (centroid) are both grid searched, the latter in the vicinity of the (independently) located hypocenter. In the preliminary stage, we considered variations of the centroid position both in the horizontal direction and depth. In the following discussions, for simplicity, we concentrate only on grid searching the centroid depth. The method is routinely used in the Seismological Laboratory of the University of Patras to calculate moment tensors in western Greece. ISOLA also proved useful in a number of earthquake studies (e.g., Zahradník, Jánský, et al., 2008; Gallovič et al., 2009; Zahradník and Gallovič, 2010). Here we use a single point-source approximation and work in three MT-inversion modes of ISOLA: DC-constrained MT (i.e., pure DC), deviatoric MT, and full MT. The noisy components at a few stations were excluded from the inversion. The best-fitting solutions of event 1 and 2 (in the two crustal models) are presented in Figure 2. In Table 3, each event is characterized by its strike, dip, rake, centroid depth, scalar moment M_0, moment magnitude M_w, the percentages of ISO, DC, and abs(CLVD), the global VR, and condition number. An example of the match between the observed and synthetic displacements is given in Figure 3; for comparison with the full-MT solution, a pure DC solution is also presented. We have chosen the DC solution with the same origin time, strike, dip, rake, and scalar moment as used in the plotted full-MT solution. Its variance reduction (VR=0.43) is considerably lower than that of the full-MT solution (VR=0.66).

As shown in Figure 2 and Table 3, the most remarkable difference between the full-MT solutions of event 1 is due to the crustal models used, especially in the case of the 10 stations, where the explosion-like mechanism in model N changes to implosion in model D. The latter has a greater variance reduction. Another important

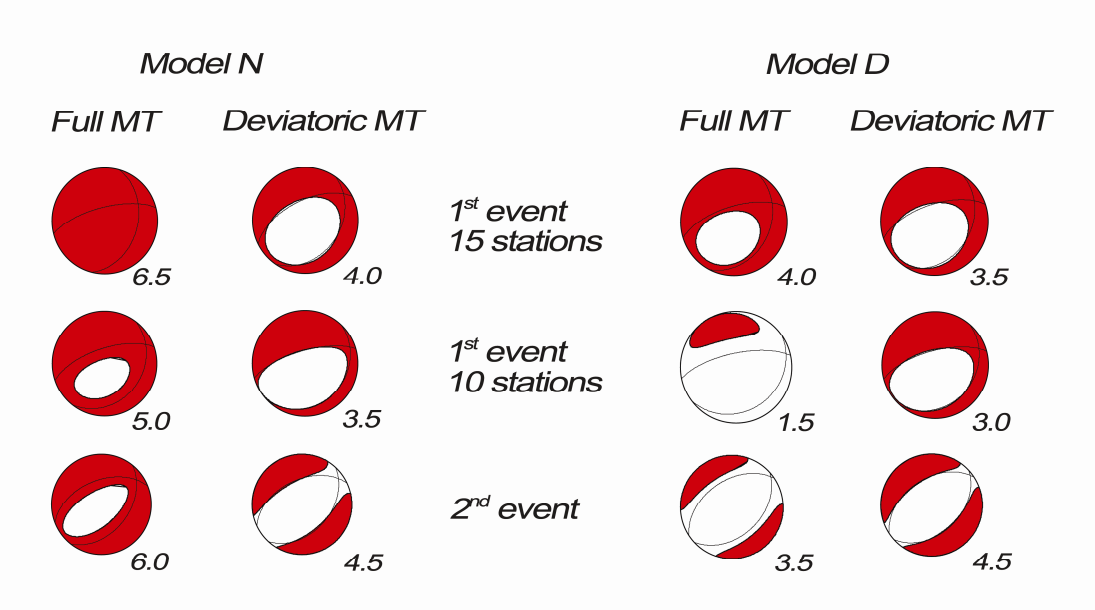

Figure 2. MT solutions for event 1 and event 2 as obtained in this study for each crustal model. The MT inversion for event 1 was run twice: using the total 15 available stations (top) and using 10 stations (middle) common with event 2 (bottom). For details, see Table 3. The computed depth (km) is shown to the right of the beachballs. The color version of this figure is available only in the electronic edition.

feature is the different centroid depth of the deviatoric and full-MT solutions, while their variance reductions are almost the same. It indicates the trade-off between the depth and the non-DC part of the MT.

We will discuss further the two cases in Table 3 (event 1) for the solutions using 15 and 10 stations. We compare these two cases because for event 2 we have only 10 stations. Therefore, for event 1 we used these 10 stations, but also the whole 15-station set. The comparison shows that the 10- and 15-station cases provide somewhat different results. In particular, in the 10-station case (event 1) we find a relatively large difference between the centroid depths in model N and model D (5 and 1.5km, respectively), and also the variation of the ISO percentage is large, even comprising the opposite sign (+32 percent in model N and –33 percent in model D). We believe that in the 10-station case (event 1), the depth and ISO in model D are less well constrained than in model N, as suggested by the condition numbers (16.27 and 4.24 in D and N, respectively). The 15-station case (event 1) has a weaker variation; for example, ISO is positive in both models N and D. The DC parameters are less affected by the assumed crustal model than the non-DC parameters. All these resolvability issues are analyzed in more detail in the next sections.

The stability of the MT solution was further examined by jackknifing the data (i.e., systematically removing one station from the inverted data set). The results are summarized in Figure 4. Event 1 has a relatively large ISO percentage in model N. Event 2 is characterized by the opposite sign of ISO in the two applied crustal models.

Table 3
Moment Tensor (MT) Inversion

Event	Model	Inversion Mode	Strike (°)	Dip (°)	Rake (°)	Depth (km)	M_w	M_0 (Nm)	DC*	CLVD†	ISO‡	VR§	CN¶
Event 1: 15 Stations Used	Model N	DC-constrained MT	241	65	−80	3.5	4.6	9.51×10^{15}	100.0	0.0	0.0	0.62	3.75
			38	26	−110								
		Deviatoric MT	243	59	−74	4.0	4.7	1.06×10^{16}	59.2	40.8	0.0	0.64	3.20
			34	33	−114								
		Full MT	255	69	−57	6.5	4.7	1.12×10^{16}	41.9	5.0	+53.1	0.66	3.34
			15	38	−144								
	Model D	DC-constrained MT	247	70	−78	2.5	4.7	1.20×10^{16}	100.0	0.0	0.0	0.67	4.11
			35	22	−120								
		Deviatoric MT	251	63	−70	3.5	4.7	1.33×10^{16}	52.4	47.6	0.0	0.70	3.59
			32	32	−124								
		Full MT	253	65	−67	4.0	4.7	1.17×10^{16}	48.6	28.0	+23.5	0.70	5.09
			27	32	−130								
Event 1: 10 Stations Used	Model N	DC-constrained MT	253	71	−79	3.5	4.6	1.01×10^{16}	100.0	0.0	0.0	0.67	3.81
			44	21	−117								
		Deviatoric MT	254	70	−78	3.5	4.6	1.02×10^{16}	87.7	12.3	0.0	0.67	3.81
			42	22	−119								
		Full MT	251	66	−74	5.0	4.6	8.49×10^{15}	57.1	10.8	+32.1	0.68	4.24
			36	27	−121								
	Model D	DC-constrained MT	256	73	−77	2.5	4.7	1.25×10^{16}	100.0	0.0	0.0	0.77	4.52
			38	20	−126								
		Deviatoric MT	254	68	−75	3.0	4.7	1.20×10^{16}	74.9	25.1	0.0	0.78	3.73
			39	25	−122								
		Full MT	258	69	−81	1.5	4.9	2.71×10^{16}	33.9	33.1	−33.0	0.78	16.27
			53	22	−112								
Event 2	Model N	DC-constrained MT	239	47	−81	5.0	4.5	5.37×10^{15}	100.0	0.0	0.0	0.65	3.65
			46	43	−99								
		Deviatoric MT	244	49	−75	4.5	4.4	4.34×10^{15}	69.4	30.6	0.0	0.65	3.45
			42	42	−106								
		Full MT	248	49	−69	6.0	4.4	4.48×10^{15}	35.9	38.8	+25.3	0.65	4.00
			38	44	−112								
	Model D	DC-constrained MT	234	46	−83	4.5	4.5	6.37×10^{15}	100.0	0.0	0.0	0.70	3.63
			45	44	−96								
		Deviatoric MT	236	46	−82	4.5	4.5	5.70×10^{15}	81.7	18.3	0.0	0.70	3.63
			46	43	−97								
		Full MT	236	47	−83	3.5	4.5	7.00×10^{15}	72.2	3.7	−24.1	0.70	6.38
			47	43	−96								

*DC, percentage of double couple.
†CLVD, percentage of compensated linear vector dipole.
‡ISO, percentage of isotropic part.
§VR, variance reduction (equation 11).
¶CN, condition number (equation 18).

NEW ANALYSIS OF ISOTROPIC COMPONENT

Figure 5a demonstrates the waveform correlation as a function of the trial depth, grid searched from 2.5 to 15 km, in steps of 0.5 km, event 1 (15 stations) and model N; the correlation is defined in equation (9). Plots such as that shown in Figure 5a represent a traditional inversion tool, used to define the optimal depth. Nevertheless, we also employ a less widely used approach: at each trial depth, we calculate the corresponding value of the ISO percentage. Although the independent variable is only depth, while the misfit and isotropic component are depth dependent, we can analyze the correlation (and depth) as a function of ISO (Fig. 5b). This plot is

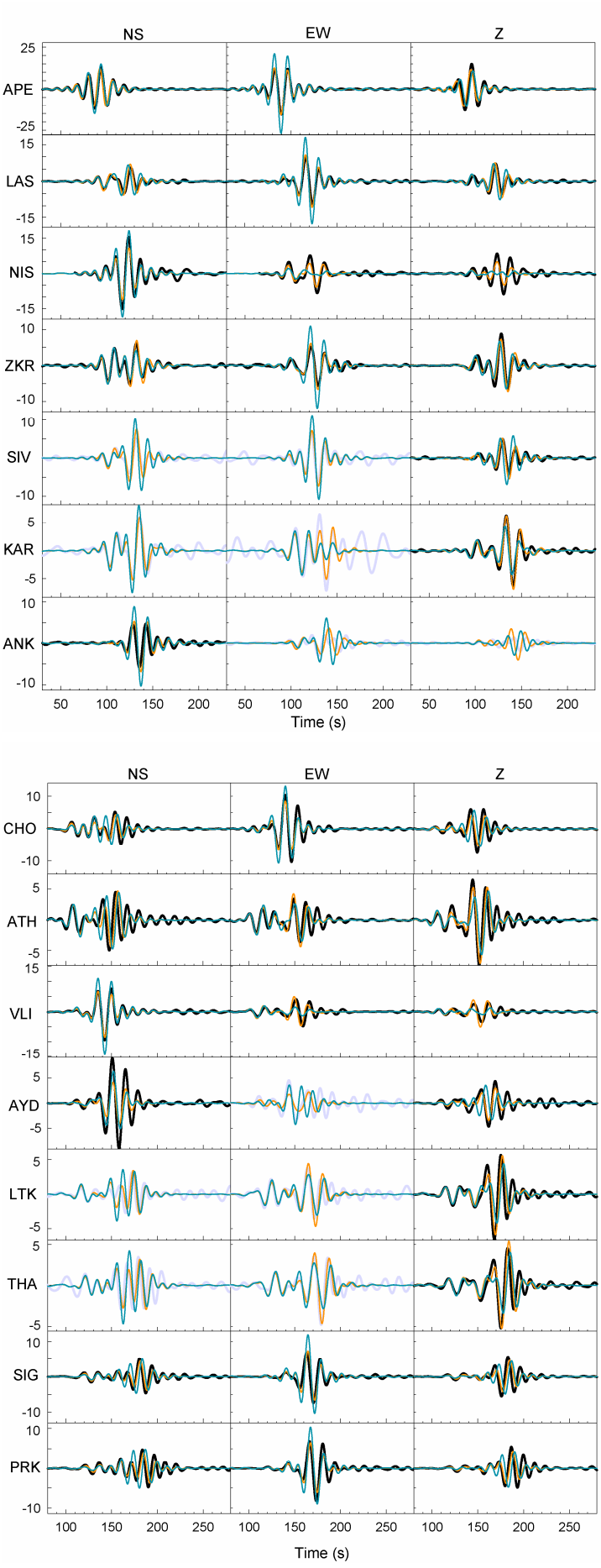

Figure 3. Comparison of observed and synthetic seismograms for event 1, using the records from all 15 stations and crustal model N. Observed traces are plotted as thick black lines, except those excluded from the inversion due to noise (bold gray). Two types of synthetics are demonstrated: the best-fitting full-MT solution (thin lighter line, variance reduction 0.66; for example, the maximum amplitude of APE-EW and SIV-EW component), and the pure DC solution (thin darker line, variance reduction 0.43; for example the maximum amplitude of LTK-EW and THA-EW component); the origin time, strike, dip, rake, and scalar moment of the latter are the same as in the full-MT solution. The vertical axis is scaled in 10^{-6} m. The color version of this figure is available only in the electronic edition.

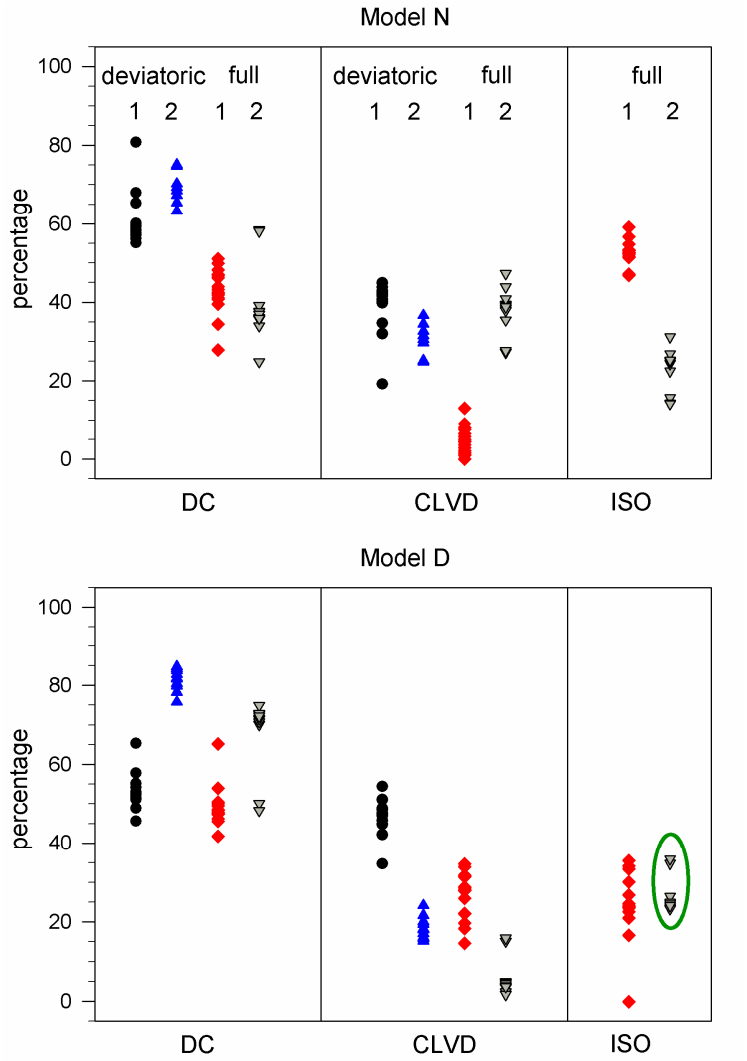

Figure 4. Stability tests regarding the percentage of DC, CLVD, and ISO as obtained by jackknifing the data, for the two structural models used (top: model N; bottom: model D). Each symbol in the plots corresponds to a single-station removal from the inversion. Numbers 1 and 2 at the top of the columns refer to event 1 and event 2, respectively. Event 1 (15 stations) and event 2 (10 stations) were inverted in the deviatoric and full-MT modes. The deviatoric solutions for events 1 and 2 are shown by the dots and upward pointing triangles, respectively. The full-MT solutions for events 1 and 2 are shown as diamonds and downward pointing triangles. Some symbols overlap due to rounding off the percentages to integer values. The CLVD and ISO percentages are shown in absolute values. The ellipse marks the case of the negative ISO. The color version of this figure is available only in the electronic edition.

analogous to the "correlation versus DC plots" introduced by Zahradník, Sokos, et al. (2008). It clearly demonstrates the trade-off between the depth and ISO percentage.

The ISO values in Figure 5b have been complemented by error bars, using a method suggested by Zahradník and Custódio (2012). It is a simple method applicable to the linear case (*H* and *O* assumed to be known; *H* = hypocenter position, *O* = origin time). In brief, the idea is as follows: a set of points inside the

6D theoretical error ellipsoid is found numerically and converted into histograms of the strike, dip, rake and ISO, thus providing also an estimate of their bounds. The minimum and maximum values of ISO, found from the histograms, define the error bars plotted in Figure 5b. Note the considerably larger uncertainty of small ISO percentages at the shallow source depths; see, for example, the large error bar of the ISO = 2.5 at the depth of 3.5 km (correlation = 0.833).

In Figure 5c we replot the content of Figure 5b in such a way that the isotropic component on the horizontal axis, so far described by ISO, is now described by $\mathrm{tr}(\mathbf{M})/3=a_6$, thus we can directly make use of the σ_{a6} values of equation (16) to plot the a_6 error bars.

The error bars introduced in Figure 5b and 5c represent important additional insight to the information carried by the misfit values. Indeed, even the solutions that have high correlation (low misfit) might be irrelevant if the parameter error is large. Large parameter errors indicate poor constraint of the studied parameter by the data. For example, as seen in Figure 5b, although the correlation takes similar values (0.84) at depths of 4.5 and 9 km (where the ISO percentage is about 30 and 65, respectively), the corresponding uncertainty of ISO is not the same; the error bar is larger for the depth of 4.5 km.

A new, deeper insight into the uncertainty of the isotropic component, fully reflecting the nonlinearity of the joint inversion of MT and the centroid depth and time, can be gained by means of the experimental PDF defined in equation (21). The example for event 1 in Figure 6 is calculated in the same source-station setup as the one used to construct Figure 5. As the numerical analysis has provided the combination of (a_1, … a_5, H,O) for each value of the independent variable a_6, we can demonstrate in the same figure also the variation $H=H(a_6)$, H being the source depth. We also demonstrate the variation of the focal mechanisms. The variation of the centroid time $O(a_6)$ is weak, and thus not shown in Figure 6. (For the depth range from 2.5 km to 15.0 km, the centroid time varied within 0.15-0.30 seconds before the origin time reported in Table 1.)

Besides the PDF constructed according to equation (21), shown in Figure 6 as the large dots, plotted in the same figure as small dots are 15 fixed-depth PDF's. They represent a modification of equation (21) in which only a_1,…a_5 and O are subjected to optimization without the depth H. The procedure is repeated for a set of chosen depth values. All depths have the same normalization constant, in this example equal to the value const of equation (21). The probability density functions at the individual depths (fixed H, variable O) are close to the theoretical Gaussian functions of the linear case (fixed H and O). The PDF function of the fully non-linear case (variable H and O), shown as the large dots, is their envelope. The envelope is also close to the Gaussian in the studied example, but this is not necessarily always the case, as demonstrated later in Figure 7. The envelope indicates the same optimal a_6 as in the individual fixed-depth cases. However, its width is much greater than that of the individual fixed-depth functions. It demonstrates how the uncertainty of a_6 increases if the depth is an unknown parameter.

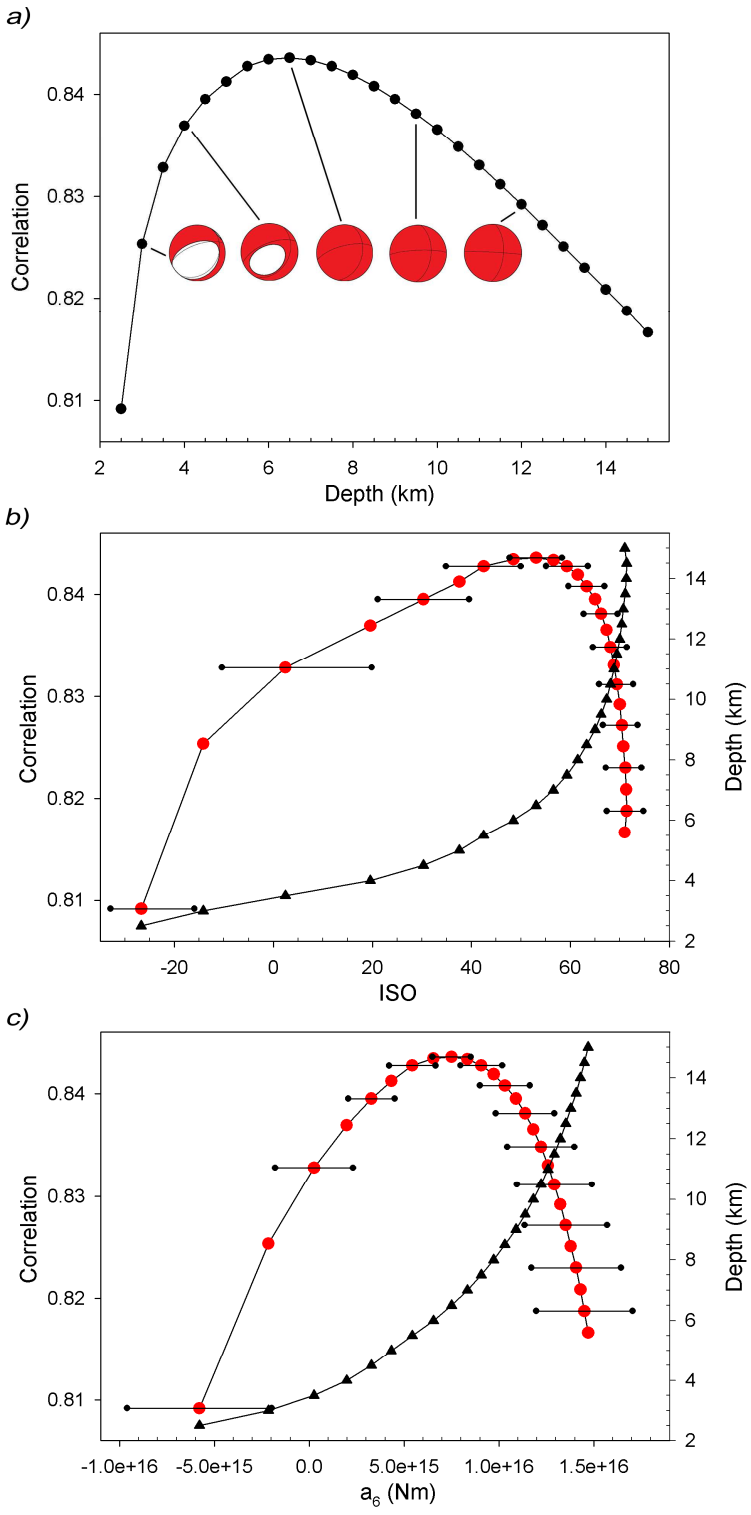

Figure 5. Uncertainty of event 1 as revealed by grid-searching the centroid depth using the entire set of 15 stations and crustal Model N. (a) Waveform correlation between observed and synthetic waveforms as a function of the trial-source depth. The full-MT solutions (beachballs) are shown for selected depths. (b) Correlation (dots) and depth (triangles) as a function of ISO percentage. (c) Correlation and depth as a function of the a_6 model parameter of this paper, $a_6 = \mathrm{tr}(\mathbf{M})/3$. The color version of this figure is available only in the electronic edition.

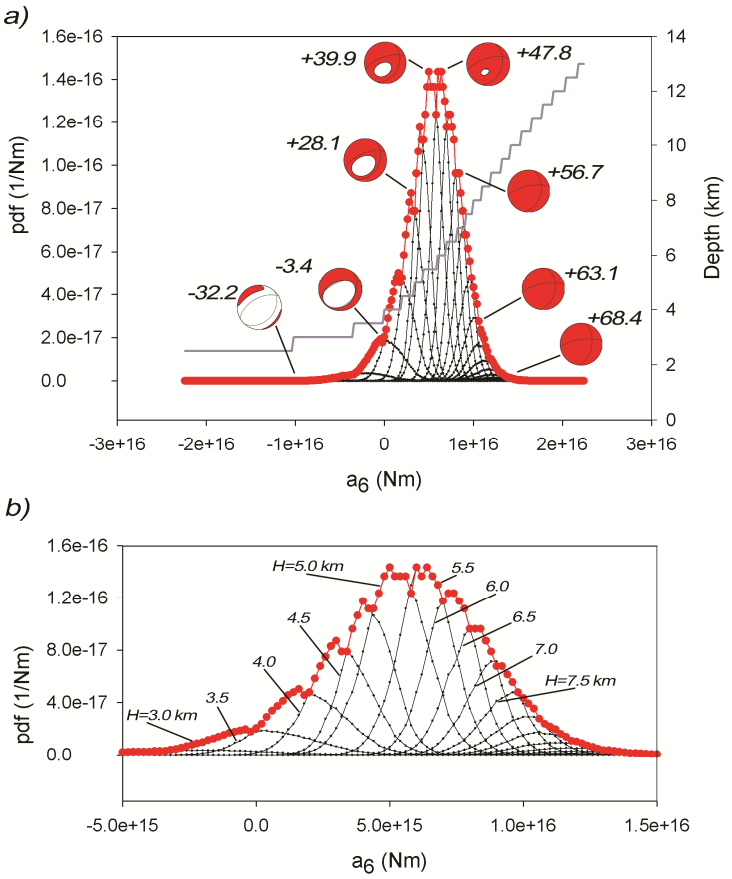

Figure 6. The uncertainty assessment of the isotropic component a_6 = tr(**M**)/3 for event 1; employing 15 stations and the crustal Model N. The experimental 1D PDF(a_6) is calculated by two methods: large dots, using equation (21) to consider the full trade-off between the moment tensor, centroid depth *H* and origin time *O*; and small dots, using the modification of equation (21), repeatedly fixing the depth value (from 1.5 km to 13.0 km with step of 0.5 km). The obtained depth variation $H=H(a_6)$ is shown by the staircase curve. Attached to selected large dots are the full-MT solutions (beachballs) and the corresponding ISO percentage. Panel (b) is a zoom of panel (a) to better visualize the individual fixed-depth curves. The color version of this figure is available only in the electronic edition.

In the nonlinear analysis presented above, both the optimal and nonoptimal solutions were derived for a fixed crustal model. Because the crustal model is also uncertain, we have to take it into consideration, too. Because the crustal model parameters do not belong to the model parameters of our inverse problem, the effect of the model should be studied by comparing alternative crustal models (the following Fig. 7).

Finally, the method of the experimental 1D PDF(a_6), proposed in equation (21), is applied to the two investigated $M_w > 4$ earthquakes, using the two available crustal models (Fig. 1b,c; Table 2). The results are summarized in Figure 7. Each function was normalized to a unit integral using (its own) normalization constant const in

equation (21). Event 1 (Fig. 7a) is processed with 15 and 10 stations. The difference between the 15- and 10-station cases is evident, but it is smaller than the difference due to the crustal model used. While event 1 is most likely characterized by $a_6 > 0$ in model N, the probability density function is considerably broader in model D, making almost no preference between $a_6 > 0$ (explosion) and $a_6 < 0$ (implosion). Event 2 (Fig. 7b) was processed only with the 10 available stations. The effect of the crustal model is the same as for event 1. Comparing the two events in model N, the isotropic component of event 2 is closer to zero, but it is also less well constrained than event 1, as indicated by the wider probability distribution in Figure 7b.

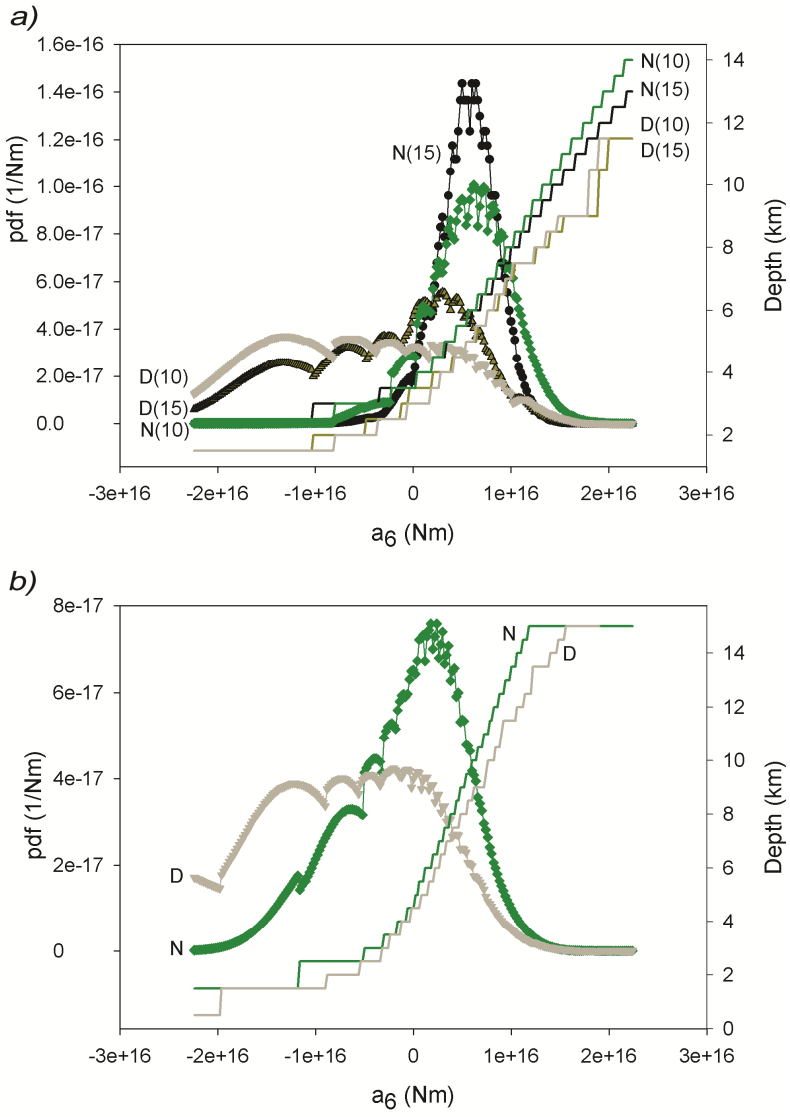

Figure 7. The uncertainty assessment of the isotropic component, PDF(a_6), calculated using equation (21) in two crustal models, N and D. (a) Event 1 is processed in model N for 15 stations (dots) and 10 stations (diamonds), and also in model D for 15 stations (upward pointing triangles) and 10 stations (downward pointing triangles). (b) Event 2 is processed with 10 stations in model N (diamonds) and D (downward pointing triangles). The corresponding relations $H(a_6)$ are also shown. The color version of this figure is available only in the electronic edition.

It is out of scope of this paper to study geological reliability of the two velocity models. We simply want to stress how strongly the assumed crustal structure can affect the uncertainty of the isotropic component, even though the considered frequencies were as low as < 0.1 Hz. Observing the large uncertainty of a_6 in model D (i.e., its wide PDF), we also recall that model D was characterized by a smaller misfit than model N (i.e., the larger VR in Table 3). This illustrates the limited meaning of the waveform misfit itself; indeed, the solution of a small misfit might yield an uncertain a_6 due to specific features of the assumed crustal model. Note that the poor resolvability of the isotropic component in model D corresponds to the poor resolvability of the shallow source depth. The main differences between the two considered crustal models are in their shallow part and different MOHO depth. As a whole, Model D is faster. The inferior resolvability of the MT in faster models was also theoretically predicted by Zahradník and Custódio (2012). In other words, if the real earth crust is like that in model D, the joint inversion of the full MT and the depth is problematic; an independent (location) constraint of the depth would be desirable, if accurate enough. If the real crust is like that in model N, the source depth (of about 6 km) is greater than in model D, and the trade-off between the isotropic component and the depth is weaker. Therefore, in this particular case, the joint inversion of the full MT and the depth is more feasible, and the necessity of an independent depth constraint is less crucial.

CONCLUSIONS

The isotropic component of the MT measures any volume change in an earthquake, and its study is significant, especially in volcanic and geothermal regions. To relate the isotropic component to a physical model of the shear dislocation, crack opening, and fluids is not straightforward, and it is beyond the scope of the present work.

In this methodic article, we focus on how to obtain the isotropic component and define its uncertainty using near-regional, low-frequency broad band waveforms (epicentral distances 60–310 km, f < 0.1 Hz). This task is more difficult than a routine deviatoric moment tensor inversion because the isotropic component is more sensitive to any uncertainties related to the hypocenter position and the crustal structure, as well as to any natural and instrumental noise. The isotropic component of a moment tensor **M** is parameterized in this study by the ISO percentage (independent of the source size) and also directly by tr(**M**)/3 (dependent on the source size). The advantage of the latter is that it represents one of the model parameters in our formulation of the inverse problem (a_6 = tr(**M**)/3).

The scope of this work is to develop a new simple method in order to construct a 1D probability density function of a_6, PDF(a_6). Towards this goal, PDF(a_6) is constructed using the experimental method of equation (21): the parameter a_6 is fixed at a series of values (in the vicinity of the optimal a_6), and for each trial a_6 value we seek the minimum misfit between the observed and synthetic seismograms. The minimization is made by the least-squares method for parameters a_1, …a_5 of the MT and by a grid search over the centroid depth and time. The results of this new technique are compared to those of the conventional analysis. To be more

specific, by conventional analysis we mean repeated calculations of MT (and its isotropic component) for a series of trial-source depths, accompanied by a stability check (jackknifing by repeatedly removing one station). The experimental PDF(a_6) and the conventional method were applied to two shallow M_w 4+ events (event 1 and event 2, respectively) in a volcanic region of the Aegean Sea, Greece, using two different crustal models.

The innovative part of this work is the experimental PDF(a_6) and its application as summarized in Figure 7. Event 1 was analyzed twice, using 15 and 10 stations, respectively. The latter case was considered to facilitate comparison with event 2, for which data from only 10 stations were available. Minor differences between the 15- and 10-station results were found. Most prominent is the effect of the crustal models used: model N (Novotný et al., 2001) and model D (Dimitriadis et al., 2010). Both structural models provide satisfactory waveform match of observed and synthetic seismograms, as evident from the variance reduction, VR ~0.7 listed in Table 3. However, if the true structure of the Earth is closer to model D, then the isotropic component is almost irresolvable, as documented by its wide PDF. If the true crust can be approximated by model N, the PDF is narrower and yields a better resolution, in particular for event 1 (a positive isotropic percentage of about 30 to 50 at depths of 4-6 km). These results have an important implication, which stems from the fact that both velocity models provide sufficient fit between the observed and synthetic waveforms. We are unable to prefer any of the two models, thus we cannot say whether the resolution of the isotropic component is relatively good (in model N) or poor (in model D). In general, if the knowledge of the velocity model is poor, it is useful to test very different velocity models (providing a reasonable waveform match, like models N and D), not only to apply a single available model and perform its statistical perturbation.

A notable feature illustrated in Figure 7 is the strong trade-off between the isotropic component and source depth. It is stronger than the trade-off of the isotropic component with the seismic moment, source angles (strike, dip, and rake) and origin time. We can even state that the isotropic component mainly trades off with depth. Therefore, in model D, waveforms require shallower depths (1.5 to 4 km for event 1) than in model N (4 to 6 km), and the shallow depths tend to provide the negative isotropic component in the studied case. The source depth is a factor considerably affecting the resolvability of the isotropic component, which is also demonstrated by the (nonmonotonic) variability of the error bars in Figure 5, calculated in the approximation of a repeatedly fixed depth. Note also the poor MT resolution at the shallow depth of 1.5 km signaled by the condition number CN as large as 16.27 in the case of event 1, 10 stations in model D (Table 3).

Although the effect of the structural model is quite obvious in Figure 7, it is true that at a given source depth the two models N and D provide a similar estimate of the a_6 parameter. This observation seems to suggest the MT inversion at the location (hypocenter) depth, especially for moderate-size earthquakes, whose hypocenter and centroid are close to each other. However, it has been shown that for shallow crustal events the depth determination is always difficult (Zahradnik, Jánský,

et al., 2008; Janský et al., 2009, 2012; Sokos et al., 2012), hence the MT inversion at the hypocenter depth cannot be generally recommended, unless dense local networks and precise crustal models are available. It might also seem that a compromising solution is to perform an MT inversion only for the deviatoric part (constrain ISO component to zero), determine the centroid depth, and then, keeping the depth value fixed rerun the inversion using the full MT decomposition. This approach, which is apparently very attractive, especially when the correlation-depth dependence in the deviatoric regime has a sharper maximum than in the full MT regime, is generally not viable. This stems from the fact that a MT deviatoric inversion for an earthquake which has a significant ISO component may result in an incorrect depth. The latter has been unambiguously proven in a simple synthetic test, even for the ideal case of noiseless data and exact Green's functions.

Finally, we would like to bring to the reader's attention one observation that is significant for those who dislike the idea of installing, learning and running new codes for the calculation of PDF(a_6) as suggested in equation (21). This observation refers to the strong similarity of the isotropic component uncertainty estimates obtained from the conventional analysis and from our new approach. This similarity becomes apparent when comparing the behavior of the ISO percentages in Figure 4 (conventional) and Figure 7 (new). Both figures illustrate the strong effect of the assumed crustal model. The isotropic component is positive, relatively large, and better resolved for event 1, under the assumption that the relevant crustal model is model N. It implies that, with the conventional methods, if the full MT inversion is run for a series of trial centroid depths and times, and if careful jackknifing of the data is performed, then a reasonable estimate of the uncertainty of the isotropic component can be obtained. This uncertainty would considerably decrease if the crustal model is very well known and the location is highly accurate; the location-constrained depth then would reduce the trade-off between the isotropic component and the source depth.

DATA AND RESOURCES

Broadband waveforms were retrieved from the permanent stations of the Hellenic Unified Seismic Network (HUSN), operated jointly by the National Observatory of Athens (NOA), the Aristotle University of Thessaloniki (AUTH), the University of Patras (UPSL) and the University of Athens (UOA). The records from one station of the National Seismic Network of Turkey (DDA) were also used. Some UPSL stations are co-operated by the Charles University in Prague. Software ISOLA (Sokos and Zahradník, 2008) was used to calculate the moment tensors. Green's functions in ISOLA were computed using the AXITRA code of Coutant (1989). The Generic Mapping Tools (GMT; Paul Wessel and Walter H. F. Smith, http://gmt.soest.hawaii.edu/, last accessed April 2013) and MATLAB (http://www.mathworks.com/products/matlab/, last accessed April 2013) were also used.

ACKNOWLEDGEMENTS

A partial financial support was obtained from the grant agencies in the Czech Republic: GAUK 14509, GACR 210/11/0854, MSM 0021620860, and SVV-2012-265308. Anastasia Kiratzi acknowledges partial support co-financed from the European Union (European Social Fund) and Greek national funds-Research Funding Program: Thales "Investing in knowledge society through the European Social Fund" and from a Greece-Turkey bilateral project. We also thank Iordanis Dimitriadis for providing the average 1D model obtained from the 3D inversion for the Columbo region. The comments and suggestions of two anonymous reviewers and of Hrvoje Tkalčić are gratefully acknowledged.

REFERENCES

Aki, K., and P. G: Richards (2002), *Quantitative seismology,* University Science Books, Sausalito, California, 704 pp.

Ambraseys, N. N. (1960). The seismic sea wave of July 9th 1956, in the Greek Archipelago, *J. Geophys. Res.* **84,** 1561–1568.

Auger, E., D'Auria, L., Martini M., Chouet, B., and P. Dawson (2006). Real-time monitoring and massive inversion of source parameters of very long period seismic signals: An application to Stromboli Volcano, Italy, *Geophys. Res. Let.* **33,** L04301, doi:10.1029/2005GL024703.

Bohnhoff, M., M. Rische, T. Meier, D. Becker, G. Stavrakakis, and H.-P. Harjes (2006). Microseismic activity in the Hellenic Volcanic Arc, Greece, with emphasis on the seismotectonic setting of the Santorini-Amorgos zone, *Tectonophysics* **423,** 17-33.

Bouchon, M. (1981). A simple method to calculate Green's functions for elastic layered media, *Bull. Seismol. Soc. Am.* **71,** 959-971.

Coutant, O. (1989). Program of numerical simulation AXITRA, *Tech. rep.*, LGIT, Grenoble, France (in French).

Davi, R., G. S. O'Brien, I. Lokmer, C. J. Bean, P. Lesage, and M. M. Mora (2010). Moment tensor inversion of explosive long period events recorded on Arenal volcano, Costa Rica, constrained by synthetics tests, *Journal of Volcanology and Geothermal Research*, **194,** 189-200.

Dimitriadis, I., E. Karagianni, D. Panagiotopoulos, C. Papazachos, P. Hatzidimitriou, M. Bohnhoff, M. Rische, and T. Meier (2009). Seismicity and active tectonics at Coloumbo Reef (Aegean Sea, Greece): Monitoring an active volcano at Santorini Volcanic Center using a temporary seismic network, *Tectonophysics* **465,** 136-149.

Dimitriadis, I., C. Papazachos, D. Panagiotopoulos, P. Hatzidimitriou, M. Bohnhoff, M. Rische, and T. Meier (2010). P and S velocity structures of the Santorini-Coloumbo volcanics system (Aegean Sea, Greece) obtained by non-linear inversion of travel times and its tectonic implications, *J. Volcanol. Geoth. Res.* **195,** 13-30.

Dreger, D. S., H. Tkalčic, and M. Johnston (2000). Dilational processes accompanying earthquakes in the Long Valley caldera. *Science* **288,** 122 (2000), DOI: 10.1126/science.288.5463.122.

Dufumier, H., and L. Rivera (1997). On the resolution of the isotropic component in moment tensor inversion, *Geophys. J. Int.* **131,** 595-606.

Ford, S. R., D. S. Dreger, and W. R. Walter (2010). Network sensitivity solutions for regional moment-tensor inversions, *Bull. Seismol. Soc. Am.* **100,** 1962-1970.

Galanopoulos, A.G. (1960). Tsunamis observed on the coasts of Greece from Antiquity to present time, *Ann. di Geofis.* **13,** 369-386.

Gallovič, F., J. Zahradník, D. Křížová, V. Plicka, E. Sokos, A. Serpetsidaki, and G-A. Tselentis (2009). From earthquake centroid to spatial-temporal rupture evolution: Mw 6.3 Movri Mountain earthquake, June 8, 2008, Greece, *Geophys. Res. Let.* **36,** L21310, doi: 10.1029/2009GL040283.

Hudson, J. A., R. G. Pearce, and R. M. Rogers (1989). Source type plot for inversion of the moment tensor, *J. Geophys. Res.* **94,** 765-774.

Janský, J., O. Novotný, V. Plicka, and J. Zahradník (2012). Earthqake location from P-arrival times only: problems and some solutions, *Stud. Geophys. Geod.* **56,** 553-566, DOI: 10.1007/s11200-011-9036-2.

Jánský, J., J. Zahradník, and V. Plicka (2009). Shallow earthquakes: shallower than expected?, *Stud. Geophys. Geod.* **53,** 261-268.

Jost, M. L., and R. B. Herrmann (1989). A students guide to and review of moment tensors, *Seismol. Res. Lett.* ***60,*** 37–57.

Julian, B. R., A. D. Miller, and G. R. Foulger (1998). Non-double-couple Earthquakes, 1, *Rev. Geophys.* **36,** 525-549.

Kikuchi, M., and H. Kanamori (1991). Inversion of complex body waves. III, *Bull. Seismol. Soc. Am.* **81,** 2335–2350.

Konstantinou, K. (2010). Crustal rheology of the Santorini–Amorgos zone: Implications for the nucleation depth and rupture extent of the 9 July 1956 Amorgos earthquake, southern Aegean, *J. Geodyn.* **50,** 400–409.

Molnar, P., and H. Lyon-Caen (1989). Fault plane solutions of earthquakes and active tectonics of the Tibetan Plateau and its margins., *Geophys. J. Int.* **99,** 123–154.

Nakano, M., H. Kumagai, and H. Inoue (2008). Waveform inversion in the frequency domain for the simultaneous determination of earthquake source mechanism and moment function, *Geophys. J. Int.* **173,** 1000-1011.

Novotný, O., J. Zahradník, and G-A. Tselentis (2001). Northwestern Turkey earthquakes and the crustal structure inferred from surface waves observed in Western Greece, *Bull. Seismol. Soc. Am.* **91,** 875-879.

Okal, E.A., C. E. Synolakis, B. Uslu, N. Kalligeris, and E. Voukouvalas (2009). The 1956 earthquake and tsunami in Amorgos, Greece. *Geophys. J. Int.* **178,** 1533–1554, doi:10.1111/j.1365–246X.2009.04237.x.

Panza, G. F., and A. Saraò (2000). Monitoring volcanic and geothermal areas by full seismic moment tensor inversion: are non-double-couple components always artifacts of modelling?, *Geophys. J. Int.* **143,** 353–364.

Papazachos, B.C. and K. Papazachou (2003). The earthquakes of Greece, Ziti Publ., pp.286.

Press, W. H., S. A. Teukolsky, W. T. Vetterling, and B. P. Flannery (1997). *Numerical recipes in Fortran 77:. The art of Scientific Computing*, Cambridge University Press, 2nd ed., 992 pp.

Riedesel, M. A., and T. H. Jordan (1989). Display and assessment of seismic moment tensors, *Bull. Seismol. Soc. Am.* **79,** 85-100.

Šílený, J. (1998). Earthquake source parameters and their confidence regions by a genetic algorithm with a 'memory', *Geophys. J. Int.* **134,** 228-242.

Šílený, F., and R. Hofstetter (2002). Moment tensor of the 1999 Dead Sea calibration shot: limitations in the isotropic source retrieval without a detailed earth model, *Tectonophysics* **356,** 157– 169.

Silver, P. G., and T. H. Jordan (1982). Optimal estimation of scalar seismic moment, *Geophys. J. Roy. Astron. Soc.* **70,** 755-787, doi: 10.1111/j.1365-246X.1982.tb05982.x.

Sokos, E. N., and J. Zahradník (2008). ISOLA a Fortran code and a Matlab GUI to perform multiple-point source inversion of seismic data. *Comput. Geosci.* **34,** 967-977.

Sokos, E. N., J. Zahradník, A. Kiratzi, J. Janský, F. Gallovič, O. Novotný, J. Kostelecký, A. Serpetsidaki, and G.-A. Tselentis (2012). The January 2010 Efpalio earthquake sequence in the western Corinth Gulf (Greece), *Tectonophysics* **530-531,** 299-309.

Templeton, D. C., and D. S. Dreger (2006). Non-double-couple earthquakes in the Long Valley volcanic region, *Bull. Seismol. Soc. Am.* **96,** 69-79.

Tkalčić, H., D. S. Dreger, G. R. Foulger, and B. R. Julian (2009). The puzzle of the 1996 Bárdarbunga, Iceland, earthquake: No volumetric component in the source mechanism, *Bull. Seismol. Soc. Am.* **99,** 3077-3085.

Vasco, D. W. (1990). Moment-tensor invariants: Searching for non-double-couple earthquakes, *Bull. Seismol. Soc. Am.* **80,** no. 2, 354–371.

Vavryčuk, V. (2001). Inversion for parameters of tensile earthquakes, *J. Geophys. Res.* **106,** 16,339-16,355.

Vavryčuk, V. (2007). On the retrieval of moment tensors from borehole data, *Geophys. Prospect.* **55,** 381-391.

Vavryčuk, V. (2011). Tensile earthquakes: Theory, modeling, and inversion, *J. Geophys. Res.* **116,** B12320, doi:10.1029/2011JB008770.

Vavryčuk, V., and D. Kuhn (2012). Moment tensor inversion of waveforms: a two-step time-frequency approach, *Geophys. J. Int.* **190,** no. 3, 1761-1776, doi: 10.1111/j.1365-245X.2012.05592.x.

Wéber, Z. (2006). Probabilistic local waveform inversion for moment tensor and hypocentral location, *Geophys. J. Int.* 165, 607-621.

Yang, X., and J. L. Bonner (2009). Characteristics of chemical explosive sources from time-dependent moment tensors, *Bull. Seismol. Soc. Am.* **99,** 36-51.

Zahradník, J., and S. Custódio (2012). Moment tensor resolvability: Application to southwest Iberia. *Bull. Seismol. Soc. Am.* 102, 1235-1254, doi: 10.1785/0120110216.

Zahradník, J., and F. Gallovič (2010). Toward understanding slip inversion uncertainty and artifacts, *J. Geophys. Res.* **115,** no. B9, B09310, doi: 10.1029/2010JB007414.

Zahradník, J., and E. Sokos (2011). Multiple-point source solution of the Mw7.2 Van earthquake, October 23, 2011, Eastern Turkey. *Research Report,* EMSC, 1 November 2011, http://www.emsc-csem.org/Files/event/239856/Van_ISOLA.pdf (last accessed April 2013).

Zahradník, J., J. Janský, and V. Plicka (2008). Detailed waveform inversion for moment tensors of M ~ 4 events: Examples from the Corinth Gulf, Greece, *Bull. Seismol. Soc. Am.* **98,** 2756-2771.

Zahradník, J., E. Sokos, G-A. Tselentis, and N. Martakis (2008). Non-double-couple mechanism of moderate earthquakes near Zakynthos, Greece, April 2006; explanation in terms of complexity, *Geophys. Prospect.* **56,** 341-356.

A2. Possible indicator of a strong isotropic earthquake component – example of two shallow earthquakes in Greece

by **Dana Křížová**[1], **Jiří Zahradník**[1], and **Anastasia Kiratzi**[2]

[1] Charles University, Faculty of Mathematics and Physics, Czech Republic

[2] Aristotle University of Thessaloniki, Department of Geophysics, Greece

ABSTRACT

For routine practice we, need simple tools to reliably identify earthquakes with large isotropic (ISO) components. This study aims to highlight a possible indicator. Non-double-couple (non-DC) components of moment tensors (MTs) play a key role in our understanding of faulting earthquake processes and/or in identifying explosions. As opposed to DC components of the calculated seismic source model, the non-DC components (compensated linear vector dipole and ISO) are more vulnerable to errors in location, inaccurate velocity modeling, and noise. Methods for analyzing resolvability of ISO are relatively complicated. We propose a simple procedure to identify an earthquake with a strong ISO component. Recent MT determinations include space and time grid search of the centroid position, mainly the depth and time. The centroid is identified with a trial source position that maximizes correlation between real and synthetic waveforms. In synthetic tests with varying ISO percentage, we compare the correlation-depth dependence for two types of MT inversion: full and deviatoric. We show that in the inversion of data with a significant ISO component under the deviatoric assumption (i.e., when ISO is neglected), we might obtain an inaccurate centroid depth. However, when we make the grid search twice, under the deviatoric-MT and full-MT assumptions, and compare the results, we can obtain an indication of the significant ISO and avoid the depth bias. This straightforward method is applied to two shallow earthquakes in Greece (the January 2012 M_w 5.3 Cretan Sea earthquake and the 26 June 2009 M_w 4.9 Santorini earthquake).

INTRODUCTION

Moment tensor (MT) calculations today belong to seismological routine. Few agencies (e.g., GeoForschungsZentrum [GFZ]) calculate the full MT, whereas most others (including Global Centroid Moment Tensor [CMT] and U.S. Geological Survey [USGS]) usually determine only the deviatoric MT, neglecting the isotropic (ISO) component. The double-couple (DC) part of MT is standard (useful and important) output from MT calculations. It is commonly parameterized by means of the strike, dip and rake angles, expressing the so-called focal mechanism (or fault-plane solution). The focal mechanism is relatively stable with respect to inaccuracies of the routinely available velocity models and also with respect to possible errors in the assumed source positions. Nevertheless, to make the focal mechanism even more reliable, the source (centroid) position and time are sometimes jointly inverted with the mechanism. Contrarily to the focal mechanism, the non-DC components of MT

are difficult to determine because they are unstable. It means that they vary a lot with small changes of the velocity model, source-station configuration, and frequency range, among others.

Previous work has focused on research of non-DC components, their limited reliability, error assessment and similar issues, starting in the 1990s (Vasco, 1990; Dufumier and Rivera, 1997; Julian et al., 1998). Here, we focus on shallow earthquakes, but studies for deep earthquakes are available (Kawakatsu, 1996; Vavryčuk, 2004). Earthquake swarms often include non-DC events. For example, in West Bohemia (Czech Republic), the non-DC components could be caused by fluid injection (Horálek et al., 2002), and a number of earthquakes in that region can be classified as tensile earthquakes (Vavryčuk, 2011). Earthquakes with noticeable compensated linear vector dipole (CLVD) or ISO components could be observed during borehole experiments. Vavryčuk et al. (2008) discovered two main types of these events. One type looked like a response to injection, while the other could be connected with anisotropy of rocks.

Full-MT calculation provides a pathway to understand the fracturing process (Song and Toksöz, 2011), how to differentiate natural from induced seismicity (Ford et al., 2009; Cesca et al., 2013). The full-MT inversion is useful in the studies of nuclear explosions (Minson end Dreger, 2008). Non-DC components can be substantial during volcanic earthquakes, for example, Long Valley caldera in California (Foulger et al., 2004; Templeton and Dreger, 2006). Among several types of non-DC volcanic events, it is worth mentioning the case of vertical-CLVD earthquakes (Shuler et al., 2013), or earthquakes with large non-DC component but missing the ISO component (Tkalčić et al., 2009). Recently, Mustać and Tkalčić (2016) used a nonlinear Bayesian inversion in which noise represents a free parameter and is implemented via empirical covariance matrix.

Despite the efforts invested into non-DC components, in practice users are still confused regarding practical questions, as for example the following: is it better to always calculate full MT, while we know that only its strike/dip/rake (and moment) are reliable? Is it instead preferable to calculate the deviatoric MT? Is the percentage of the DC part (hereafter, DC%) well determined if derived from the deviatoric MT? More specifically, the objective of this article is to analyze how the deviatoric constraint affects the MT inversion results such as the DC%, the centroid depth, and the strike/dip/rake angles. The main innovative product is a simple indicator of events with strong ISO components, easily applicable to routine observatory practice.

This article is structured as follows: first, we briefly summarize methods that we use to invert waveforms into MT. Then, we introduce two real events that occurred in Greece: the 2012 Cretan Sea and the 2009 Santorini earthquakes. Next, we perform synthetic tests using the same source-station geometry as for the two real events. We vary the strength of the non-DC components and compare the full-MT and deviatoric-MT inversions. We arrive at a hypothesis that events with a significant ISO component can be detected by a simple comparison of the full-MT and deviatoric-MT inversions, and that the centroid depth determination of such

events, under deviatoric constraint, may be highly inaccurate. Finally, we return to the two real events and show that the Santorini (volcanic) earthquake has a significant ISO component, whereas ISO of the Cretan Sea earthquake seems to be negligible (i.e., the latter appears to be a common tectonic earthquake).

METHOD

Basic Equations

Moment tensor **M** of an earthquake is expressed in the form of a linear combination of six elementary (dimensionless) moment tensors $\mathbf{M}^i$**:**

$$M_{pq} = \sum_{i=1}^{6} a_i M^i_{pq} \ . \tag{1}$$

We use the elementary tensors as in the discrete-wavenumber code AXITRA of Coutant (1989):

$$M^1 = \begin{pmatrix} 0 & 1 & 0 \\ 1 & 0 & 0 \\ 0 & 0 & 0 \end{pmatrix} \quad M^2 = \begin{pmatrix} 0 & 0 & 1 \\ 0 & 0 & 0 \\ 1 & 0 & 0 \end{pmatrix} \quad M^3 = \begin{pmatrix} 0 & 0 & 0 \\ 0 & 0 & -1 \\ 0 & -1 & 0 \end{pmatrix}$$

$$M^4 = \begin{pmatrix} -1 & 0 & 0 \\ 0 & 0 & 0 \\ 0 & 0 & 1 \end{pmatrix} \quad M^5 = \begin{pmatrix} 0 & 0 & 0 \\ 0 & -1 & 0 \\ 0 & 0 & 1 \end{pmatrix} \quad M^6 = \begin{pmatrix} 1 & 0 & 0 \\ 0 & 1 & 0 \\ 0 & 0 & 1 \end{pmatrix}. \tag{2}$$

The $\mathbf{M}^1$-$\mathbf{M}^5$ tensors represent five DC focal mechanisms, whereas $\mathbf{M}^6$ is a purely ISO source. The *a*-coefficients in equation (1), or simply *a*, are related to **M** as

$$\mathbf{M} = \begin{pmatrix} -a_4 + a_6 & a_1 & a_2 \\ a_1 & -a_5 + a_6 & -a_3 \\ a_2 & -a_3 & a_4 + a_5 + a_6 \end{pmatrix} \ . \tag{3}$$

The moment trace is related with just a single *a*-coefficient, $a_6 = \mathrm{tr}(\mathbf{M})/3$. The scalar seismic moment is defined by Silver and Jordan (1982) as

$$M_0 = \sqrt{\frac{\sum_{p=1}^{3}\sum_{q=1}^{3}(M_{pq})^2}{2}} \ . \tag{4}$$

The MT decomposition used here is $\mathbf{M} = \mathbf{M}_{ISO} + \mathbf{M}_{DEV}$, in which $\mathbf{M}_{ISO}$ and $\mathbf{M}_{DEV}$ stand for the ISO and deviatoric part, respectively, and $\mathbf{M}_{DEV} = \mathbf{M}_{DC} + \mathbf{M}_{CLVD}$ (e.g., Julian et al., 1998, p. 530). The relative size of the ISO, DC and CLVD components is expressed in percentages, and the sum of their absolute values is 100%. The so-called deviator formulation assumes $\mathbf{M} = \mathbf{M}_{DEV}$, and in this case the sum of DC and CLVD percentages is 100%. The definition of the percentages has not yet been unified in literature; we follow equations (8a)–(8c) of Vavryčuk (2001).

The source of finite extent and duration is approximated by a point source (centroid). Assuming that the centroid position and centroid time are known, the displacement at a station can be written as

$$u_i(t) = \sum_j^6 a_j \left(\sum_p \sum_q M_{pq}^j * G_{ip,q}\right) = \sum_{j=1}^6 a_j E_i^j(t) \qquad (5)$$

(Aki and Richards, 2002). Here, **G** is Green's tensor and $\mathbf{E}^j$ denotes the *j*th elementary seismogram corresponding to the *j*th elementary MT. The Green's functions are calculated in 1D velocity models by the discrete wave number method (Bouchon, 1981), including near-field terms. Full displacement waveforms are inverted without any phase separation. Artificial time shifts of complete seismograms, sometimes used to compensate for deficiencies of the velocity model, are not used because we consider their application poorly justified (Zahradník et al., 2008). We suppose that the moment-rate function is a delta function, which is a good approximation at frequencies below the corner frequency of the event. Then, equation (5) can be understood as a linear inverse problem for unknown *a*, hence, the unknown **M**. The full-MT inversion seeks the value of all six *a*'s, whereas the deviatoric inversion (DEV) assumes a_6=0; therefore, only the first five *a*'s are calculated. The inverse problem is solved by the least-squares method. If the centroid position and time belong to the unknown parameters, they are sought through a spatiotemporal grid search in vicinity of a previously estimated position, and (together with **M**) they collectively represent the CMT solution. The grid search maximizes the correlation between the observed (*u*) and synthetic (*s*) seismograms, defined by

$$Corr = \frac{\int us}{\sqrt{\int u^2 s^2}}, \qquad (6)$$

in which $\int us = \sum_i \int u_i(t) s_i(t) dt$ and summation is over components and stations. The match between the observed and synthetic seismograms is measured by the global variance reduction (VR):

$$VR = 1 - \frac{\int (u - s)^2}{\int u^2} = Corr^2 . \qquad (7)$$

This equation follows from equation (6) and from the fact that if synthetics *s* are found by the least-squares misfit minimization of $\int(u-s)^2$, then $\int us = \int ss$ (see, e.g., equations 1-6 of Kikuchi and Kanamori, 1991).

To examine how well or ill posed the inverse problem is, we additionally use the condition number (CN, equation 18 of Křížová et al., 2013). It is a relative measure; a larger CN signalizes a worse (less stable) resolvability of MT. To measure the angular departure of any two DC solutions, under comparison, we use Kagan angle (Kagan, 1991). The solutions are comparable (quite similar) if the angle is < 10°-20°. (e.g., see Zahradník and Custódio, 2012). We implemented this method using ISOLA software (Sokos and Zahradník, 2008, 2013).

Technical Details

Before instrumental correction and band-pass filtering, the integrated raw displacement data are always carefully checked to detect possible disturbances in an attempt to prevent harming the CMT inversion (Zahradík and Plešinger, 2005, 2010; Vackář et al., 2015). The frequency range of the waveform inversion (e.g., 0.05-0.08 Hz) used in this article is quite standard for near-regional applications of a similar type, where the low- and high-frequency limits are determined by the noise (either instrumental or natural) and by the ability to model observed data with existing velocity models, respectively. Following our previous work (Křížová et al., 2013; their fig. 1b,c and table 2), we use two velocity models: the model proposed by Novotný et al. (2001; obtained from regional surface-wave dispersion) and the model of Dimitriadis et al. (2010; obtained from nonlinear inversion of travel times and applicable to the broader region of Santorini Island). Hereafter, they are called N-model and D-model, for brevity.

DATA

Although we basically focus on synthetics tests, we start with real data because in the synthetics tests we will use the same source-station configuration. We investigate two shallow events of the south-central Aegean region: the 27 January 2012 M_w 5.3 Cretan Sea earthquake and the 26 June 2009 M_w 4.9 Santorini earthquake (Fig. 1a and 1b, respectively). For their preliminary agency reports, we refer to the European-Mediterranean Seismological Centre (EMSC) web pages (see Data and Resources). MT solutions for both of the events are also available online (see Data and Resources). The Cretan Sea earthquake is the strongest event of the January 2012 earthquake sequence in Cretan Sea. The Santorini earthquake is the strongest event of the June 2009 earthquake sequence near Santorini Island.

The selection of the two events is motivated by the following:

1. both events were well recorded by broadband instruments of a reasonable azimuthal coverage;
2. both events occurred at a region where tectonic and volcanic events occur, making them candidates for possibly large ISO components;
3. these two earthquakes were previously studied by Kiratzi (2013) and Křížová et al. (2013), and so a good preliminary estimate of their parameters is available;
4. the previous analyses have revealed that the events may have a quite different ISO content, in particular a large ISO during the Santorini earthquake.

Table 1 summarizes standard CMT parameters of the events, calculated here, inverting only for the deviatoric part of the tensor, using the N-model, and the station configuration of Figure 1. In the following, first we make synthetic tests and demonstrate how the MT calculation is affected by neglecting the ISO component. Then, we try to find and show similar effects on real data. For both cases, we assume a fixed horizontal position of the centroid, varying only the depth.

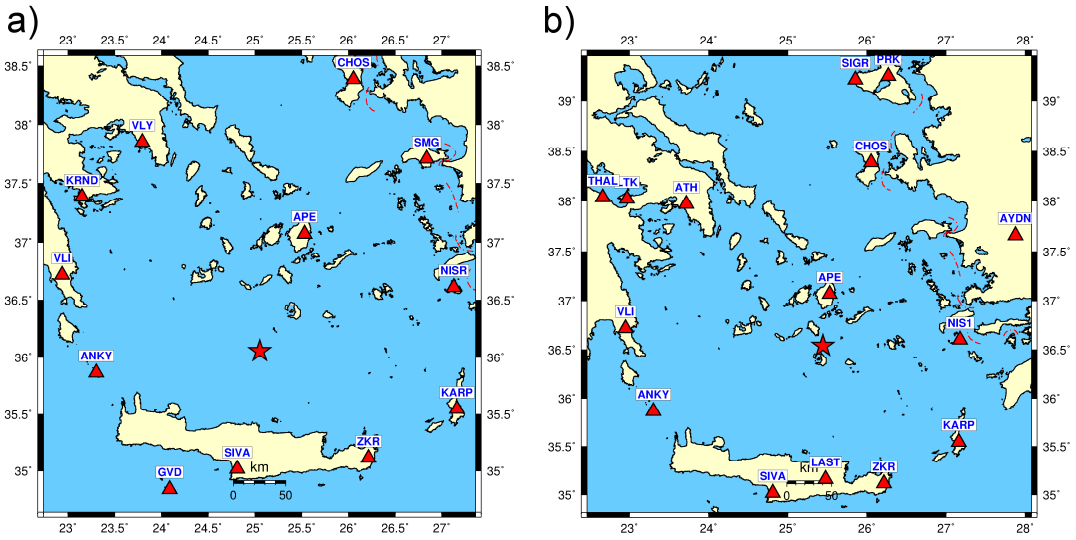

Figure 1. Studied earthquakes (asterisks) and stations (triangles) used in our analysis for (a) Cretan Sea and (b) Santorini. Table 1 provides more information on the earthquakes. The color version of this figure is available only in the electronic edition.

Table 1

Earthquake Centroid Moment Tensor (MT) Parameters of the Cretan Sea Earthquake and Santorini Earthquake Calculated in This Work

	Earthquakes	
	Cretan Sea	Santorini
Date (yyyy/mm/dd)	2012/01/27	2009/06/26
Time (hh:mm:ss.s in UTC)	01:33:24.5	20:37:37.7
Latitude (°N)	36.056	36.540
Longitude (°E)	25.053	25.445
Depth (km)	8	4
M_w	5.3	4.6
M_0 (N·m)	1.18×10^{17}	1.07×10^{16}
Strike/dip/rake (°)	188/80/−112	243/59/−74
Strike/dip/rake (°)	76/24/−23	34/33/−114
DC*	94.4	59.2
VR†	64.2	64.5

*DC, percentage of double couple.
†VR, variance reduction in percent.

RESULTS: SYNTHETIC DATA

Motivation of the synthetic tests comes from observatory practice. Besides the centroid position and the strike/dip/rake angles, we are often interested in the DC% because this is the simplest parameter characterizing a possible deviation of the earthquake from pure shear faulting. We seek to understand how the obtained DC% depends on the adopted MT-inversion mode.

Moment Tensor

Consider a target earthquake of a full-MT $\mathbf{M} = \mathbf{M}_{ISO} + \mathbf{M}_{CLVD} + \mathbf{M}_{DC}$. If we invert waveforms corresponding to this **M** under the assumption that the MT is purely deviatoric, we obtain $\mathbf{M'} = \mathbf{M'}_{CLVD} + \mathbf{M'}_{DC}$. It is obvious that, in general, $\mathbf{M'}_{CLVD}$ does not equal $\mathbf{M}_{ISO} + \mathbf{M}_{CLVD}$; therefore, $\mathbf{M'}_{DC}$ does not equal $\mathbf{M}_{DC}$. Thus, we get a biased estimate of the DC%. How large is the DC% bias, and how does it depend on the size of the ISO component (ISO%)? These are the questions we are interested in. A related question is how the other source parameters, such as the strike/dip/rake angles and the centroid depth, may differ between the full-MT and deviatoric-MT inversion modes.

Designing the Synthetic Tests

All tests have a common feature. We calculate synthetic waveforms for an assumed centroid position and for a given full MT. We then invert the synthetic waveforms in either a full-MT or deviatoric-MT mode and we leave the centroid depth and time free. We investigate the effects of the deviatoric constraint on the obtained source parameters (strike/dip/rake, depth, DC%, etc.). Three tests are made (A–C), each one with six subtests (1-6).

Tests A and B (Tables A3 and A4) differ in the centroid depth and strike/dip/rake angles of the simulated events, corresponding to the two selected real earthquakes. The subtests differ in their ISO% (rounded to integer values): ±90, ±46, and ±30 for test A and ±90, ±48, and ±32 for test B. The plus and minus signs correspond to explosion and implosion, respectively. For simplicity, all models have CLVD% = 0. Synthetic data are forward simulated and inverted using the same velocity model (N-model), unless differently specified.

Technically, the subtests are created as follows: we choose the strike/dip/rake angles and calculate the *a*-coefficients a_1, ..., a_5, of the deviatoric MT, (see equation 3). Then, we create full MTs of several ISO components by choosing appropriate values of the sixth coefficient a_6 (Tables A1 and A2). For synthetics tests, we have chosen a_1, ..., a_5 coefficients that are close to solutions for full-MT inversions in real cases (it is because we are changing the ISO component across subtests; therefore, full-MT inversion was used). The true depth for test A is 8 km (Table 2) and for test B is 6 km (Table 3). The 6 km depth is preferred because the former 4 km depth (Table 1) was calculated for deviatoric solution only.

Test C is more complicated (Table A5). The assumed source parameters are as in Test B (Tables A1 and A2); however, to illustrate possible effects of inaccurate velocity models, we forward simulate synthetic waveforms in one model (N-model), but invert them in the other (D-model). That is why in Test C, variance reduction (equation 7) is always less than 85%.

The MT-inversion results for synthetic tests A-C (Figs. 2–6) including the subtests 1-6, mentioned in corresponding Tables A3–A5, reveal a number of interesting features, which are discussed in the following sections.

Focal Mechanism

First, we focus on the fault-plane solution by looking at the nodal lines. These lines are the result of the inversion (sub-tests 1–6, mentioned in corresponding Tables A3–A5). For full-MT inversion in Test A, we see (Fig. 2a) that these nodal lines do not significant change for all sub-tests 1–6. A similar result is obtained for Test B (Fig. 2c). In most subtests of Test A (Fig. 2b), the nodal lines of the deviatoric inversion differ only marginally from the correct solution. However, there are two exceptions, corresponding to the MT with the largest ISO ±89.5%. For these cases, the deviatoric inversion produces a MT whose CLVD is greater than 90%, and the fault-plane solution of the deviatoric inversion differs quite significantly from the correct one. The deviation, expressed in terms of the Kagan angle, is 47° and 37° for ISO = –89.5% and +89.5%, respectively. On the other hand, for ISO = ±29.8%, the Kagan angle is smaller than 10°. The subtests of Test B (Fig. 2d), representing a similar experiment but with different strike/dip/rake angles and a slightly shallower depth, give almost the same results (see Tables A3-A5 for details).

In Test C, where the inversion is performed for the incorrect velocity model, we obtain deviations from the correct solution even in the full-MT inversion (Fig. 2e). The latter is the case of subtests C1D and C2D, with real ISO= –90.3% and +90.4% in which we obtain only ISO=–70.1 and +75.1, respectively. For subtest C2D (full), we get a Kagan angle as large as 91°. For two smaller (absolute) values of ISO, the full-MT inversion gives a higher variance reduction and small Kagan angle. The deviatoric inversion in the incorrect model (Fig. 2f) provides relatively small deviation of the nodal lines from the correct solution. It means that, in this example, the inversion of the fault-plane solution is robust.

DC% and Depth

We seek to see how much the DC% deviates from the correct values when neglecting the ISO source component during the MT inversion. This question is answered in Figure 3a. The prescribed (correct) values are shown by filled circles for test A and filled squares for tests B and C, which differ across sub-tests 1–6. We should mention that we generate synthetic data without noise and then invert them, which is why the results for full-MT inversion in N-model are considered to be correct. The performance of Test A is easy to understand. In most subtests 1–6 with variable ISO% of the input data, the DC% is well reproduced in the deviatoric inversion (empty circles are near the filled circles) because ISO% is projected into CLVD%, thus keeping the correct DC%, except two cases. The two exceptions, subtests 3 and 5, correspond to the input ISO of –46% and –30%, which did not project into CLVD, but instead they apparently enriched the DC source content, that is increased DC%. The enrichment is so high that the resulting DC% of subtests 3 and 5 is practically the same (> 90%), not reflecting the different DC% of the input data. We also note that in all the subtests, the retrieved DC% never drops below the true value. Values of Kagan angle are shown in Figure 3b, and the source depth was changed due to the deviatoric assumption (Fig. 3c). The results of Test B are analogous to Test A (marked in Fig. 3a with filled and empty squares, respectively).

Table 2
Cretan Sea Earthquake

Earthquake	DC	CLVD	ISO	CN	VR (%)	Depth (km)	Strike (°)	Dip (°)	Rake (°)
N (full)	83.2	7.2	−9.6	2.56	64.5	8	187	81	−113
							79	24	−20
N (deviatoric)	94.4	5.6	0.0	2.03	64.2	8	188	80	−112
							76	24	−23

Inversion is in full-MT and deviatoric-MT modes. N, N-model; ISO, isotropic; CN, condition number; CLVD, compensated linear vector dipole.

Table 3
Santorini Earthquake

Earthquake	DC	CLVD	ISO	CN	VR	Depth (km)	Strike (°)	Dip (°)	Rake (°)
N (full)	50.2	1.4	48.4	3.90	65.7	6	253	67	−61
							18	35	−139
N (deviatoric)	59.2	40.8	0.0	3.20	64.5	4	243	59	−74
							34	33	−114
D (full)	52.5	4.4	43.1	3.64	69.4	5	250	65	−65
							21	34	−132
D (deviatoric)	60.4	39.6	0.0	3.38	69.0	3	246	62	−73
							33	31	−119

Inversion is in full-MT and deviatoric-MT modes. N, N-model; D, D-model.

Test C (also in Fig. 3a,b), in which the inversion is done intentionally with a different velocity model than the one used to produce the synthetic data, is more complicated. Both velocity models are described in Figures 1b,c and table 2 of Křížová et al. (2013). The prescribed (correct) values are those of test B due to the incorrect velocity model, in this case test C. For the deviatoric-MT inversion, the DC% is almost always biased for the low input DC% (subtest 1, also accompanied by an erroneous retrieved depth). However, for the full-MT inversion the retrieved DC% is relatively close to the true one (or somewhat lower). The DC% for the full-MT inversion is retrieved well in subtests 1 and 2, but in subtests 3–6 it is lower than the true value. Our results show that an incorrect velocity model introduces bias in estimating the DC% in both the full-MT and deviatoric-MT inversions.

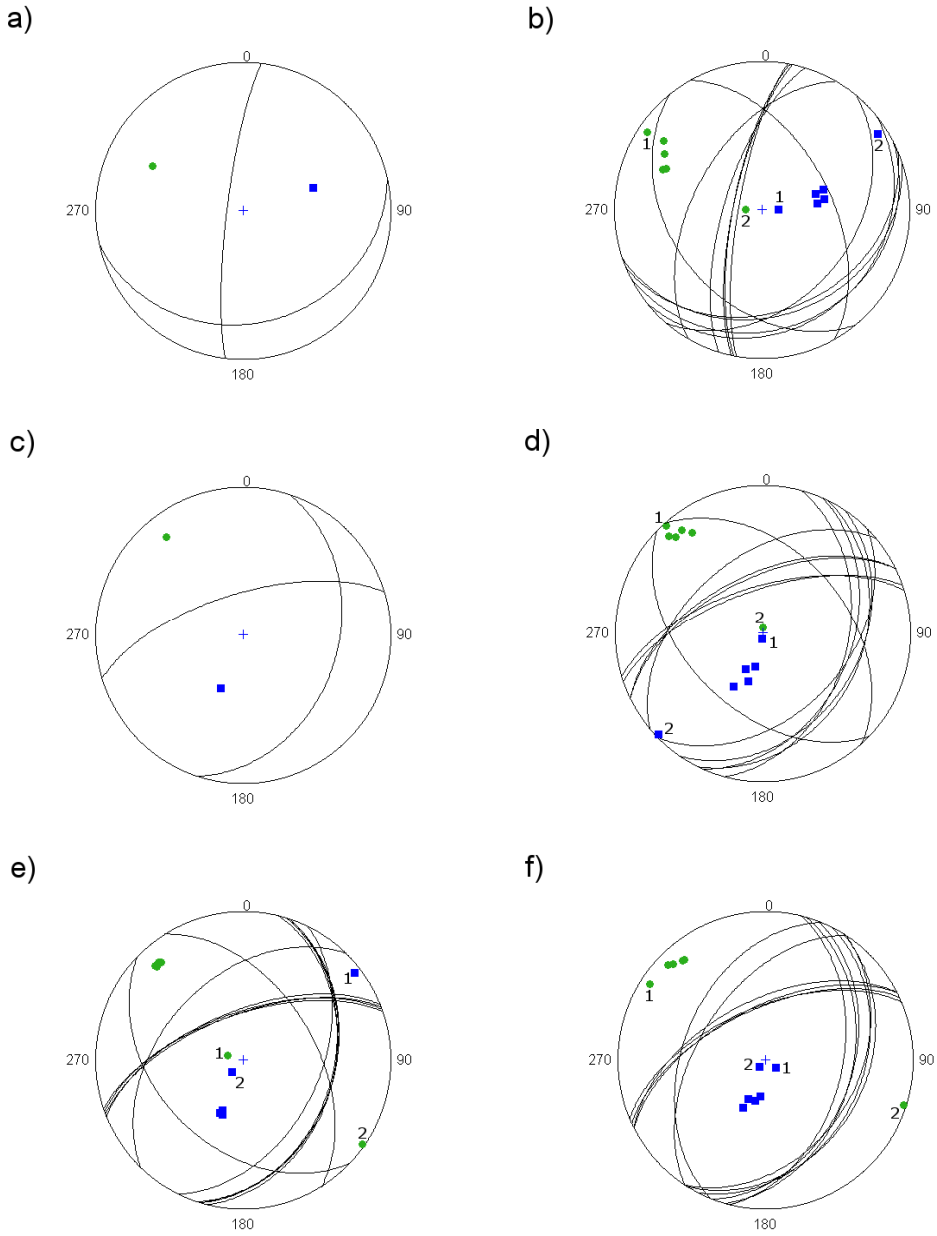

Figure 2. Nodal lines are the result of the inversion (sub-tests 1–6). Squares are symbols for P-axis and circles stands for T-axis. (a)Test A, full moment tensor (MT); (b) Test A, deviatoric MT; (c) Test B, full MT; (d) Test B, deviatoric MT; (e) Test C, full MT; (f) Test C, deviatoric MT. (Each inversion is made in full-MT mode [a, c, e] and deviatoric-MT mode [b, d, f]. For b, d, e and f, we marked P-axis and T-axis for sub-tests 1 and 2.) The color version of this figure is available only in the electronic edition.

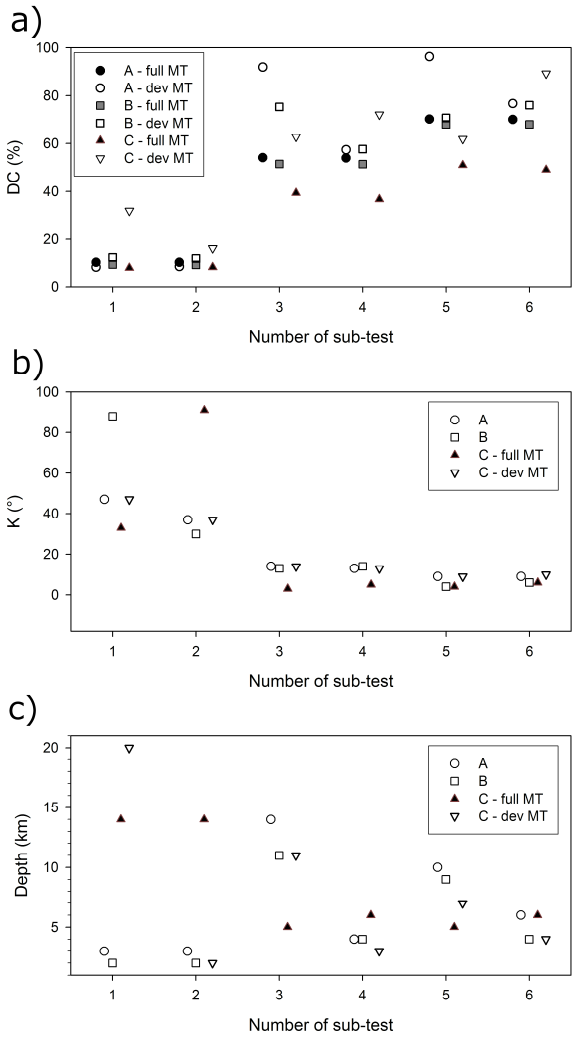

Figure 3. Results corresponding to Tables A3–A5. (a) Double-couple percentage (DC%): the input data (the correct solution) are mentioned, such as full MT in N-model. The remaining symbols, explained in legend, are the result of the inversion (subtests 1–6). (b) Kagan angle: for test A and B is the difference between full MT and deviatoric (dev) MT and for test C is the difference between full MT for B and results from inversion in wrong velocity model. (c) Source depth obtained for each subtest. The color version of this figure is available only in the electronic edition.

Correlation versus Source Depth

Here, we analyze whether there is any simple feature in these complex results, at least for some specific values of ISO%. As seen in Figures 2 and 3, subtests 1 and 2 of the largest ISO% seem to behave differently in all aspects (the fault-plane solution, DC%, depth). Therefore, we further concentrate on the variation of the waveform correlation with trial source depth, and we will show that indeed the events with a large ISO% may have a specific correlation-depth behavior. Recall that the source depth prescribed in synthetic data is 8 km for test A and 6 km for tests B and C. Synthetic seismograms created for the full-MT source at these depths are inverted either in the full-MT or deviatoric-MT mode, while the trial depth is free (tests A–C in Figs. 4–6).

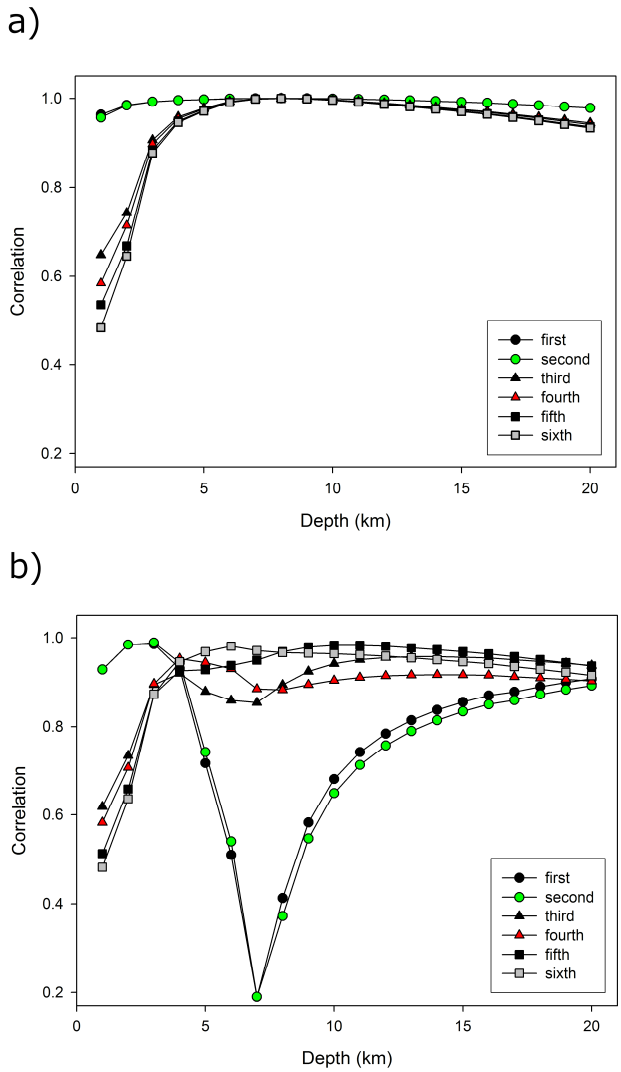

Figure 4. Waveform correlation for synthetic test A (subtests are for variable isotropic percentage [ISO%], see legend and Table A3). Correct source depth is 8 km. Synthetic waveforms due to full MT are inverted in two modes: (a) full MT and (b) deviatoric MT. The color version of this figure is available only in electronic edition.

Synthetic Data Inverted in Full-MT Mode

We start with the synthetic data inverted in full-MT mode, and, as seen from the correlation-depth curves (Figs. 4a, 5a, and 6a), no pronounced local maxima can be detected. In other words, for this particular event-station geometry and velocity model, the centroid depth resolvability is almost none. The (weak) depth variation is almost independent of ISO%. There is a weak dependence on depth for subtests 3–6, but the shape of curves is almost the same. The correlation seems to be least dependent on depth in subtests 1 and 2; the curves (with circles) are almost flat. Note an interesting feature of Figure 6a (the same MT as in Fig. 5a, but the full-MT inversion is made with wrong velocity model): Despite the use of the inappropriate velocity model, the depth dependence in Figure 6a has a similar shape as in Figure 5a, only the correlation values are lower.

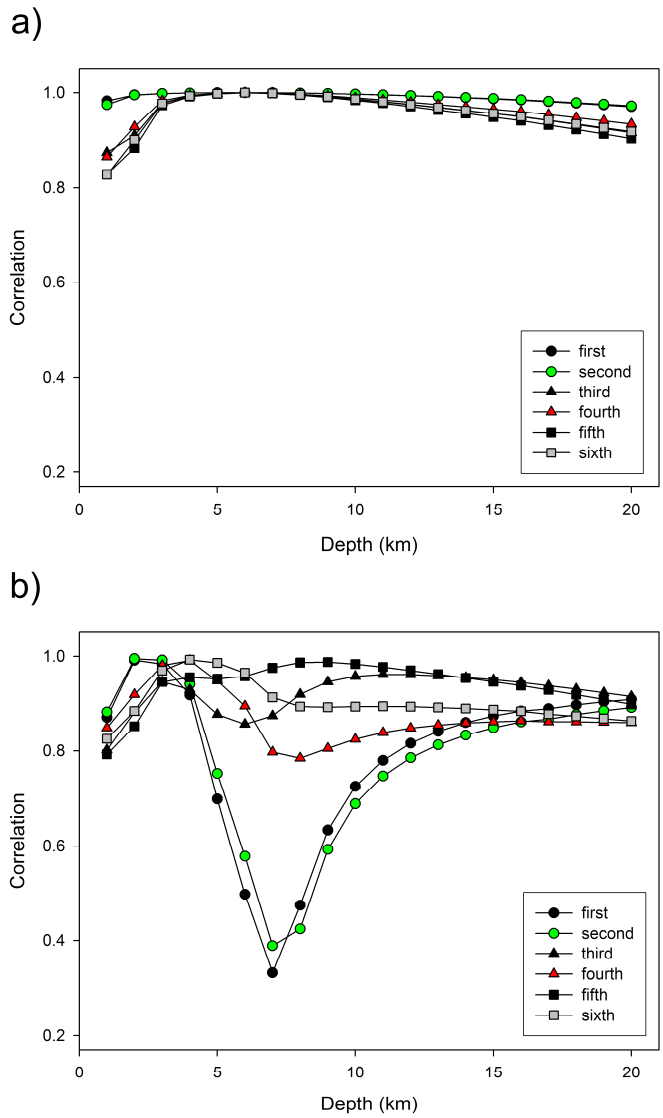

Figure 5. Waveform correlation for synthetic test B (subtests are for variable ISO%, see legend and Table A4). Correct source depth is 6 km. Synthetic waveforms due to full MT are inverted in two modes: (a) full MT and (b) deviatoric MT. The color version of this figure is available only in electronic edition.

Synthetic Data Inverted in Deviatoric-MT Mode

The inversion of the same synthetic data in deviatoric-MT mode (Figs. 4b, 5b, and 6b), clearly shows that neglecting the ISO component has a strong effect upon the correlation-depth variations. In particular, subtests 1 and 2 show very deep local minima, but weaker local minima can also be observed in the other subtests. The minima are close (but not identical) to the true source depth. This remarkable feature is common to tests A–C. The tests indicate that if a real event has a very large ISO% (low DC%), the correlation-depth graph may get an apparent minimum near the correct source depth, that is, the depth will be incorrectly determined. For example, as in Figures 4b and 5b, the source depth can be erroneously identified with the local correlation maximum at the depth < 5km.

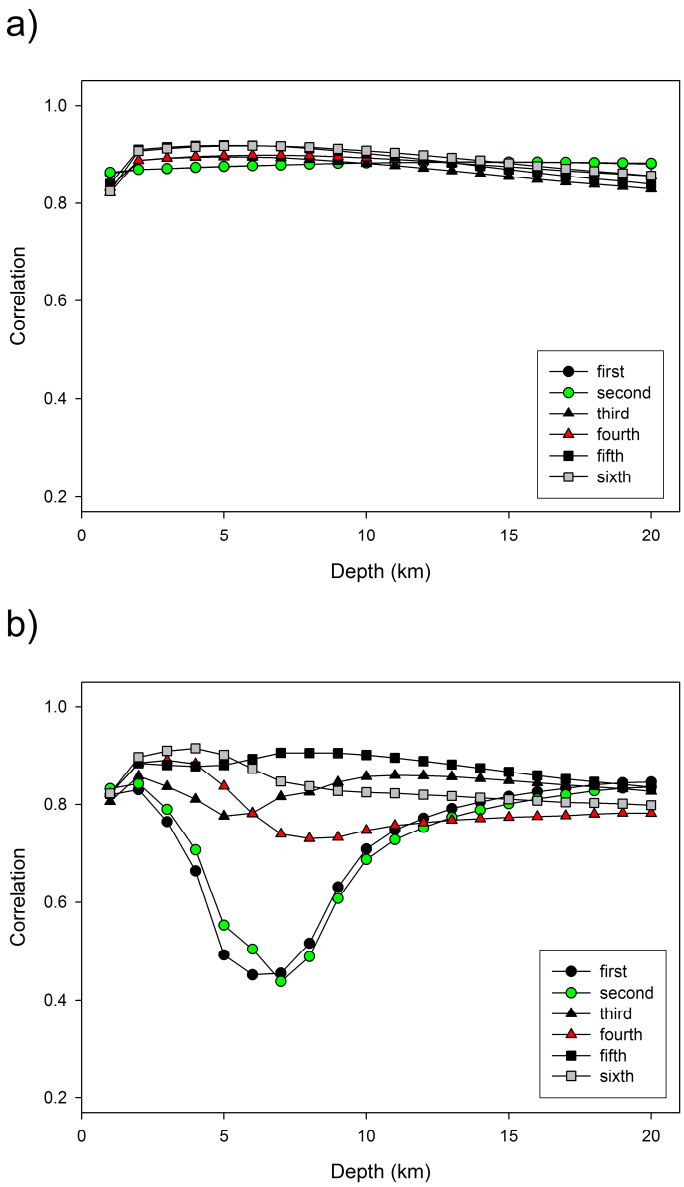

Figure 6. As in Figure 5, but the inversion is made in a different model (D-model, whereas the forward simulation used N-model; see legend and Table A5). (a) Full MT. (b) Deviatoric MT. The color version of this figure is available only in electronic edition.

The significantly different correlation-depth profiles can be simply explained. Imagine a source at depth *D* with a large ISO component and negligible CLVD. This ISO component constitutes a significant part of the waveforms. In the full-MT inversion, the waveforms can be best fitted at the depth *D*. However, in the deviatoric-MT inversion, the true waveforms are approximated with synthetics lacking the ISO part. It means that real data are interpreted in terms of an inappropriate model (DC and CLVD only), thus deteriorating the match at depth *D*. Because the inappropriate model does not contain ISO, real data could be partially fit only by a source model at depth *D* having a different focal mechanism, biased with respect to the true one in a way compensating the missing ISO. However, if no biased deviatoric MT can compensate the lack of ISO, a correlation minimum is

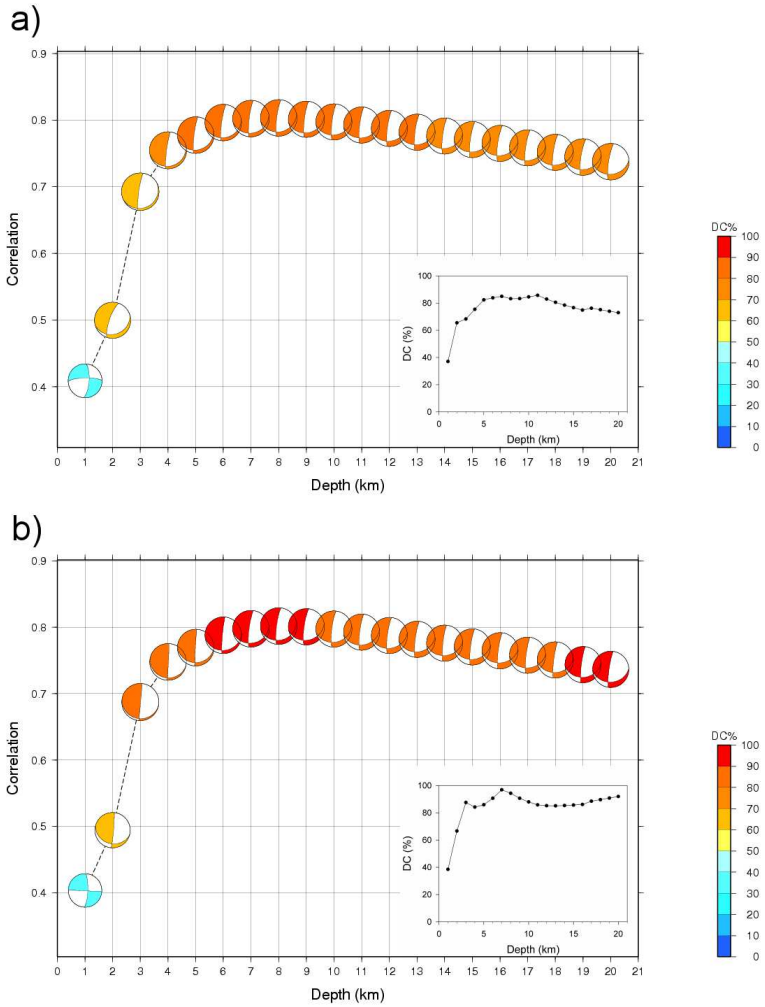

Figure 7. Waveform correlation for the Cretan Sea earthquake. Real waveforms are inverted in two modes: (a) full MT and (b) deviatoric MT. The color version of this figure is available only in electronic edition.

created. At another trial depth, $D' \neq D$, some deviatoric-MT source model can exist (e.g., a model with a spurious CLVD, and/or with biased strike, dip, and rake angles) that produces synthetics fitting real data almost as well as the full-MT synthetics at depth D. Hence, the source depth estimate in the deviatoric-MT inversion may be biased from D to D'.

The previous detailed synthetic tests have some practical implications. We think that the message of the synthetic tests is quite strong. They suggest that if the data processing indicates a small DC%, the correlation-depth analysis should be made twice, both in the full-MT and deviatoric-MT modes. If these two results strongly differ from each other, they may indicate the presence of a large ISO component. More sophisticated methods (e.g., Křížová et al., 2013) may then be applied as a next step toward checking relevance of the large ISO%.

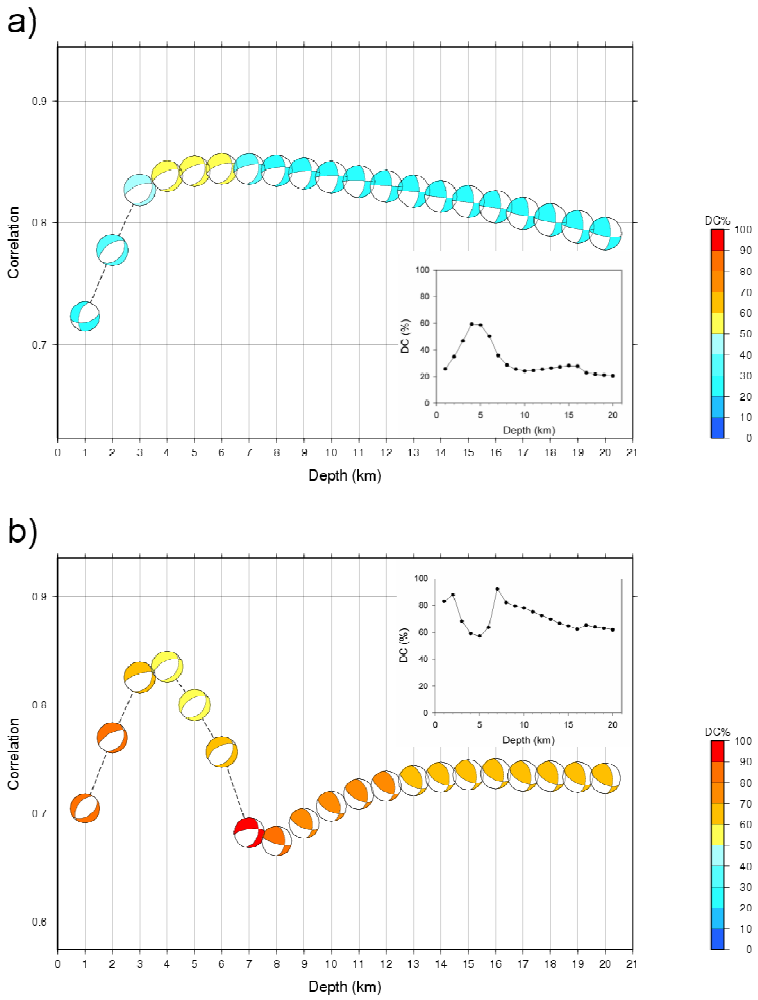

Figure 8. Waveform correlation for the Santorini earthquake. Real waveforms are inverted in two modes: (a) full MT and (b) deviatoric MT. The color version of this figure is available only in electronic edition.

RESULTS - REAL DATA

The inversion results using the observed waveforms from the two earthquakes as introduced in Table 1 are summarized in Tables 2 and 3, and Figures 7 and 8 for the Cretan Sea and Santorini Island events, respectively. To more deeply investigate possible non-DC components, we follow the approach of the Synthetic Data Inverted in Deviatoric-MT Mode section and study the depth-dependent correlation in two modes: full and deviatoric. For Cretan sea earthquake, our CLVD value (6%) is smaller than the CLVD value (43%) obtained in previous modeling, using a different code and station geometry (Kiratzi, 2013). For the Santorini earthquake, we expect a large ISO component because standard deviatoric CMT inversion indicated a DC% as low as 59%. Two velocity models for Santorini earthquake were used (D-model and N-model), but the results are similar; thus, we present in Figure 8 only the latter.

The two events are very different. The Cretan Sea has a large DC% for both inversion modes in a broad range of the trial source depths, and the correlation-depth variations are almost identical. These are indications of a low ISO component. The

Santorini earthquake has a lower DC% at the depths where the correlation takes its maximum values. Most importantly, the full-MT and deviatoric-MT inversions provide considerably different correlation-depth dependences. For the Santorini earthquake, we obtain a weak correlation maximum at a depth of 6 km in the full-MT mode, contrasting with a very pronounced local minimum in the deviatoric-MT mode at a depth of 8 km, and also featuring a local maximum at the depth of 4 km. Compared with the synthetic tests, we interpret these features as an indicator for a large ISO component of the Santorini Island event. On the other hand, the missing local minimum in correlation function for Cretan Sea earthquake indicates a relatively low ISO component. We also believe that the correlation maximum at 4 km is a biased estimate of the centroid depth; the true depth could be closer to 6-8 km. The present conclusion of the large ISO% of the Santorini earthquake is in good agreement with the independently obtained results of Křížová et al. (2013).

CONCLUSIONS

For any earthquake, we may apply several methods attempting to resolve its CMT and to estimate its uncertainty. Although the CMT calculations belong to routine tasks, the uncertainty estimate is more of a research problem, particularly regarding the ISO component. This work provides a hypothesis that some simple tools, applicable in the routine MT inversion, could relatively easily identify earthquakes with strong ISO, which can be used in routine seismological practice.

Our recommendation has as follows: if routine processing of an earthquake indicates a small DC%, then the waveform inversion should be made in two modes: the full MT and the deviatoric MT. The processing should include a careful examination of the waveform correlation as a function of the trial centroid depth. If the two inversion modes (full and deviatoric) provide remarkably different correlation-depth functions, and in particular, if the correlation of the deviatoric inversion poses a deep local minimum, although in the full-MT inversion such a minimum is absent, we have an indication of a strong ISO component. The likely source depth is close to that local minimum. Because in routine practice just the maximum of the correlation-depth function provides an estimate of the centroid depth, here we see that in case of the deviatoric inversion of an event with large ISO this traditional approach fails. In this sense, deviatoric inversions of events with large ISO component should be applied with caution because the maximum of the correlation-depth function may return an incorrect depth (and possibly also an incorrect fault-plane solution).

This hypothesis has been supported by extensive synthetic tests. Interestingly, the tests indicated that the mentioned features of the correlation-depth functions of the events with large ISO components (i.e., deep local minima present in the deviatoric-MT inversion but absent in the full-MT inversion) are rather robust. Indeed, these characteristic features were found even in the case when synthetic waveforms simulated in one velocity model were inverted in another model available for the same region.

Our approach has been tested on two shallow earthquakes in Greece, the 27 January 2012 M_w 5.3 Cretan Sea event and the 26 June 2009 M_w 4.9 Santorini event. Their behavior was quite different, indicating a significantly stronger ISO component for the Santorini earthquake. This indication is in agreement with the previously detailed analysis of the large ISO, made with a more complex research tool (Křížová et al., 2013).

As a final remark, we propose that the events indicated in the standard CMT processing as potential candidates for large ISO (using our proposed approach) be further analyzed by more sophisticated methods.

DATA AND RESOURCES

Broadband waveforms were retrieved from the permanent stations of the Hellenic Unified Seismic Network (HUSN), operated jointly by the National Observatory of Athens (NOA, doi:10.7914/SN/HL), the Aristotle University of Thessaloniki (AUTH, doi:10.7914/SN/HT), the University of Patras (UPSL, doi:10.7914/SN/HP), and the University of Athens (UOA). The records from one station of the National Seismic Network of Turkey (DDA) were also used. A number of UPSL stations are co-operated by the Charles University in Prague. Software ISOLA (Sokos and Zahradník, 2008) was used to calculate the moment tensors. Green's functions in ISOLA were computed using the AXITRA code of Coutant (1989). The Generic Mapping Tools (GMT; Paul Wessel and Walter H. F. Smith, http://gmt.soest.hawaii.edu/, last accessed July 2016) and MATLAB (http://www.mathworks.com/products/matlab/, last accessed July 2016) were also used. Preliminary agency reports, including moment tensor solutions, are mentioned on the European-Mediterranean Seismological Centre (EMSC) webpages (www.emsc-csem.org/, last accessed July 2016).

ACKNOWLEDGMENTS

Partial financial support of this work was obtained from the Czech Science Foundation Grant Number GACR-14-04372S. We also acknowledge partial support from THALES project (MIS377335), funded by the European Union (European Social Fund, ESF) and Greek national funds. The comments and suggestions of C. P. Evangelidis are gratefully acknowledged.

REFERENCES

Aki, K., and P. G: Richards (2002), *Quantitative seismology,* University Science Books, Sausalito, California, 704 pp.

Bouchon, M. (1981). A simple method to calculate Green's functions for elastic layered media, *Bull. Seismol. Soc. Am.* **71**, 959-971.

Cesca, S., Rohr, A., and T. Dahm (2013). Discrimination of induced seismicity by full moment tensor inversion and decomposition. *J. Seismol.* **17,** no. 1, 147-163.

Coutant, O. (1989). Program of numerical simulation AXITRA, *Res. Rept.*, LGIT, Grenoble, France (in French).

Dimitriadis, I., C. Papazachos, D. Panagiotopoulos, P. Hatzidimitriou, M. Bohnhoff, M. Rische, and T. Meier (2010). P and S velocity structures of the Santorini-Coloumbo volcanics system (Aegean Sea, Greece) obtained by non-linear inversion of travel times and its tectonic implications, *J. Volcanol. Geoth. Res.* **195**, 13-30.

Dufumier, H., and L. Rivera (1997). On the resolution of the isotropic component in moment tensor inversion, *Geophys. J. Int.* **131**, 595–606.

Ford, S. R., Dreger, D. S., & Walter, W. R. (2009). Identifying isotropic events using a regional moment tensor inversion. *J. Geophys. Res.* **114,** no. B1, doi: 10.1029/2008JB005743.

Foulger, G. R., Julian, B. R., Hill, D. P., Pitt, A. M., Malin, P. E., & Shalev, E. (2004). Non-double-couple microearthquakes at Long Valley caldera, California, provide evidence for hydraulic fracturing. *J. Volcanol. Geoth. Res.* **132,** no. 1, 45-71.

Horálek, J., J. Šílený, and T. Fischer (2002). Moment tensors of the January 1997 earthquake swarm in NW Bohemia (Czech Republic): double-couple vs. non-double-couple events. *Tectonophysics*, **356,** no. 1, 65-85.

Julian, B. R., A. D. Miller, and G. R. Foulger (1998). Non-double-couple Earthquakes, 1. Theory, *Rev. Geophys.* **36**, 525-549.

Kagan, Y. Y. (1991). 3-D rotation of double-couple earthquake sources, *Geophys. J. Int.* **106**, 709-716, doi 10.1111/j.1365-246X.1991.tb06343.x.

Kawakatsu, H. (1996). Observability of the isotropic component of a moment tensor. *Geophys. J. Int.* **126,** no. 2, 525-544.

Kikuchi, M., and H. Kanamori (1991). Inversion of complex body waves. III, *Bull. Seismol. Soc. Am.* **81,** 2335-2350.

Kiratzi, A. (2013). The January 2012 earthquake sequence in the Cretan Basin, south of the Hellenic Volcanic Arc: Focal mechanisms, rupture directivity and slip models, *Tectonophysics,* **586,** 160-172, doi: 10.1016/j.tecto.2012.11.019.

Křížová, D., J. Zahradník, and A. Kiratzi (2013). Resolvability of Isotropic Component in Regional Seismic Moment Tensor, Inversion, *Bull. Seismol. Soc. Am.* **103,** no. 4, 2460 - 2473, doi: 10.1785/0120120097.

Minson, S. E., and D. S. Dreger (2008). Stable inversions for complete moment tensors. *Geophys. J. Int.* **174,** no. 2, 585-592.

Mustać, M., and H. Tkalčić (2016). Point source moment tensor inversion through a Bayesian hierarchical model. *Geophys. J. Int.* **204,** no. 1, 311-323, doi: 10.1093/gji/ggv458.

Novotný, O., J. Zahradník, and G-A. Tselentis (2001). Northwestern Turkey earthquakes and the crustal structure inferred from surface waves observed in Western Greece, *Bull. Seismol. Soc. Am.* **91**, 875-879.

Shuler, A., G. Ekström, and M. Nettles (2013), Physical mechanisms for vertical-CLVD earthquakes at active volcanoes, *J. Geophys. Res.* **118**, 1569–1586, doi:10.1002/jgrb.50131.

Silver, P. G., and T. H. Jordan (1982). Optimal estimation of scalar seismic moment, *Geophys. J. R. Astron. Soc.* **70**, 755-787, doi: 10.1111/j.1365-246X.1982.tb05982.x.

Sokos, E. and J. Zahradník (2013). Evaluating centroid moment tensor uncertainty in new version of ISOLA software, *Seismol. Res. Lett.* **84**, 656-665.

Sokos, E. N., and J. Zahradník (2008). ISOLA a Fortran code and a Matlab GUI to perform multiple-point source inversion of seismic data, *Comput. Geosci.* **34**, 967-977.

Song, F., and M. N. Toksöz (2011). Full-waveform based complete moment tensor inversion and source parameter estimation from downhole microseismic data for hydrofracture monitoring, *Geophysics* **76,** no. 6, WC103-WC116.

Templeton, D. C., and D. S. Dreger (2006). Non-double-couple earthquakes in the Long Valley volcanic region, *Bull. Seismol. Soc. Am.* **96**, 69–79.

Tkalčić, H., D. S. Dreger, G. R. Foulger, and B. R. Julian (2009). The puzzle of the 1996 Bárdarbunga, Iceland, earthquake: No volumetric component in the source mechanism, *Bull. Seismol. Soc. Am.* **99**, 3077–3085.

Vackář J., J. Burjánek, and J. Zahradník (2015). Automated detection of disturbances in seismic records; MouseTrap code. *Seismol. Res. Lett.* **86**, 442-450.

Vasco, D. W. (1990). Moment-tensor invariants: Searching for non-double-couple earthquakes, *Bull. Seismol. Soc. Am.* **80**, no. 2, 354–371.

Vavryčuk, V. (2001). Inversion for parameters of tensile earthquakes, *J. Geophys. Res.,* **106**, 16,339-16,355.

Vavryčuk, V. (2004). Inversion for anizotropy from non-double-couple components of moment tensors. *J. Geophys. Res.* **109**, no. B07306, doi: 10.1029/2003JB002926.

Vavryčuk, V. (2011), Tensile earthquakes: Theory, modeling, and inversion, *J. Geophys. Res.*, **116**, no. B12320, doi:10.1029/2011JB008770.

Vavryčuk, V., M. Bohnhoff, Z. Jechumtálová, P. Kolář, and J. Šílený (2008). Non-double-couple mechanisms of microearthquakes induced during the 2000 injection experiment at the KTB site, Germany: A result of tensile faulting or anisotropy of a rock? *Tectonophysics*, **456,** no. 1, 74-93.

Zahradník, J., and S. Custódio (2012). Moment tensor resolvability: Application to southwest Iberia. *Bull. Seismol. Soc. Am.*, **102**, 1235-1254, doi: 10.1785/0120110216.

Zahradník, J., and A. Plešinger (2005). Long-period pulses in broadband records of near earthquakes *Bul. Seismol. Soc. Am.* **95**, no. 5, 1928-1939.

Zahradník, J., and A. Plešinger (2010). Toward understanding subtle instrumentation effects associated with weak seismic events in the near field. *Bull. Seismol. Soc. Am.* **100**, 59-73.

Zahradník, J., J. Janský, and V. Plicka (2008). Detailed waveform inversion for moment tensors of M ~ 4 events: Examples from the Corinth Gulf, Greece, *Bull. Seismol. Soc. Am.*, **98**, 2756-2771.

APPENDIX

Three synthetic tests were made (A–C), each one with six subtests (1–6). Tables A1 and A2 show the input data for these calculations. Tables A3–A5 are listed as a supplement to Figures 2-6.

Table A1

a-Coefficients Used to Generate Moment Tensor (MT) Models

Parameter	Test A	Tests B and C
a_1	-0.494837×10^{17}	-0.379445×10^{16}
a_2	0.964645×10^{16}	0.450544×10^{16}
a_3	0.102082×10^{18}	0.613149×10^{14}
a_4	-0.934958×10^{16}	-0.228232×10^{16}
a_5	-0.201239×10^{17}	-0.195328×10^{16}

Table A2

a_6-Coefficients Used to Generate MT Models

Calculation	Test A	Tests B and C
1	-0.1×10^{19}	-0.1×10^{18}
2	0.1×10^{19}	0.1×10^{18}
3	-0.1×10^{18}	-0.1×10^{17}
4	0.1×10^{18}	0.1×10^{17}
5	-0.5×10^{17}	-0.5×10^{16}
6	0.5×10^{17}	0.5×10^{16}

Table A3

Synthetic Test A. Data with Full MT Inverted in Full and Deviatoric Modes, Using Correct Velocity Model

Earthquake	DC	CLVD	ISO	CN	VR	Depth (km)	Strike (°)	Dip (°)	Rake (°)	K (°)*
A1N (full)	10.5	0.0	−89.5	2.56	99.98	8	186	81	−112	
							76	24	−21	
A1N (deviatoric)	8.5	91.5	0.0	3.81	97.00	3	331	52	96	47
							140	38	81	
A2N (full)	10.5	0.0	89.5	2.56	99.98	8	187	80	−112	
							76	24	−22	
A2N (deviatoric)	8.8	91.2	0.0	3.81	97.73	3	209	52	−96	37
							39	38	−82	
A3N (full)	54.1	0.0	−45.9	2.56	99.96	8	187	80	−112	
							76	24	−22	
A3N (deviatoric)	91.9	8.1	0.0	1.75	91.56	14	196	68	−113	
							67	33	−44	
A4N (full)	54.0	0.0	45.9	2.56	99.96	8	187	80	−112	14
							76	24	−22	
A4N (deviatoric)	57.4	42.6	0.0	2.57	90.69	4	191	74	−102	13
							51	20	−52	
A5N (full)	70.2	0.0	−29.8	2.56	99.95	8	187	80	−112	
							76	24	−22	
A5N (deviatoric)	96.3	3.7	0.0	1.54	96.52	10	191	74	−114	9
							70	28	−34	
A6N (full)	70.1	0.0	29.8	2.56	99.95	8	187	80	−112	
							76	24	−22	
A6N (deviatoric)	76.7	23.3	0.0	2.74	96.17	6	190	77	−106	9
							62	20	−39	

All calculations are for 12 stations. CLVD is stated in absolute value. DC, double couple; ISO, isotropic; CN, condition number; VR, variance reduction. Synthetic waveforms due to full MT are inverted under deviatoric constraint (ISO% = 0). The forward simulation and the inversion are made in same velocity model. Results for full MT for input data are put into the table for comparison. Subtests 1–6 differ in their ISO% values but share almost the same strike/dip, rake, and depth.

*K, Kagan angle (reference solution is the result for full MT in each subtest).

Table A4

Synthetic Test B. Data with Full MT Inverted in Full and Deviatoric Modes, Using Correct Velocity Model

Earthquake	DC	CLVD	ISO	CN	VR	Depth (km)	Strike (°)	Dip (°)	Rake (°)	K (°)*
B1N (full)	9.6	0.1	−90.3	3.90	99.95	6	252	66	−61	
							18	36	−138	
B1N (deviatoric)	12.5	87.5	0.0	4.42	98.23	2	318	42	93	88
							133	47	86	
B2N (full)	9.4	0.1	90.4	3.90	99.96	6	252	66	−60	
							18	36	−138	
B2N (deviatoric)	12.1	87.9	0.0	4.42	98.92	2	229	47	−86	30
							44	42	−93	
B3N (full)	51.5	0.1	−48.4	3.90	99.92	6	252	66	−61	
							18	36	−138	
B3N (deviatoric)	75.3	24.7	0.0	2.22	91.40	11	243	56	−65	13
							23	40	−122	
B4N (full)	51.4	0.1	48.5	3.90	99.94	6	252	66	−61	
							18	36	−138	
B4N (deviatoric)	57.7	42.3	0.0	3.20	97.87	4	244	58	−73	14
							34	34	−115	
B5N (full)	68.0	0.0	−31.9	3.90	99.91	6	252	66	−61	
							18	36	−138	
B5N (deviatoric)	70.7	29.3	0.0	2.31	96.96	9	252	64	−55	4
							14	42	−139	
B6N (full)	68.0	0.0	32.0	3.90	99.93	6	252	66	−61	
							18	36	−138	
B6N (deviatoric)	76.0	24.0	0.0	3.20	98.18	4	251	65	−67	6
							25	32	−130	

As in Table A3, but the input data (results for full-MT solution) have different strike/dip, rake, and depth than in test A. All calculations are for 15 stations (components with good signal-to-noise ratio are used).

*K, Kagan angle (reference solution is the result for full MT in each subtest)

Table A5

Synthetic Test C. Data with Full MT Inverted in Full and Deviatoric Modes Using Different Velocity Model

Earthquake	DC	CLVD	ISO	CN	VR	Depth (km)	Strike (°)	Dip (°)	Rake (°)	K (°)*
C1D (full)	8.2	21.7	−70.1	4.18	78.59	14	223	44	−76	33
							25	47	−102	
C1D (deviatoric)	32.0	68.0	0.0	2.82	71.17	20	202	42	−83	47
							13	47	−96	
C2D (full)	8.5	16.4	75.1	4.18	78.46	14	328	50	99	91
							133	40	78	
C2D (deviatoric)	16.3	83.7	0.0	5.17	71.17	2	213	51	−89	37
							32	38	−90	
C3D (full)	39.3	11.2	−49.5	3.64	79.32	5	251	65	−59	3
							17	38	−137	
C3D (deviatoric)	62.8	37.2	0.0	2.18	72.95	11	242	56	−64	14
							20	40	−123	
C4D (full)	36.7	13.8	49.5	3.02	79.72	6	248	65	−59	5
							14	38	−137	
C4D (deviatoric)	72.1	27.9	0.0	3.38	77.83	3	242	60	−73	13
							31	33	−116	
C5D (full)	51.0	15.5	−33.5	3.63	83.55	5	250	64	−60	4
							17	38	−135	
C5D (deviatoric)	61.9	38.1	0.0	2.59	81.56	7	247	61	−59	9
							16	41	−132	
C6D (full)	49.1	16.9	34.0	3.02	83.47	6	248	63	−60	6
							16	38	−134	
C6D (deviatoric)	89.3	10.7	0.0	3.10	82.50	4	245	61	−69	10
							26	34	−123	

Synthetic waveforms due to full MT are inverted under deviatoric constraint (ISO% = 0). The forward simulation was made in N-model and the inversion in D-model. Results for full-MT solution in N-model are in Table A4. Subtests 1–6 differ in their ISO% values but share the same strike/dip, rake, and depth, as also seen in test B. All calculations are for 15 stations (components with good signal-to-noise ratio are used).

*K, Kagan angle (reference solution is the result for full MT in N-model, mentioned in Table A4, in each subtest).

Supplementary material: Additional results for chosen earthquakes and for synthetic tests

All Figures in Supplementary material are correlation diagrams and in right corner the beach ball for the best solution is added (its colour is always red and have no connection to DC scale which is used in correlation diagrams).

The results are discused in the main text of this thesis, so here is no summary of calculations.

S1. Jackknife tests

All jackknife tests are calculated for the geographic coordinates which were used for calculations in articles Křížová et al. (2013) for Santorini Island earthquakes and in Křížová et al. (2016) for Cretan Sea earthquake. Summary of results for jackknife tests for two Santorini Islands earthquakes for both used models (D and N) for deviatoric MT and full MT are in the Figure 4 in Křížová et al. (2013).

The solutions for earthquakes which were processed during jackknife tests are relatively stable. So, the shapes of correlation diagrams are almost same in each group of outcomes (for chosen earthquake, crustal model and type of MT inversion). Like a representative sample we show in the Figures (below in this Supplementary material) results for calculation using all stations and for comparison two results of jackknife tests where station ZKR is excluded in the first case and station CHOS is excluded in the second case. We chose this results because all components from stations ZKR and CHOS are used during common calculations for both Santorini Island earthquakes and also for Cretan Sea earthquake. Results for remaining jackknife tests are mentioned only in Tables (below in this Supplementary material).

Note that there is a first boundary in both crustal models (N and D) in the depth of 1.0 km and in the correlation diagrams we can often see some artefact of calclulation using the Green's functions which are calculated in 1D velocity models by the discrete wavenumber method (Bouchon, 1981).

S1.1. Jackknife tests for Santorini earthquake swarm - strongest event

Results are summarized in the Tables S1. – S2. and in the Figures S1. and S2. The depth step is 0.5 km in this case.

Table S1.: Jackknife tests for Santorini Island earthquake swarm – strongest event, model N

Model N	Full MT							Deviatoric MT					
excluded station	strike; dip; rake (°)			DC	CLVD	ISO	VR	strike; dip; rake (°)			DC	CLVD	VR
none	255	69	-57	41.9	5.0	53.1	65.5	243	59	-74	59.2	40.8	64.3
	15	38	-144					34	33	-114			
APE	265	82	-43	27.9	13.0	59.1	65.4	242	66	-78	80.8	19.2	64.9
	3	47	-169					36	26	-113			
LAST	256	68	-57	48.2	0.1	51.7	64.3	245	59	-72	56.2	43.8	63.1
	16	38	-143					32	34	-117			
NIS1	254	68	-63	51.1	2.1	46.8	65.1	251	67	-75	68.0	32.0	63.9
	21	33	-138					36	26	-121			
ZKR	254	67	-57	43.2	3.6	53.2	64.7	242	58	-73	57.4	42.6	63.5
	14	39	-142					33	35	-114			
SIVA	255	68	-57	42.2	4.7	53.1	66.0	243	59	-74	59.2	40.8	64.8
	15	37	-144					34	33	-114			
KARP	255	68	-57	42.5	4.2	53.3	66.9	243	59	-74	58.4	41.6	65.8
	15	38	-144					34	34	-114			
ANKY	255	69	-52	34.4	9.0	56.6	66.9	241	58	-73	59.6	40.4	65.1
	10	41	-148					32	34	-114			
CHOS	252	67	-61	49.9	2.8	47.3	65.1	242	59	-73	58.3	41.7	64.0
	17	36	-138					32	34	-115			
ATH	253	68	-61	41.1	7.5	51.4	66.2	243	60	-74	59.3	40.7	64.8
	16	34	-141					34	32	-114			
VLI	257	69	-54	44.0	1.2	54.8	65.3	248	64	-71	55.1	44.9	64.2
	14	40	-146					30	31	-123			
AYDN	256	68	-62	47.0	5.7	47.3	66.0	246	60	-75	65.3	34.7	65.2
	20	34	-140					37	32	-114			
LTK	254	69	-59	39.5	7.9	52.6	66.4	243	59	-74	60.2	39.8	65.1
	15	36	-143					34	33	-114			
THAL	254	69	-58	40.8	6.5	52.7	66.2	242	59	-74	59.8	40.2	64.8
	15	36	-143					34	33	-114			
SIGR	256	69	-56	46.2	1.7	52.1	65.9	244	59	-72	57.7	42.3	64.6
	15	38	-144					32	34	-117			
PRK	256	68	-57	46.7	0.9	52.4	66.0	244	59	-72	57.1	42.9	64.8
	15	38	-144					32	34	-116			

Table S2.: Jackknife tests for Santorini Island earthquake swarm – strongest event, model D

Model D	Full MT							Deviatoric MT					
excluded station	strike; dip; rake (°)			DC	CLVD	ISO	VR	strike; dip; rake (°)			DC	CLVD	VR
none	253	65	-67	48.6	28.0	23.5	69.6	251	63	-70	52.4	47.6	69.5
	27	32	-130					32	32	-124			
APE	254	65	-62	50.0	14.6	35.4	62.8	251	62	-69	55.2	44.8	62.6
	23	36	-134					32	34	-123			
LAST	252	65	-68	49.5	33.9	16.6	69.0	252	65	-70	52.8	47.2	68.9
	29	32	-128					32	30	-126			
NIS1	252	67	-74	65.2	34.7	-0.1	71.4	252	67	-74	65.3	34.7	71.4
	36	27	-122					36	27	-122			
ZKR	250	64	-66	47.8	22.1	30.1	68.9	251	64	-70	52.3	47.7	68.7
	24	34	-130					31	31	-125			
SIVA	253	65	-67	47.5	31.5	21.0	71.1	253	64	-96	51.1	48.9	71.0
	28	32	-130					31	32	-126			
KARP	252	66	-68	50.5	26.0	23.5	72.3	250	64	-71	54.2	45.8	72.1
	27	31	-129					32	31	-123			
ANKY	249	64	-64	48.3	18.3	33.4	71.9	248	62	-69	53.0	47.0	71.6
	22	35	-132					29	33	-124			
CHOS	251	65	-67	47.4	28.7	23.9	69.1	250	63	-70	51.4	48.6	69.0
	26	33	-130					31	32	-124			
ATH	253	65	-66	45.6	31.8	22.6	69.5	253	63	-69	48.9	51.1	69.4
	27	33	-130					32	32	-125			
VLI	254	65	-64	41.8	31.4	26.8	70.0	251	62	-68	45.6	54.4	69.8
	25	34	-132					30	34	-125			
AYDN	254	66	-68	54.0	22.0	24.0	70.5	252	64	-71	57.8	42.2	70.3
	29	31	-129					35	30	-122			
LTK	253	65	-66	47.7	28.6	23.7	69.7	251	63	-69	51.5	48.5	69.6
	27	33	-130					32	32	-124			
THAL	253	65	-66	47.5	28.3	24.2	69.9	251	63	-69	51.4	48.6	69.8
	27	33	-130					32	32	-124			
SIGR	253	65	-66	47.5	27.9	24.6	69.3	251	63	-69	51.5	48.5	69.1
	27	33	-131					32	32	-124			
PRK	252	65	-64	46.2	19.7	34.1	69.6	251	63	-70	51.2	48.8	69.4
	24	34	-132					32	32	-124			

For the calculations of full MT where the station NIS1 was excluded we get ISO = -0.1, but for this case we have CN = 6.30.

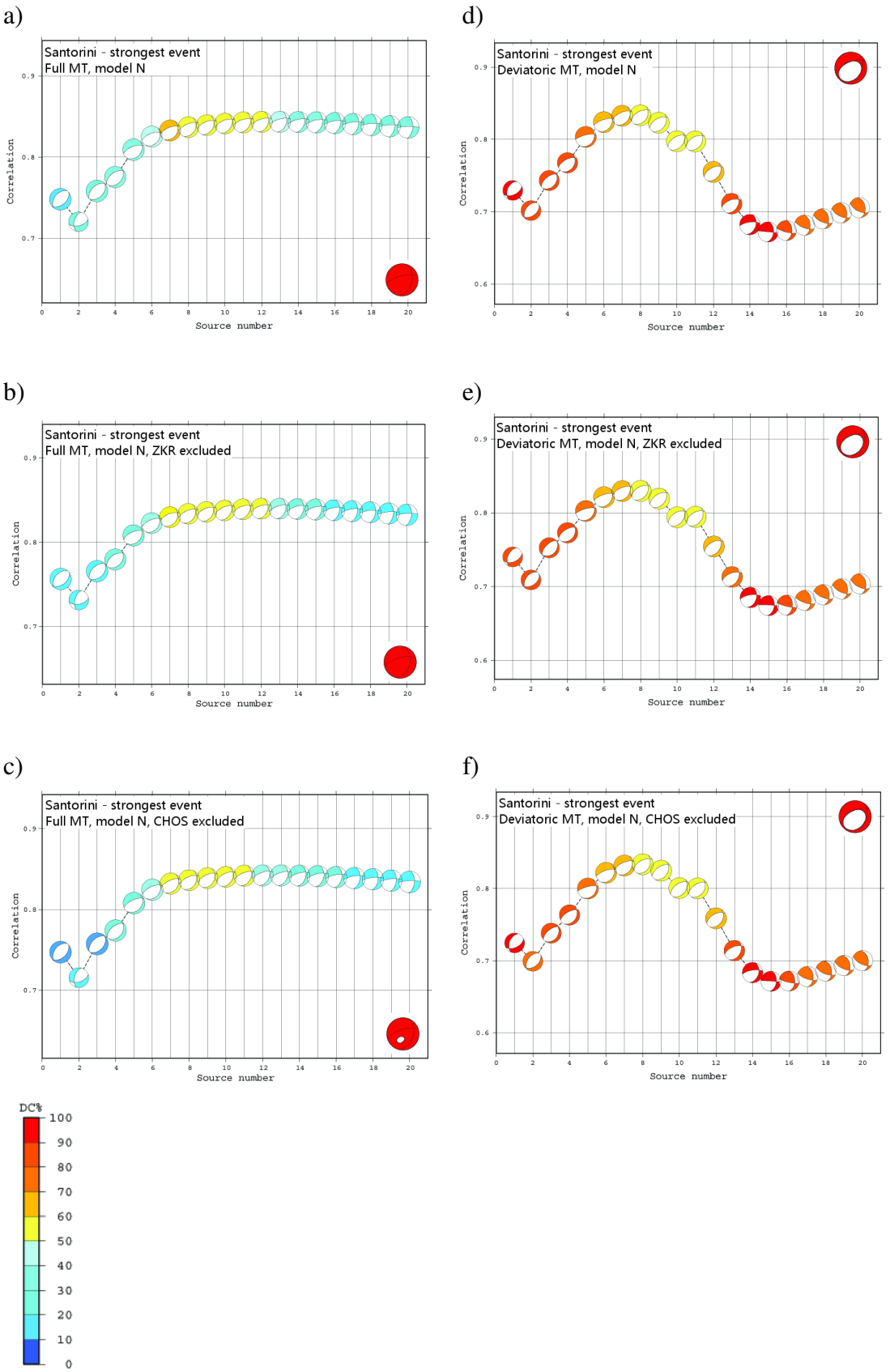

Figure S1. Correlation diagrams for Santorini Island earthquake swarm – strongest event, model N. In the left column are solutions for full MT inversion; in the right column are results for deviatoric MT.

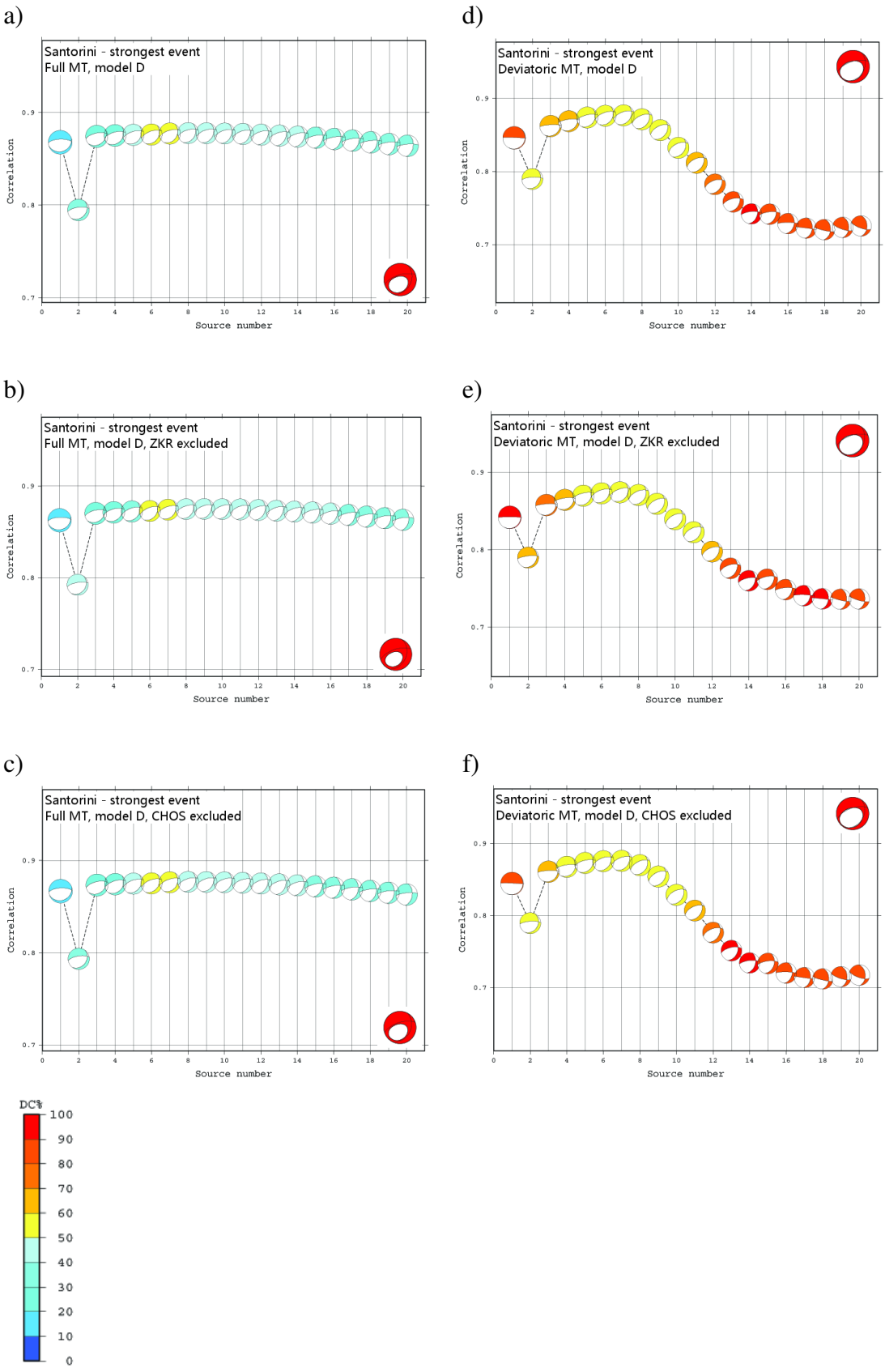

Figure S2. Correlation diagrams for Santorini Island earthquake swarm – strongest event, model D. In the left column are solutions for full MT inversion; in the right column are results for deviatoric MT.

S1.2. Jackknife tests for Santorini earthquake swarm - second strongest event

Results are summarized in the Tables S3. – S4. and in the Figures S3. and S4. The depth step is 0.5 km in this case.

Table S3.: Jackknife tests for Santorini Island earthquake swarm – second strongest event, model N

Model N	Full MT							Deviatoric MT					
excluded station	strike; dip; rake (°)			DC	CLVD	ISO	VR	strike; dip; rake (°)			DC	CLVD	VR
none	248	49	-69	35.9	38.8	25.3	65.3	244	49	-75	69.4	30.6	65.0
	38	44	-112					42	42	-106			
APE	221	47	-108	37.0	47.3	15.7	61.7	225	46	-103	63.3	36.7	61.6
	67	45	-71					64	44	-76			
LAST	245	51	-73	39.1	38.4	22.5	63.3	240	49	-80	75.1	24.9	62.8
	39	41	-109					46	41	-100			
ZKR	257	51	-59	24.9	43.9	31.2	63.5	250	49	-71	65.5	34.5	63.3
	34	47	-122					42	44	-110			
KARP	248	49	-68	36.1	39.5	24.4	77.4	245	49	-75	68.5	31.5	76.8
	38	44	-113					42	42	-106			
CHOS	249	50	-65	37.6	35.5	26.9	63.9	245	48	-73	75.8	25.2	63.5
	34	45	-116					40	43	-108			
ATH	246	49	-72	35.7	39.1	25.2	65.7	243	49	-76	70.3	29.7	65.5
	39	43	-109					43	42	-105			
VLI	249	49	-68	36.9	37.9	25.3	63.2	246	49	-74	67.3	32.7	62.8
	37	44	-113					42	43	-107			
LTK	245	50	-73	34.0	40.9	25.1	67.0	242	49	-78	68.5	31.5	66.8
	40	42	-108					44	41	-103			
SIGR	251	50	-65	58.4	27.3	14.3	65.6	249	49	-68	75.1	24.9	65.3
	35	45	-116					37	44	-113			
PRK	248	48	-68	58.1	27.7	14.2	65.2	247	48	-70	74.8	25.2	64.9
	37	45	-113					39	44	-110			

Table S4.: Jackknife tests for Santorini Island earthquake swarm – second strongest event, model D

Model D	Full MT							Deviatoric MT					
excluded station	strike; dip; rake (°)			DC	CLVD	ISO	VR	strike; dip; rake (°)			DC	CLVD	VR
none	236	47	-83	72.2	3.7	-24.1	70.0	236	46	-82	81.7	18.3	69.8
	47	43	-96					46	43	-97			
APE	232	44	-91	70.1	3.4	-26.4	61.9	231	44	-92	75.8	24.2	61.7
	54	45	-88					54	54	-87			
LAST	235	50	-85	71.5	3.9	-24.6	69.4	235	49	-84	80.5	19.5	69.3
	48	39	-95					46	40	-96			
ZKR	238	48	-83	72.7	2.3	-25.0	68.7	237	48	-83	78.3	21.7	68.7
	48	41	-97					47	42	-97			
KARP	235	48	-85	74.9	1.7	-23.4	84.1	234	47	-85	79.9	20.1	83.9
	49	41	-94					48	42	-94			
CHOS	236	46	-83	71.5	4.9	-23.6	68.8	235	46	-83	84.8	15.2	68.6
	46	43	-97					45	43	-97			
ATH	237	46	-83	50.1	15.1	-34.8	70.1	237	46	-82	82.9	17.1	69.8
	48	43	-96					45	44	-98			
VLI	240	46	-80	48.3	15.9	-35.9	68.1	240	46	-77	84.2	15.8	68.2
	47	44	-99					43	46	-77			
LTK	238	46	-82	70.8	4.7	-24.5	71.1	237	46	-81	81.9	18.1	70.9
	46	44	-98					45	44	-98			
SIGR	237	46	-83	71.6	4.4	-24.0	69.6	236	46	-82	82.9	17.1	69.3
	47	44	-97					46	44	-97			
PRK	236	46	-83	72.9	3.9	-23.2	69.4	236	46	-83	83.8	16.2	69.2
	47	43	-96					46	43	-96			

This event is characterized by the opposite sign of ISO in the two applied crustal models.

CN for full MT calculations in model D with excluded station:

none = 6.38; APE = 6.99; LAST = 6.32; ZKR = 6.57; KARP = 6.42; CHOS = 6.31; ATH = 8.28; VLI = 8.11; LTK = 6.41; SIGR = 6.28; PRK = 6.31.

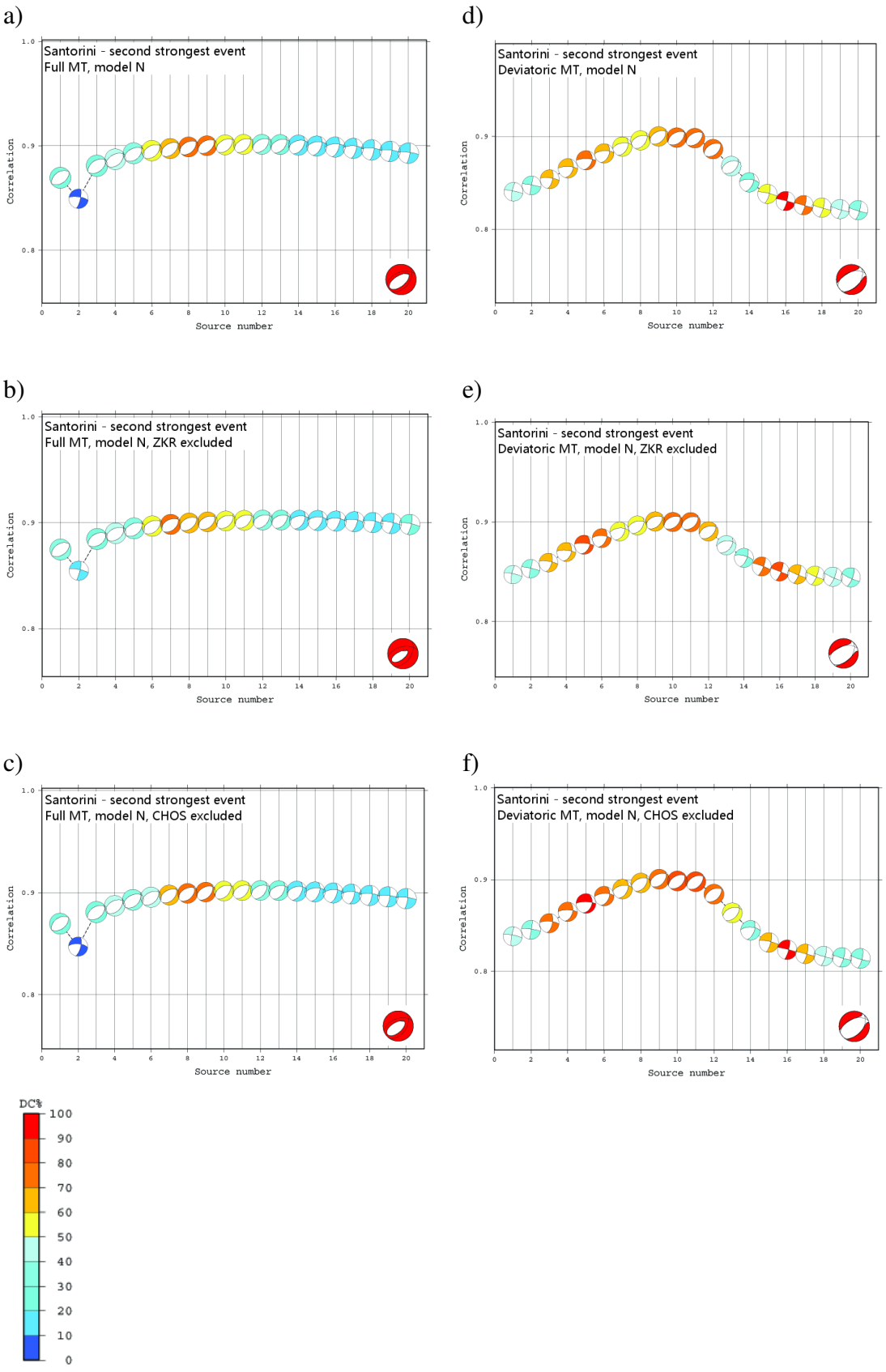

Figure S3. Correlation diagrams for Santorini Island earthquake swarm – second strongest event, model N. In the left column are solutions for full MT inversion; in the right column are results for deviatoric MT.

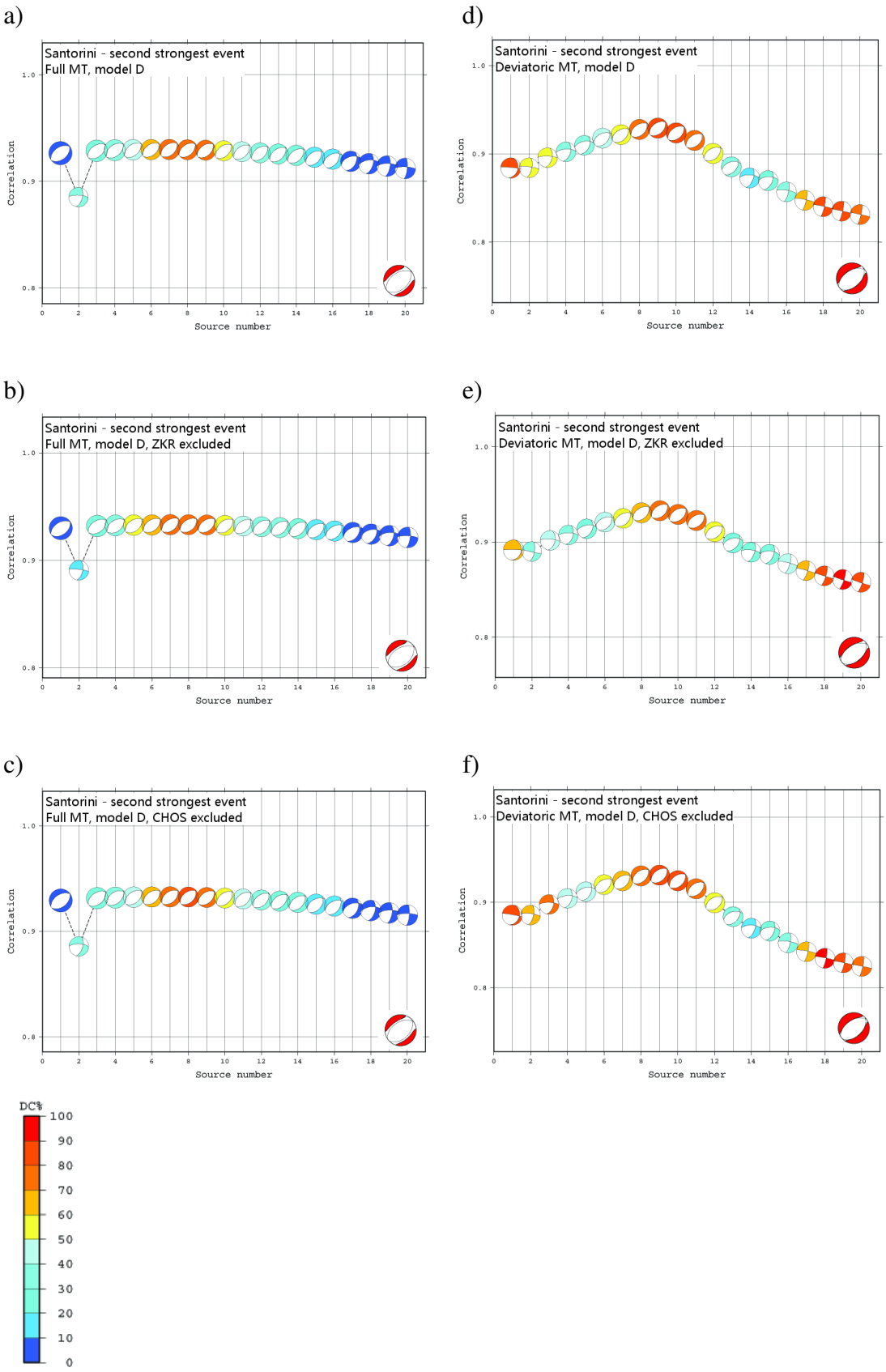

Figure S4. Correlation diagrams for Santorini Island earthquake swarm – second strongest event, model D. In the left column are solutions for full MT inversion; in the right column are results for deviatoric MT.

S1.3. Jackknife tests for Cretan Sea earthquake

Results are summarized in the Table S5. and in the Figure S5. The depth step is 1.0 km in this case.

Table S5.: Jackknife tests for Cretan Sea earthquake swarm

Model N	Full MT							Deviatoric MT					
excluded station	strike; dip; rake (°)			DC	CLVD	ISO	VR	strike; dip; rake (°)			DC	CLVD	VR
none	187	81	-113	83.2	7.2	-9.6	64.5	188	80	-112	94.4	5.6	64.2
	79	24	-20					76	24	-23			
SIVA	189	83	-105	84.8	0.8	-14.4	67.2	189	82	-108	94.9	5.1	66.5
	75	16	-24					77	19	-23			
APE	187	80	-109	84.8	0.4	-14.8	63.6	188	78	-111	98.5	1.5	63.2
	73	21	-25					72	24	-28			
ZKR	188	80	-112	82.0	8.8	-9.2	65.2	189	79	-113	87.7	12.3	65.1
	77	23	-23					76	26	-25			
ANKY	186	82	-115	81.2	7.0	-11.8	62.1	187	80	-114	94.4	5.6	61.7
	80	26	-17					77	26	-22			
GVD	185	84	-118	90.4	6.1	-3.5	66.9	186	83	-118	94.2	5.8	66.8
	84	28	-12					84	28	-13			
NISR	189	81	-112	87.4	7.3	-5.3	65.1	189	80	-112	93.5	6.5	65.0
	78	23	-22					77	23	-24			
KARP	188	79	-113	84.8	5.3	-9.9	63.1	189	78	-112	96.4	3.6	62.8
	76	25	-24					74	25	-27			
VLI	187	82	-113	83.0	4.5	-12.5	63.6	188	79	-114	94.4	5.6	63.1
	79	24	-19					77	26	-23			
KRND	187	83	-111	81.2	9.8	-9.0	66.5	188	82	-113	87.6	12.4	66.2
	81	22	-17					80	24	-19			
VLY	187	81	-114	77.6	11.2	-11.2	64.8	188	79	-115	86.1	13.9	64.5
	78	25	-21					76	27	-23			
SMG	188	81	-113	84.4	6.0	-9.6	64.0	189	79	-112	95.7	4.3	63.8
	79	24	-20					76	24	-24			
CHOS	187	81	-113	86.5	3.9	-9.6	64.7	188	79	-113	98.1	1.9	64.4
	78	25	-20					76	25	-24			

CN for full MT calculations with excluded station:
none = 2.56; SIVA = 3.26; APE = 2.57; ZKR = 2.69; ANKY = 2.54; GVD = 2.85; NISR = 2.59; KARP = 2.49; VLI = 2.51; KRND = 2.58; VLY = 2.61; SMG = 2.59; CHOS = 2.51;

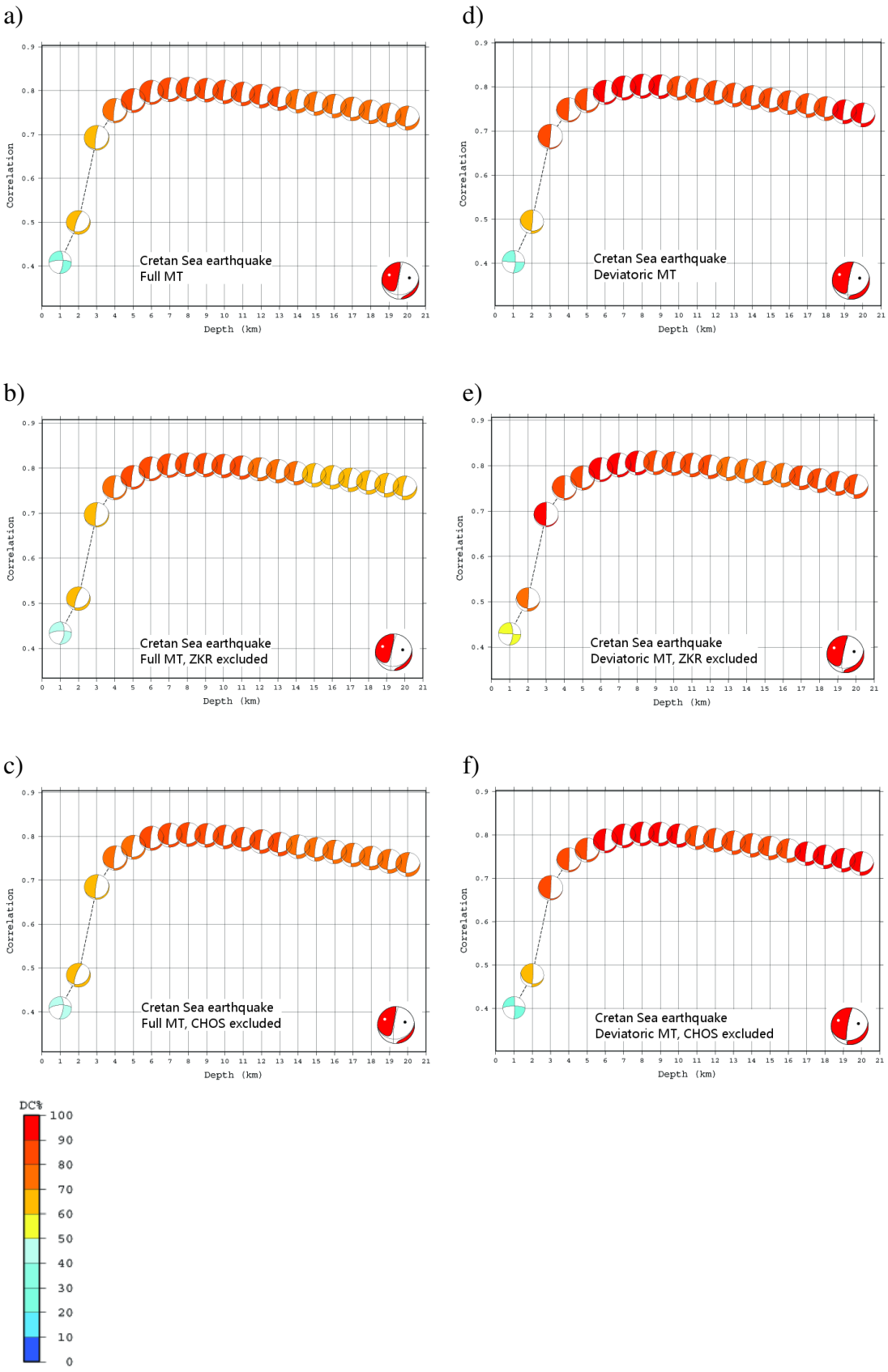

Figure S5. Correlation diagrams for Cretan sea earthquake – model N. In the left column are solutions for full MT inversion; in the right column are results for deviatoric MT.

S2. Correlation diagrams for synthetic tests

Results are summarized in the Tables A3 – A5 and Figures 4. – 6. in Křížová et al. (2016) and here in the Figures S6. – S11.

Recall that the source depth prescribed in synthetic data is 8 km for Test A, and 6 km for Tests B and C. Synthetic seismograms created for the full-MT source at these depths are inverted either in the full-MT or deviatoric-MT mode, while the trial depth is free.

In the Figure S6.b is for the subtest A2 – full MT shown as a result beach ball which probably has not the right color (it is no reason for solution like this). In our opinion it could be due to version of GMT 4 (http://gmt.soest.hawaii.edu/). The similar situation is in the Figure S8.a for the subtest B1 – full MT. The question is if the nodal lines on beach balls make sense even if the ISO component of MT is (in absolute value) higher than 90%.

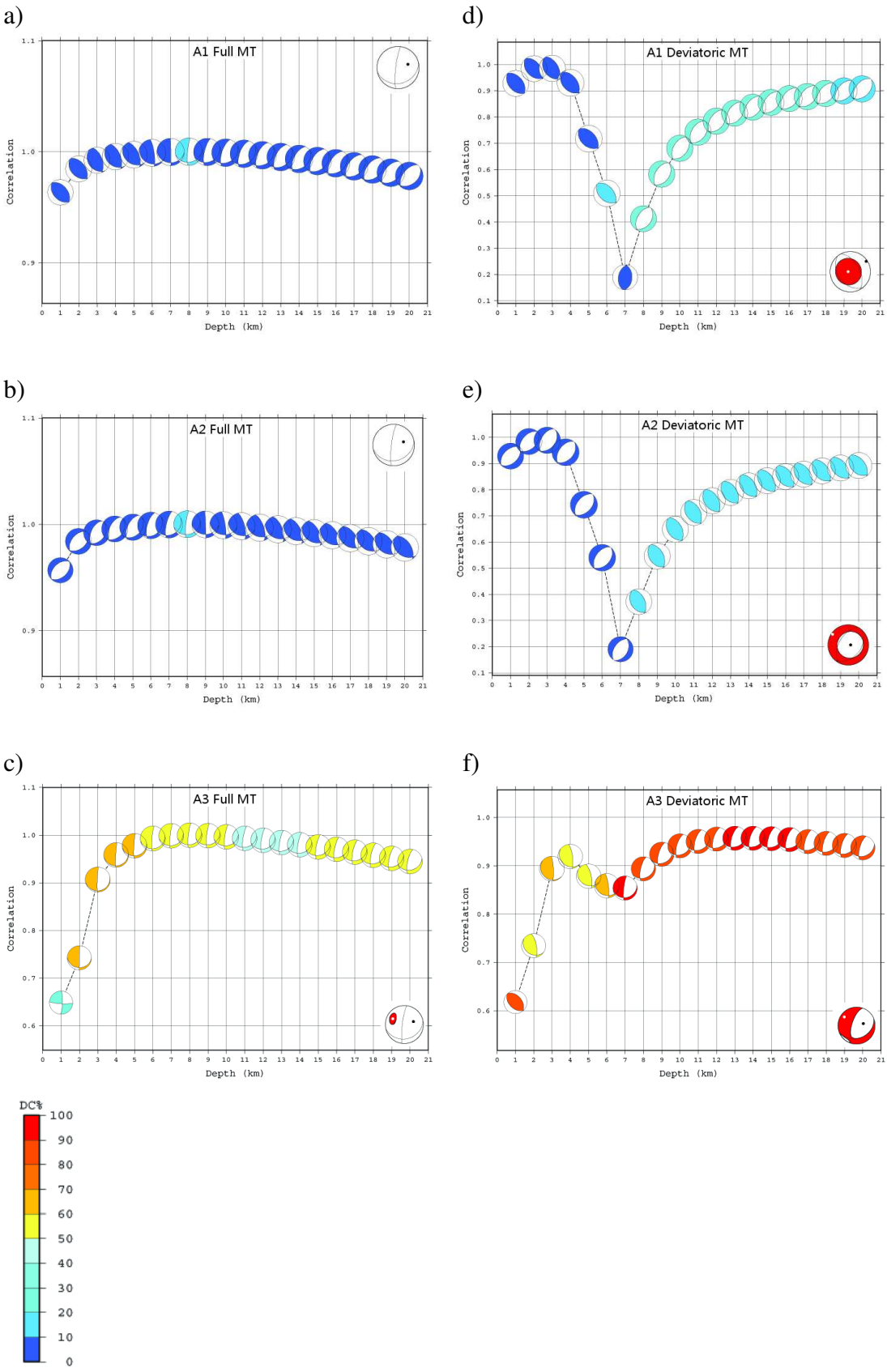

Figure S6. Correlation diagrams for test A (part I.) and subtests 1 – 3. In the left column are solutions for full MT inversion; in the right column are results for deviatoric MT.

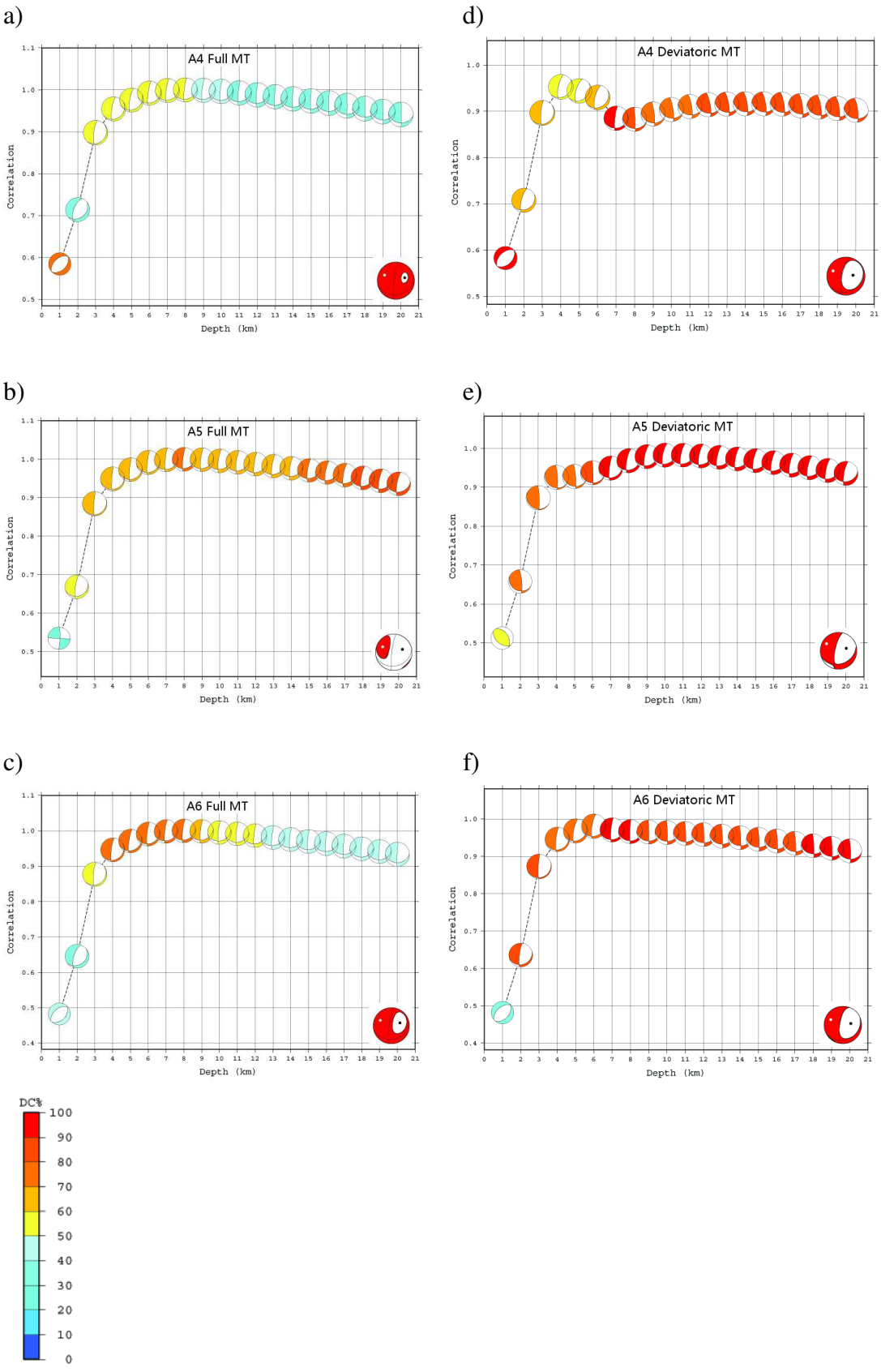

Figure S7. Correlation diagrams for test A (part II.) and subtests 4 – 6. In the left column are solutions for full MT inversion, in the right column are results for deviatoric MT.

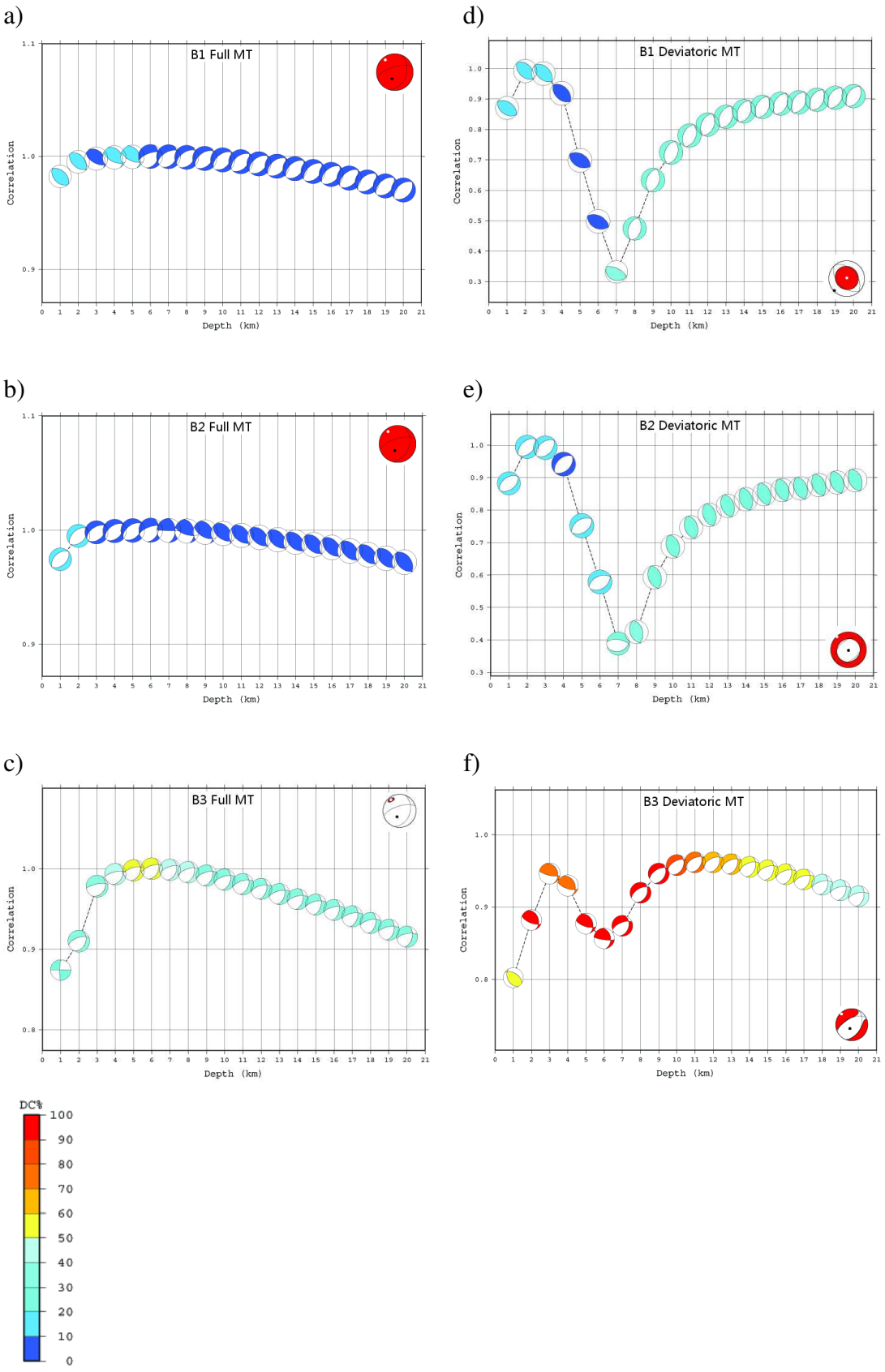

Figure S8. Correlation diagrams for test B (part I.) and subtests 1 – 3. In the left column are solutions for full MT inversion; in the right column are results for deviatoric MT.

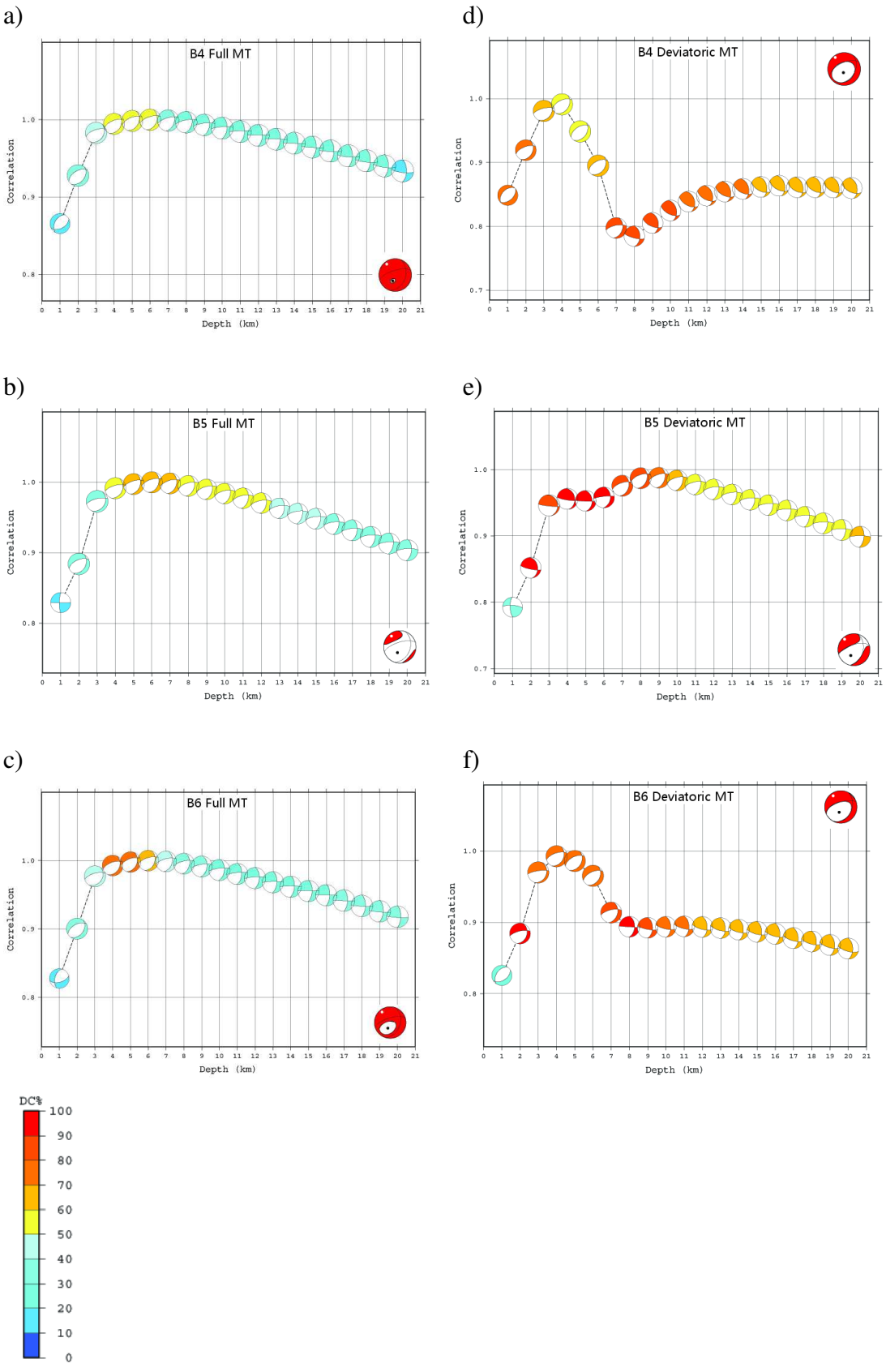

Figure S9. Correlation diagrams for test B (part II.) and subtests 4 – 6. In the left column are solutions for full MT inversion; in the right column are results for deviatoric MT.

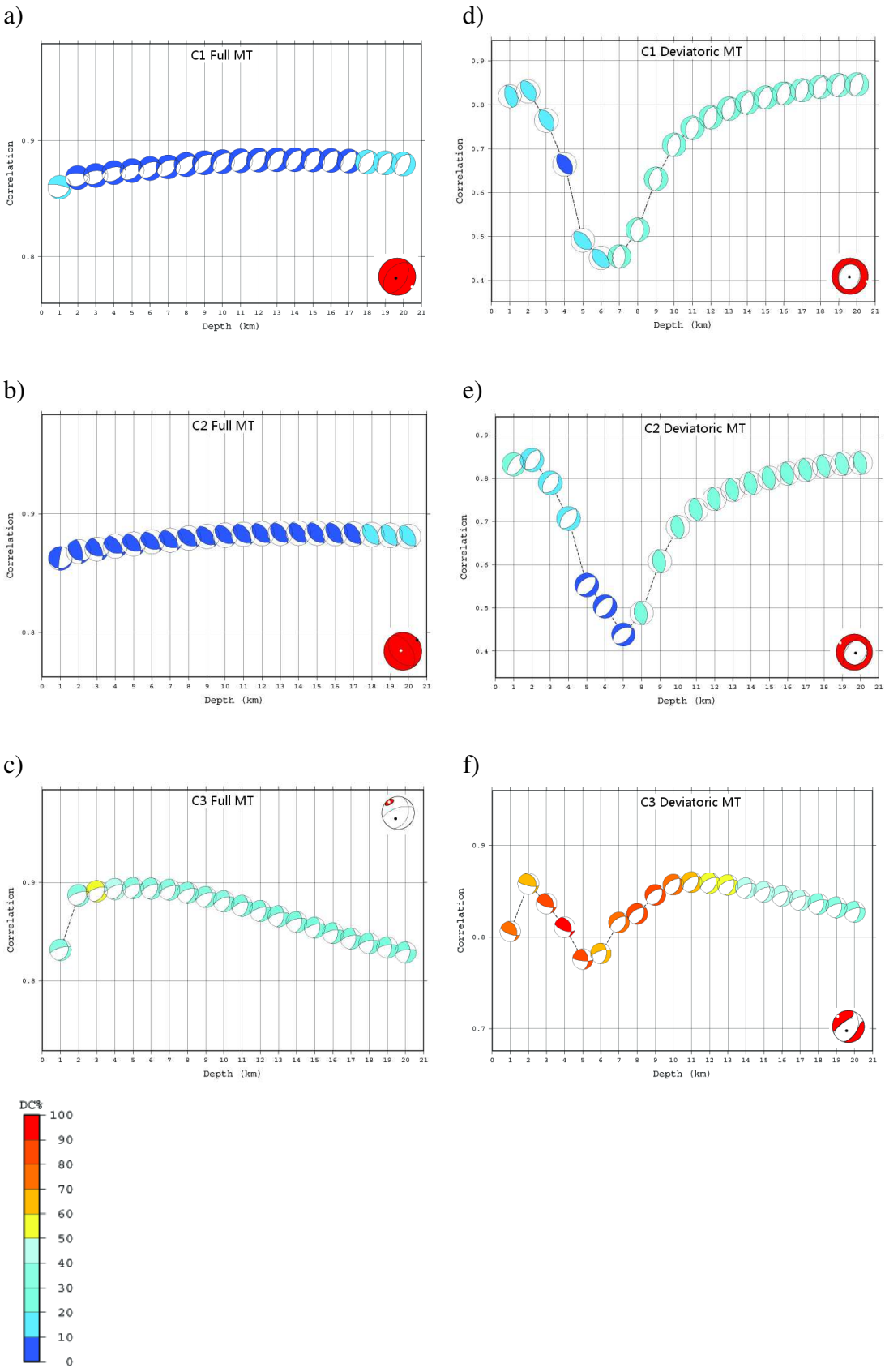

Figure S10. Correlation diagrams for test C (part I.) and subtests 1 – 3. In the left column are solutions for full MT inversion; in the right column are results for deviatoric MT.

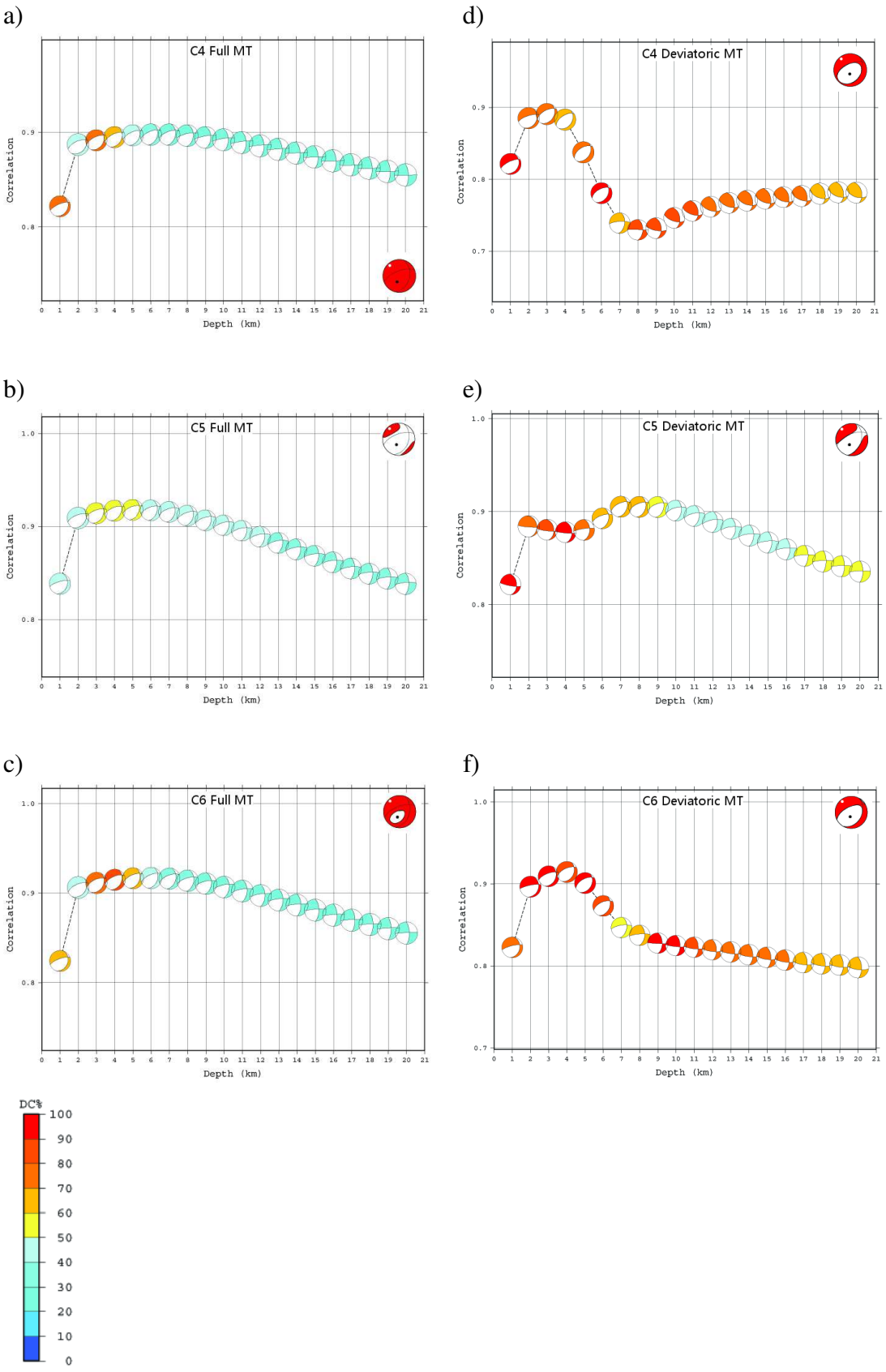

Figure S11. Correlation diagrams for test C (part II.) and subtests 4 – 6. In the left column are solutions for full MT inversion; in the right column are results for deviatoric MT.

List of Figures

List of Tables

List of Abbreviations

AUTH	Aristotle University of Thessaloniki
CLVD	Compensated Linear Vector Dipole
CMT	Centroid Moment tensor
DC	Double Couple
DDA	National Seismic Network of Turkey
DEV	Deviatoric part of Moment tensor
ELSTAT	Hellenic Statistical Authority
EMSC	European-Meditertanean Seismological Centre
FDSN	Federation of Digital Seismographic Networks
GFZ	GeoForschungsZentrum
GMT	Greenwitch Mean Time x GMT ... The Generic Mapping Tools
H	centroid depth
HUSN	Hellenic Unified Seismic Network
IRIS	Incorporated Research Institutions for Seismology
ISC	International Seismological Centre
ISO (VOL)	Isotropic (volumetric) component
ISOLA	ISOLated Asperities
model D	crustal velocity model (Dimitriadis et al., 2010)
model N	crustal velocity model (Novotný et al., 2001)
MT	Moment tensor
NOA	National Observatory of Athens
O	centroid time
Orfeus	Observatories & Research Facilities for European Seismology
PTN axes	pressure, tension, normal axes of Moment tensor
SAC	Seismic Analysis Code
SEED	Standard for the Exchange of Earthquake Data
TDMT_INVC	Time-Domain Moment Tensor INVerse Code
UOA	University of Athens
UPSL	University of Patras Seismological Laboratory
USGS	U.S. Geological Survey
UTC	Coordinated Universal Time

Cartesian coordinate systems:

NED	first coordinate *x* is positive from south to north, second *y* is positive from west to east and the last *z* downward
USE	positive upward, southward and eastward
ENU	positive eastward, northward and upward
NWU	positive northward, westward and upward

Components of records:

NS	north-south
EW	east-west
Z	vertical component

The station codes are not considered abbreviations in this thesis. (They are listed in the Table 2.2.)

Notation

a_1 ... a_5, a_6	scalar coefficients of Moment tensor
c_{ijkl}	components of a fourth-order tensor, are independent of strain
CN	condition number
corr	correlation between observed and synthetic seismograms
$\Delta\chi^2$	theoretical misfit
E^j	elementary seismogram corresponding to the *j*th elementary Moment tensor
$\tilde{\mathbf{E}}$	design matrix
G	Green's tensor
λ	eigenvalue of $\mathbf{E}^T\mathbf{E}$
M	Magnitude (M_w ... moment magnitude) x M ... Moment tensor
M_{DEV}; M_{ISO}; M_{DC}; M_{CLVD}	Decomposition of Moment tensor
M_0	Scalar seismic moment
misfit	match between real and best-fitting seismograms
μ	according to Passyanos et al. (1996)
pdf	1D Gaussian probability density function
Q_p, Q_s	attenuation quality factors
ρ	density
s	synthetic seismogram (displacement)
σ_{a6}	standard deviation
t	time
u	displacement
v_p, v_s	velocity of p and s waves
V_i	i-th singular vector
VR	variance reduction
w_i	i-th singular value